

Stereoselective Ruthenium-Catalyzed Olefin Metathesis

Thesis by

D. William Ward

In Partial Fulfillment of the Requirements

for the Degree of

Doctor of Philosophy

California Institute of Technology

Pasadena, California



2003

(Submitted July 10, 2003)

© 2003

Donald William Ward

All Rights Reserved

For Emily and My Family

Acknowledgments

It is difficult to use the small amount of space available here to express gratitude to all those who have made invaluable contributions to my time at Caltech. I would like to begin by expressing my gratitude to Prof. Bob Grubbs. The freedom which Bob grants to the members of his group allows them to progress beyond the role of mere student and causes them to become true participants in a scientific community. Bob provides valuable input at the right moments, and also allows research to run its natural course when necessary. I would also like to thank my research committee for their time and commitment, including Profs. John Bercaw, Mitchio Okumura, and Jonas Peters.

I would like to thank the many people with whom I have worked directly on this research, including Steve Goldberg, Jacob Berlin, Dean Toste, Jon Seiders, Larry Henling, Mike Day, Melanie Sanford, Choon Woo Lee, Janis Louie, and Chris Bielawski.

There are of course many other coworkers in the Grubbs group who have had a big impact on my day-to-day life. I especially appreciate the kind helpfulness of many of the students and postdocs who were in the group when I joined, including Melanie Sanford, Todd Younkin, Matthias Scholl, Dave Lyn, Helen Blackwell, Tom Kirkland, Mike Koschko, JP Morgan, Tina Trnka, Mike Ulman, Eric Connor, Helen Blackwell, and Delwin Elder. These people were always available with inexhaustible patience when I had many questions.

I've also enjoyed sharing time in the group with many others: Andrew Waltman, Stu Cantrill, Jen Love, Justin Gallivan, Hyunjin Kim, Dan Sanders, and Christie Morrill. These kind people made day-to-day life so much easier, and have helped me to ponder life's eternal question: "What *is* the muguet?"

Caltech's SURF program will always have my gratitude for introducing me to the Institute. I would especially like to thank the SURF director, Ms. Carolyn Merkel, and my SURF advisors, Profs. Joe Shepherd and Paul Robinson.

I have also been grateful for those people who really keep the gears at Caltech moving, including Linda Syme, Rick Gerhardt, Tom Dunn, Steve Gould, Joe Drew, and Chris Smith.

Others who have made my time at Caltech much more enjoyable include Leroy Hood, Vipin, the National Registry of Historic Places, Gimpy, the late-night Dandy, Tex-Slash-Slash, Squeaky, "the Eye," Willie Nelson (frequently spotted on campus), surgical Elvis, Red Dog, and all great Americans who have selflessly ridden the rails and upheld the hobo creed.

Abstract

Ruthenium complexes ligated with *N*-heterocyclic carbenes, such as (IMesH₂)(PCy₃)(Cl)₂Ru=CHPh [IMesH₂ = 1,3-dimesityl-4,5-dihydroimidazol-2-ylidene], constitute the latest class of olefin metathesis catalysts and are particularly desirable for their high activity and tolerance of most common functional groups. This thesis primarily describes studies aimed at understanding and controlling the stereoselectivity of this type of complex, including enantioselectivity and *cis/trans* selectivity.

Chapter 2 describes the basic design of novel chiral *N*-heterocyclic carbene ruthenium complexes active for olefin metathesis. A series of catalysts based on this design is prepared and studied by variable-temperature NMR spectroscopy and X-ray crystallography.

Chapter 3 relates the utilization of these chiral ruthenium-based olefin metathesis catalysts in enantioselective desymmetrization reactions of achiral trienes to produce cyclic ethers. Selectivity trends are identified and catalysts are optimized with the best result showing a 90% enantiomeric excess of product. A stereochemical model is proposed based on the outcome of these reactions.

Chapter 4 relates efforts to develop a useful test for measuring the inherent stereoselectivity of a wide array of ruthenium-based olefin metathesis catalysts by converting them to relatively inactive Fischer-alkylidenes in a single-turnover reaction with dihydrofuran. A group of approximately twenty olefin metathesis catalysts is tested with this technique, and the resulting data are found to correlate well with the results of the ring-closing metathesis of macrocycles. Several trends are discussed, and a stereochemical model consistent with the results of these reactions is described.

Chapter 5 details a novel route for the synthesis of telechelic polymers through the ring-opening metathesis polymerization (ROMP) of highly strained bicyclic monomers.

Table of Contents

Chapter 1: Introduction	1
Introduction to Olefin Metathesis.....	2
Stereoselectivity in Olefin Metathesis.....	4
Developing Stereoselective Ruthenium-Based Olefin Metathesis Catalysts.....	13
Thesis Research.....	15
References.....	16
Chapter 2: Synthesis and Characterization of Chiral Ruthenium-Based Olefin Metathesis Catalysts	21
Abstract.....	22
Introduction.....	23
Results and Discussion.....	23
Experimental Section.....	30
References and Notes.....	41
Chapter 3: Enantioselective Ruthenium-Catalyzed Ring-Closing Metathesis	43
Abstract.....	44
Introduction.....	45
Results.....	46
Discussion.....	52

Experimental Section.....	64
References and Notes.....	70

Chapter 4: Testing the Inherent Stereoselectivity of Ruthenium-Based Olefin

Metathesis Catalysts	73
Abstract.....	74
Introduction.....	75
Results.....	79
Discussion.....	87
Experimental Section.....	92
References and Notes.....	95

Chapter 5: Novel Method for the Synthesis of Telechelic

Poly(oxanorbornene)	97
Abstract.....	98
Introduction.....	99
Results and Discussion.....	102
Conclusion.....	107
Experimental Section.....	109
References and Notes.....	112

Appendix: X-Ray Crystallographic Data	113
--	-----

List of Figures

Chapter 1: Figure 1.	Mechanism of the olefin metathesis reaction.....	2
Figure 2.	Olefin metathesis reactions.....	3
Figure 3.	Applications of olefin metathesis.....	4
Figure 4.	Cis double bonds in natural products.....	5
Figure 5.	Olefin metathesis catalysts that exhibit <i>cis</i> -selectivity.....	6
Figure 6.	First example of enantioselective olefin metathesis.....	7
Figure 7.	Kinetic resolution of dienes through RCM.....	8
Figure 8.	Functional groups listed in descending order of reactivity with early and late transition metal olefin metathesis catalysts.....	14
Figure 9.	Activity and functional group compatibility of olefin metathesis catalysts.....	15
Chapter 2: Figure 1.	Desymmetrization of the IMesH ₂ /ruthenium system 2.1	24
Figure 2.	Possible rotational isomers of chiral mono- <i>o</i> -substituted complexes.....	26
Figure 3.	<i>Ortho</i> -methyl naphthyl complex 2.22	27
Figure 4.	X-Ray crystal structure of complex 2.23	29
Chapter 3: Figure 1.	Chiral olefin metathesis catalysts.....	45
Figure 2.	Relative activity of molybdenum-alkylidene isomers.....	52
Figure 3.	Effect of chiral bisalkoxide ligand.....	53

Figure 4. Molybdenum-catalyzed enantioselective metathesis stereochemical model.....	54
Figure 5. Possible geometries of olefin complex intermediate.....	55
Figure 6. Lowest-energy metallacyclobutane according to computation...56	
Figure 7. Olefin complexes of ruthenium.....	57
Figure 8. Steric interaction between alkylidene and NHC ligands.....	59
Figure 9. Stereochemical model A.....	60
Figure 10. Stereochemical model B.....	61
Figure 11. Stereochemical model C.....	62
Chapter 4: Figure 1. Cis double bonds in natural products.....	75
Figure 2. Olefin metathesis catalysts that exhibit cis selectivity.....	76
Figure 3. Attempted <i>cis</i> -selective catalyst design.....	77
Figure 4. E:Z ratios of reactions of dihydrofuran with olefin metathesis complexes.....	81
Figure 5. Enantioselectivity/ <i>trans</i> -selectivity correlation.....	88
Figure 6. <i>Syn</i> and <i>anti</i> rotamers in <i>cis/trans</i> selectivity.....	89
Figure 7. X-Ray crystal structure of complex 2.22	91
Figure 8. Disfavoring of <i>cis</i> product formation through alkylidene steric interaction.....	91
Chapter 5: Figure 1. ¹ H NMR spectrum of low-molecular-weight semitelechelic poly(oxanorbornene) 5.10	103

Figure 2. ^1H NMR spectrum of low molecular weight telechelic poly(oxanorbornene) 5.12	105
---	-----

List of Schemes

Chapter 1: Scheme 1. Chiral molybdenum catalysts ligated with BINOL derivatives.....	9
Scheme 2. Enantioselective desymmetrizations via ring-closing metathesis.....	10
Scheme 3. Syntheses of <i>endo</i> - and <i>exo</i> - brevicomin.....	11
Scheme 4. Asymmetric ring-opening metathesis/ring-closing metathesis (AROM/RCM).....	12
Scheme 5. Asymmetric ring-opening metathesis/cross metathesis (AROM/CM).....	13
Chapter 2: Scheme 1. Synthesis of chiral catalysts.....	25
Scheme 2. Preparation of bis(pyridine) analogue to complex 2.20	28
Chapter 3: Scheme 1. Presumed mechanism of kinetic resolution via enantioselective ring-closing metathesis.....	46
Scheme 2. Desymmetrization of achiral triene substrates 3.7-3.9	47
Scheme 3. Enantioselective desymmetrization of achiral triene 3.9 by catalyst 3.13	50
Scheme 4. Mechanism of ruthenium-catalyzed olefin metathesis.....	55
Scheme 5. Reaction of IMesH ₂ /ruthenium system with diphenylacetylene.....	56

Scheme 6. Reaction mechanism featuring “swinging” metallacyclobutane moiety.....	57
Scheme 7. Synthesis of ruthenium-olefin complex 3.23	58
Chapter 4: Scheme 1. Single-turnover reactions with dihydrofuran.....	78
Scheme 2. Synthesis of complexes 4.7 and 4.8	79
Scheme 3. Synthesis of complex 4.12	80
Scheme 4. Macrocyclization through ring-closing metathesis.....	86
Chapter 5: Scheme 1. Ru-catalyzed preparation of HTPBD 5.5	99
Scheme 2. ADMET/depolymerization synthesis of telechelic poly(oxanorbornene).....	101
Scheme 3. Synthesis of semitelechelic poly(oxanorbornene).....	102
Scheme 4. Synthesis of telechelic poly(oxanorbornene) 5.12	105
Scheme 5. Synthesis of telechelic poly(norbornene) derivative 5.15	108

List of Tables and Charts

Chapter 3: Table 1. Enantioselective desymmetrization of triene 3.7 by catalysts 3.1-3.6	48
Table 2. Enantioselective desymmetrization of triene 3.8 by catalysts 3.4-3.6	49
Table 3. Enantioselective desymmetrization of triene 3.9 by catalysts 3.5 and 3.6	50
Table 4. Enantioselective desymmetrization of triene 3.9 by catalysts 3.6 and 3.14	51
Table 5. Enantioselective desymmetrization of achiral triene 3.25	63
Chapter 4: Chart 1. E:Z ratios in the macrocyclization of 4.29	87
Chapter 5: Table 1. Data for semitelechelic poly(oxanorbornene) 5.10	103
Table 2. Data for telechelic poly(oxanorbornene) 5.12	106
Table 3. Data for telechelic poly(oxabornene) 5.12 with adjusted catalyst loadings.....	107

Chapter 1: Introduction

Introduction to Olefin Metathesis

In organic chemistry, carbon-carbon bond-forming reactions remain of central importance. With the discovery and development of homogeneous late-metal catalysts, olefin metathesis has emerged over the past decade as a powerful reaction that is widely used in organic synthesis and polymer science.¹⁻⁴ Discovered in the 1950s, olefin metathesis is the transition-metal-mediated disproportionation of carbon-carbon double bonds. Since the 1970s, olefin metathesis has been understood to proceed through a mechanism in which an olefin coordinates to a transition metal alkylidene complex, undergoes [2+2] cycloaddition with the metal alkylidene to form a metallacyclobutane, and cleaves productively to regenerate a metal-alkylidene complex and a coordinated olefin product (Figure 1).^{2,5-9}

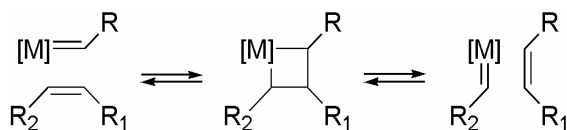


Figure 1. Mechanism of the olefin metathesis reaction.

Despite the apparent simplicity of this mechanism, the olefin metathesis reaction comprises several applications of tremendous variety, including ring-opening metathesis polymerization (ROMP),^{2,10-14} acyclic diene metathesis polymerization (ADMET),¹⁵⁻¹⁹ ring-closing metathesis (RCM),²⁰⁻²⁷ and cross metathesis (CM) (Figure 2).²⁸⁻³² Each of these processes represents a unique manifestation of the olefin metathesis reaction. For example, in ROMP, the reaction is thermodynamically driven by the relief of ring-strain of cyclic monomers in the formation of polymer. On the other hand, the monomers in ADMET are driven to polymerize via the removal of volatile olefin side-products

(ethylene) generated in the course of the metathesis reaction. As in ADMET, the loss of volatile side products is a driving force in the cross metathesis (CM) reaction, and the judicious matching of substrates with appropriate steric and electronic characteristics leads to a synthetically useful reaction by preferentially producing a particular product instead of a statistical mixture of metathesis products.

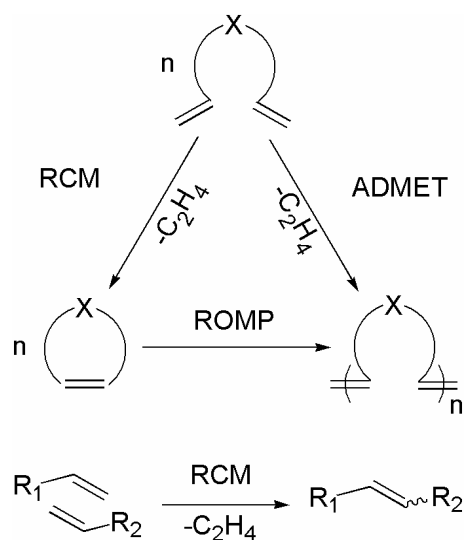


Figure 2. Olefin metathesis reactions.

The versatility of the olefin metathesis reaction has led to its use in a number of notable and disparate applications (Figure 3). For instance, the ROMP and cross-linking of dicyclopentadiene monomer produce tough resins of industrial importance. Ring-closing metathesis has been employed as a key step in the synthesis of an advanced intermediate in the total synthesis of epothilone A.^{23,26,27} Furthermore, metathesis has also been employed in supramolecular chemistry by closing copper-templated phenanthroline-containing cyclic olefins to form catenanes.^{33,34} Other applications not depicted include the ROMP of highly functionalized norbornene derivatives with pendant

sugars, amino acids, and vancomycin subunits for biological applications³⁵⁻³⁷ and the use of olefin metathesis to cyclize polypeptides and to cross-link peptides.³⁸⁻⁴⁰

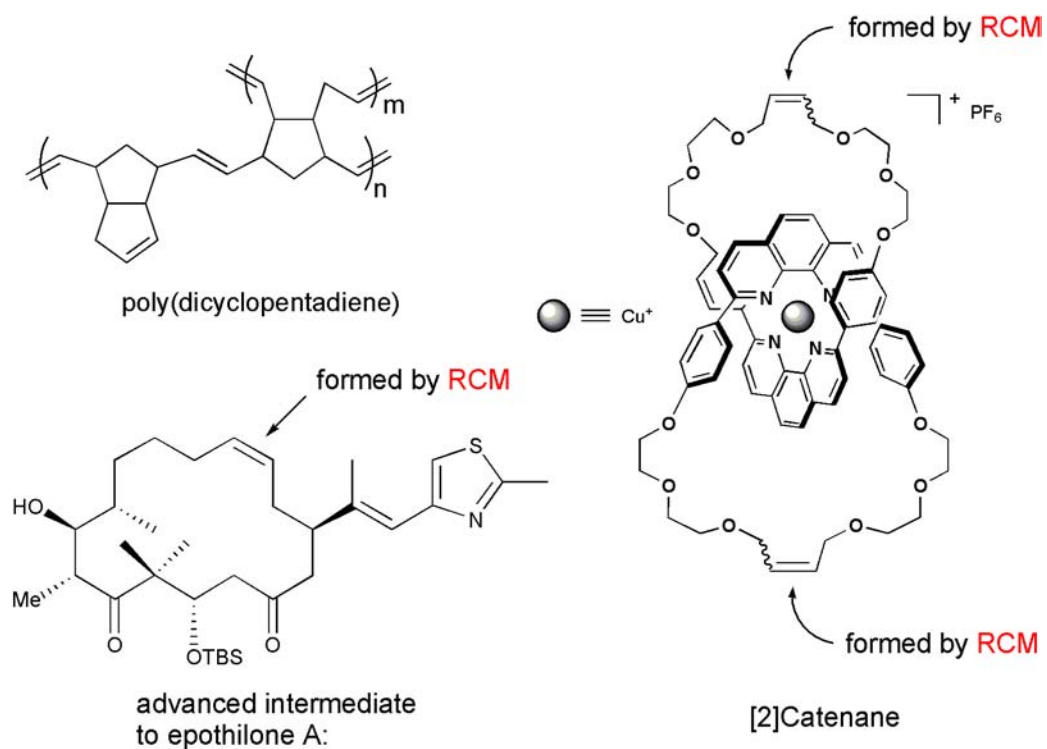


Figure 3. Applications of olefin metathesis.

Stereoselectivity in Olefin Metathesis

While much of the research effort in olefin metathesis has focused on boosting the activity, stability, functional-group compatibility, and applicability of olefin metathesis catalysts, stereoselectivity remains relatively elusive and undeveloped. As a result, achieving high enantioselectivity and cis/trans selectivity remains a major goal in olefin metathesis.

Cis/trans selectivity

An important problem in organic synthesis continues to be the control of the *cis/trans* isomerism of double bonds.⁴¹ As the equilibrium ratio of these isomers is generally impure for olefin metathesis products (*trans*:*cis* ~ 4:1 to 9:1), catalysts that provide either pure *trans* or pure *cis* formation are desired. Given the thermodynamic preference for *trans* olefin, the synthesis of pure *cis* products is anticipated to be particularly difficult. The development of a *cis*-selective catalytic route, however, remains especially attractive due to an abundance of *cis* olefins in natural products (Figure 4). For instance, the stereoselective synthesis of the *cis* olefins contained in the

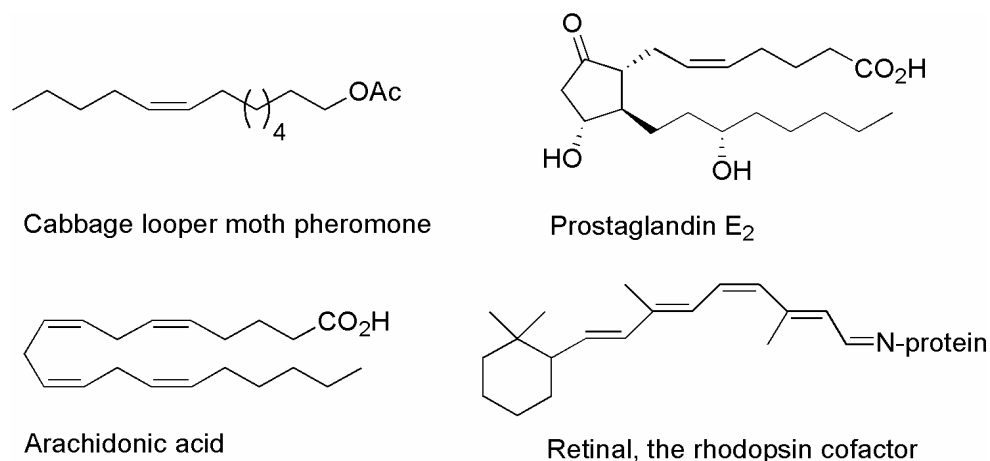


Figure 4. *Cis* double bonds in natural products.

majority of insect pheromones derived from C12 through C23 fatty acids is often critical since the *trans* isomer may inhibit the activity of its *cis* counterpart.^{42,43} Many biological processes involve the isomerization of a particular olefin from *cis* to *trans*, and investigation of these processes depends on the development of methods for *cis* olefin synthesis.^{44,45} Furthermore, *cis* olefins are present in a large number of bioactive molecules, including the prostaglandins.⁴⁶⁻⁴⁹

The occurrences of *cis* selectivity reported in the synthesis of small molecules via olefin metathesis are few. Early, ill-defined systems composed of tungsten or molybdenum salts and organotin/organoaluminums are capable of facilitating ROMP to give high *cis* polymer.^{50,51} Well-defined systems that display some measure of *cis* selectivity (Figure 5) include the cyclometallated aryloxy alkylidene tungsten (VI) catalyst (**1.1**)⁵² and *cis*-dialkyl-Cp*-diene tantalum complexes (**1.2**).⁵³ These complexes catalyze the ROMP of norbornene with the resulting polymers exhibiting greater than 98% *cis* linkages. Additionally, the tungsten catalyst has demonstrated high *cis* selectivity in cross metathesis, albeit at low conversions. However, these systems are highly sensitive to water and maintain a low compatibility with functional groups, making the development of user-friendly, *cis*-selective catalysts a worthwhile goal.

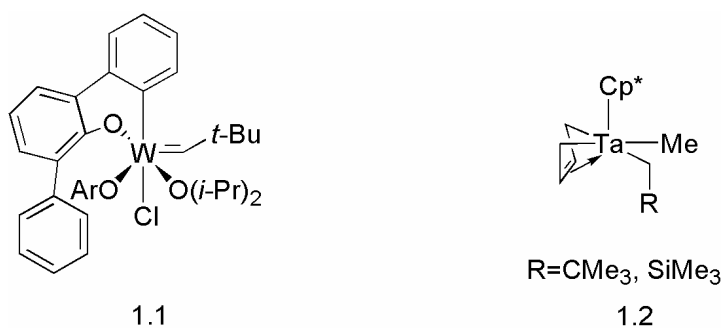


Figure 5. Olefin metathesis catalysts that exhibit *cis*-selectivity.

Enantioselectivity

The first strides in enantioselective olefin metathesis were made with Schrock's development of molybdenum alkylidenes appended with chiral diolate ligands for the production of highly tactic ROMP polymers.⁵⁴ In this report, the authors observe that "one might also consider the possibility that [the reported] catalysts...could selectively

polymerize or ring-close one enantiomer in a racemic mixture.” Since then, a family of molybdenum alkylidene catalysts ligated with chiral bisalkoxide ligands has produced a prodigious body of enantioselective metathesis reactions. A few years following Schrock’s portentous observation, the Grubbs group reported the first examples of enantioselective olefin metathesis utilizing a molybdenum alkylidene species ligated with (1*R*,2*R*)-2’,2’,2’’,2’’-tetrakis(trifluoromethyl)-1,2-bis(2’-hydroxymethyl)cyclopentane (**1.3**) (Figure 6).^{55,56} In these reports, chiral catalysts are employed in order to effect the kinetic resolution of racemic dienes through enantioselective ring-closing metathesis, albeit with modest enantiomeric excesses ($k_{rel} < 3$). For example, in the kinetic resolution of chiral diene **1.4**, catalyst **1.3** ring-closes the *R* enantiomer 2.2 times faster than the *S* enantiomer.

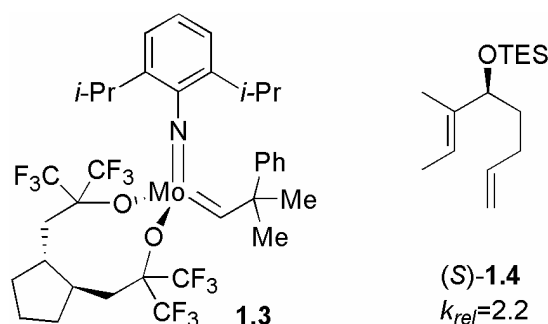


Figure 6. First example of enantioselective olefin metathesis.

Following these reports, the Hoveyda and Schrock groups collaborated to improve the enantioselectivity of catalysts of this motif.⁵⁷ By ligating the molybdenum alkylidene species with more rigid chiral diolate species, more selective catalysts were achieved. For example, molybdenum alkylidene complex **1.5** is ligated with a rigid biphen-derived ligand and efficiently catalyzes the ring-closing metathesis kinetic resolution of dienes **1.6-1.8** with high selectivity ($k_{rel} > 21$) (Figure 7).⁵⁸

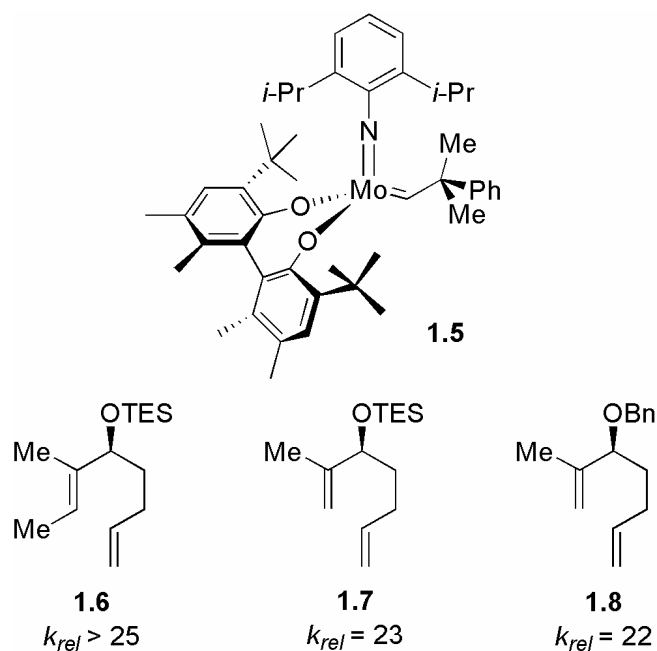
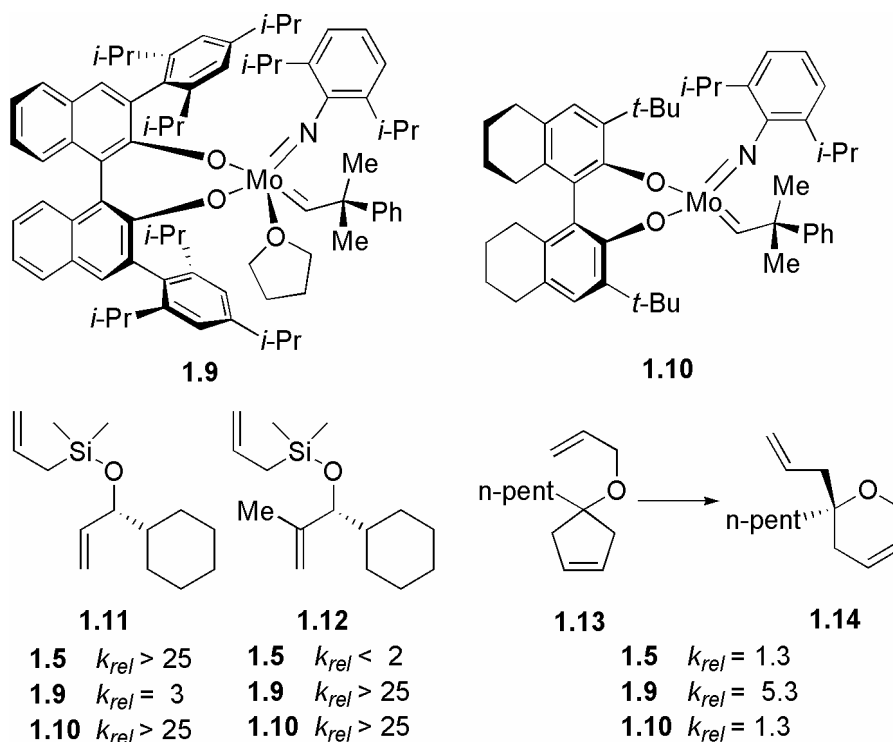


Figure 7. Kinetic resolution of dienes through RCM.

Although catalyst **1.5** efficiently and selectively promotes the formation of optically pure or enriched carbo- and heterocycles through asymmetric ring-closing metathesis, a challenge with catalysts of this motif has proven to be the development of a single catalyst that effects efficient enantioselective olefin metathesis for a broad array of substrates does not exist. This problem has in some measure been addressed by the development of catalysts complementary to **1.5**, such as molybdenum complexes **1.9**⁵⁹ and **1.10**,^{60,61} which have been ligated with a chiral BINOL derivative and a hydrogenated chiral BINOL derivative, respectively (Scheme 1). Although it is difficult to predict which complexes will enantioselectively catalyze a particular reaction, these complexes are complementary in their selectivity. For example, while only complexes **1.5** and **1.10** efficiently resolve diene **1.11**, substrate **1.12** (which contains only one additional methyl group) is selectively resolved only by complexes **1.9** and **1.10**. On the

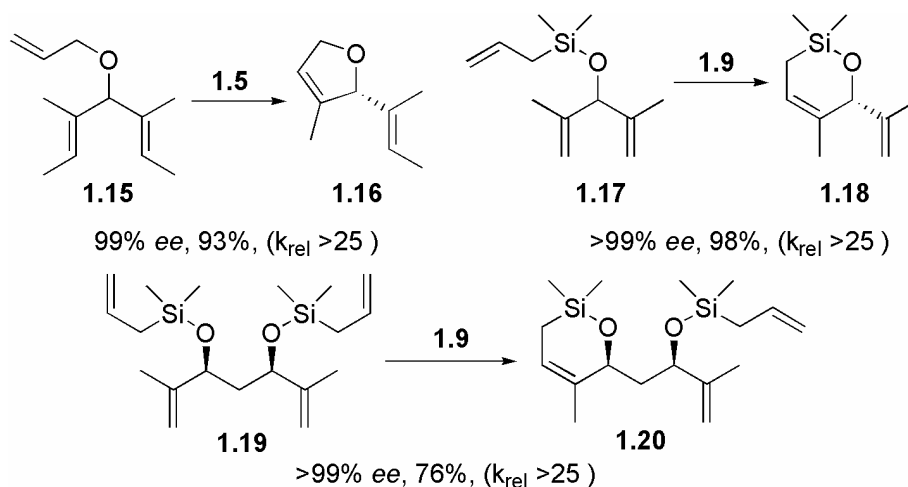
other hand, in the enantioselective synthesis of cyclic ether **1.14**, complex **1.9** exhibits significantly greater selectivity ($k_{rel} > 5$) than that of complexes **1.5** or **1.10** ($k_{rel} = 1.3$).



Scheme 1. Chiral molybdenum catalysts ligated with BINOL derivatives.

The synthesis of cyclic ether **1.14** (Scheme 1) is an example of the desymmetrization of an achiral molecule to form enantioenriched product. This type of enantioselective desymmetrization remains one of the most attractive types of reactions for olefin metathesis because of the theoretical possibility of achieving complete conversion of starting material to enantiopure product. By comparison, kinetic resolution offers a theoretical maximum of only 50 percent conversion to enantiopure product. Catalyst **1.5** is highly efficient in the enantioselective desymmetrization of achiral trienes to form five-membered cyclic ethers (Scheme 2).⁶² For example, in the case of achiral

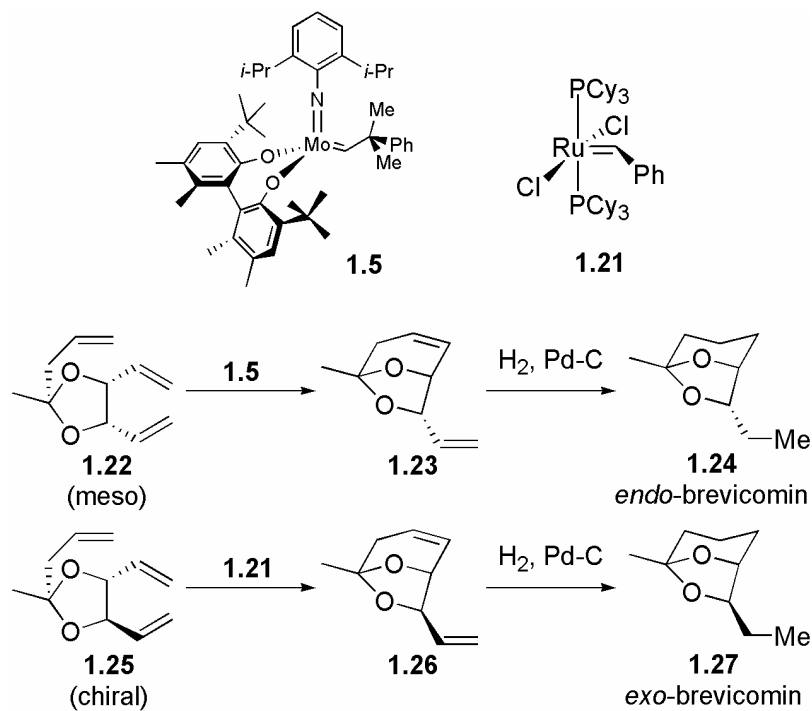
triene **1.15**, catalyst **1.5** is presumed to react first with the substrate's mono-substituted central olefin and then to react preferentially with one of the two pendant olefins in an enantiodetermining ring-closing step to provide cyclic ether **1.16** in 99% *ee* and high conversion. Complementarily, catalyst **1.9** is an efficient catalyst for enantioselective reactions to form six-membered cyclic ethers, and ring-closes achiral triene **1.17** to give cyclic ether **1.18** in greater than 99% *ee* and 98% conversion.⁵⁹ Finally, the versatility of enantioselective desymmetrization is exhibited in the reaction of **1.9** with achiral tetraene **1.19**. This reaction is, in practice, similar to a kinetic resolution, as the catalyst preferentially ring-closes one pair of olefins over another pair in order to provide chiral product **1.20** in greater than 99% *ee*.⁶³



Scheme 2. Enantioselective desymmetrizations via ring-closing metathesis.

The utility of the enantioselective desymmetrization reaction is exemplified in the total synthesis of *endo*-brevicomine **1.24** reported by the Burke group at the University of Wisconsin (Scheme 3).⁶⁴ In this report, *meso*-ketal triene **1.22** undergoes an enantioselective-desymmetrization ring-closing metathesis transformation with catalyst

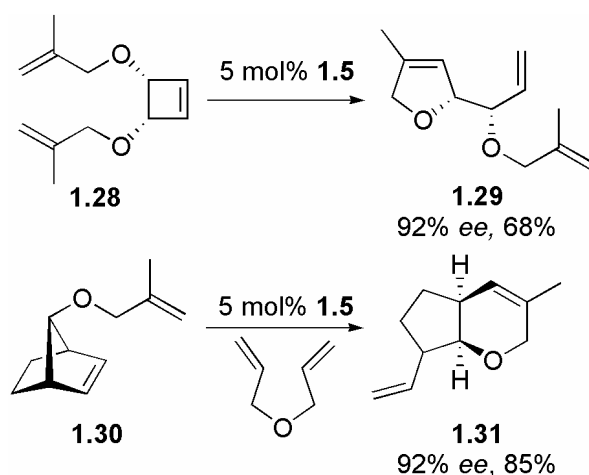
1.5 in order to provide enantioenriched product **1.23** in 55-59% *ee*. Hydrogenation of **1.23** provides *endo*-brevicommin **1.24** as the major product. By contrast, utilization of the achiral bisphosphine catalyst **1.21** in the synthesis of *exo*-brevicommin **1.27** requires the use of an enantiopure starting material.



Scheme 3. Syntheses of *endo*- and *exo*-brevicommin.

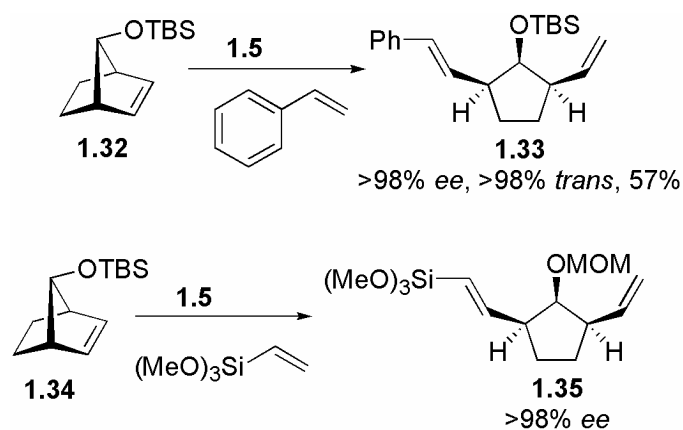
Enantioselective desymmetrization can also be employed to produce complex unsaturated carbo- and heterocycles in a single step using a powerful class of reactions, tandem asymmetric ring-opening metathesis/ring-closing metathesis (AROM/RCM).⁶⁵ In AROM/RCM, chiral metathesis catalysts react enantioselectively with achiral cyclic substrates in a ring-opening step, followed by intramolecular ring-closing with a pendant olefin to provide optically enriched product. For example, in substrate **1.28**, the cyclobutene moiety is ring-opened by chiral molybdenum alkylidene **1.5**, which then

reacts selectively with a pendant disubstituted olefin to yield unsaturated five-membered cyclic ether **1.29** in 92% *ee* (Scheme 4). Similarly, *meso*-bicyclic norbornene derivative **1.30** is ring-opened by chiral catalyst **1.5**, which then ring-closes intramolecularly with its pendant olefin in order to produce the complex bicyclic unsaturated ether **1.31** in 92% *ee*, all in a single step.



Scheme 4. Asymmetric ring-opening metathesis/ring-closing metathesis (AROM/RCM).

Asymmetric ring-opening metathesis/cross metathesis (AROM/CM) comprises the enantioselective ring-opening of a cyclic substrate followed by *intermolecular* cross metathesis with a partner olefin.^{66,67} For example, catalyst **1.5** reacts enantioselectively with strained cyclic substrate **1.32**, and forms product **1.33** in greater than 98% *ee* by reacting with the cross-partner olefin (styrene) instead of intramolecularly with a pendant olefin as in (AROM/RCM) (Scheme 5). Similarly, protected norbornene derivative **1.34** undergoes AROM/CM with trimethoxyvinylsilane as its cross-partner to produce the chiral five-membered carbocycle **1.35** in greater than 98% *ee*.



Scheme 5. Asymmetric ring-opening metathesis/cross metathesis (AROM / CM).

Developing Stereoselective Ruthenium-Based Olefin Metathesis Catalysts

Despite the remarkable enantioselectivity of the molybdenum alkylidene catalysts described above, the development of ruthenium-based enantioselective olefin metathesis catalysts has remained of considerable interest. The main motivation in developing ruthenium-based catalysts arises from the combined benefits of the extraordinary air/moisture stability and functional-group compatibility exhibited by ruthenium-based catalysts. The Schrock and Hoveyda groups have directed considerable efforts toward the improvement of the stability and synthetic utility of molybdenum alkylidene catalysts, including the development of *in situ* preparative routes⁶⁰ and polymer-supported catalysts⁶⁸. However, none of these approaches compares to the potential robustness and functional-group tolerance offered by ruthenium-based catalysts, which have long been demonstrated to react preferentially with olefins over other functional groups such as acids, alcohols, aldehydes, and ketones (Figure 8).⁶⁹ Additionally, the development of enantioselective ruthenium-based olefin metathesis catalysts may address the specific

substrate-to-catalyst matching that is required for effective use of the molybdenum class of catalysts.

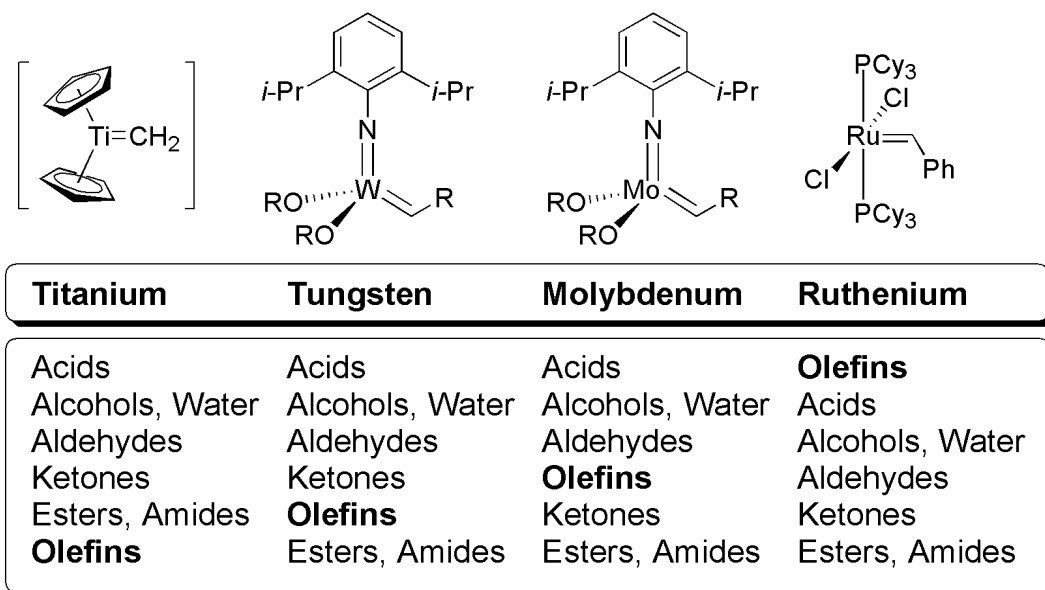


Figure 8. Functional groups listed in descending order of reactivity with early and late transition metal olefin metathesis catalysts.

Traditionally, the high activity of the molybdenum- and early-transition-metal-based olefin metathesis catalysts has helped to compensate for their relatively poor stability and functional-group compatibility. However, with the advent of ruthenium-based olefin metathesis catalysts ligated with *N*-heterocyclic carbenes, the activity of ruthenium-based catalysts now rivals that of the earlier transition metals (Figure 9),⁷⁰⁻⁷² making ruthenium-based catalysts ideal candidates for development as enantioselective catalysts. Furthermore, the *N*-heterocyclic carbene ligand, unlike the phosphine ligands of earlier ruthenium-based metathesis catalysts, is highly suitable for modification as a chiral ligand.

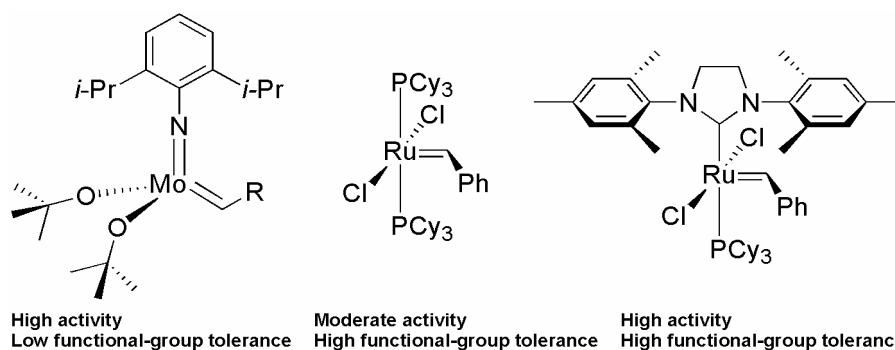


Figure 9. Activity and functional group compatibility of olefin metathesis catalysts.

Thesis Research

This thesis primarily relates advances made in controlling the stereoselectivity of ruthenium-based olefin metathesis catalysts, including enantioselectivity and cis/trans selectivity. **Chapter 2** details the synthesis and characterization of the organometallic complexes utilized in this work. **Chapter 3** pertains to the utilization of chiral ruthenium-based olefin metathesis catalysts in enantioselective desymmetrization to produce cyclic ethers. A stereochemical model is proposed based on the stereochemical outcome of these reactions. **Chapter 4** relates efforts to develop a probe for the inherent cis/trans selectivity of a wide array of ruthenium-based olefin metathesis catalysts. The implications of this study on the general approach to controlling stereoselectivity are also discussed. **Chapter 5** relates a novel route for the synthesis of telechelic polymers through ring-opening metathesis polymerization (ROMP).

References

1. Trnka, T. M.; Grubbs, R. H. *Acc. Chem. Res.* **2001**, *34*, 18-29.
2. Ivin, K. J. *J. Mol. Catal. A: Chem.* **1998**, *133*, 1-16.
3. Randall, M. L.; Snapper, M. L. *J. Mol. Catal. A: Chem.* **1998**, *133*, 29-40.
4. Grubbs, R. H.; Chang, S. *Tetrahedron* **1998**, *54*, 4413-4450.
5. Katz, T. J.; McGinnis, J. J. *Am. Chem. Soc.* **1977**, *99*, 1903-1912.
6. Katz, T. J.; Rothchild, R. *J. Am. Chem. Soc.* **1976**, *98*, 2519-2526.
7. Katz, T. J.; McGinnis, J. J. *Am. Chem. Soc.* **1975**, *97*, 1592-1594.
8. Grubbs, R. H.; Burk, P. L.; Carr, D. D. *J. Am. Chem. Soc.* **1975**, *97*, 3265-3267.
9. Grubbs, R. H.; Carr, D. D.; Hoppin, C.; Burk, P. L. *J. Am. Chem. Soc.* **1976**, *98*, 3478-3483.
10. Bazzi, H. S.; Sleiman, H. F. *Macromolecules* **2002**, *35*, 624-629.
11. Charvet, R.; Novak, B. M. *Macromolecules* **2001**, *34*, 7680-7685.
12. Davidson, T. A.; Wagener, K. B. *J. Mol. Catal. A: Chem.* **1998**, *133*, 67-74.
13. Hillmyer, M. A.; Nguyen, S. T.; Grubbs, R. H. *Macromolecules* **1997**, *30*, 718-721.
14. Pu, L.; Wagaman, M. W.; Grubbs, R. H. *Macromolecules* **1996**, *29*, 1138-1143.
15. Malecka, E.; Marciniak, B.; Pietraszuk, C.; Church, A. C.; Wagener, K. B. *J. Mol. Catal. A: Chem.* **2002**, *190*, 27-31.
16. O'Donnell, P. M.; Brzezinska, K.; Powell, D.; Wagener, K. B. *Macromolecules* **2001**, *34*, 6845-6849.
17. Schwendeman, J. E.; Church, A. C.; Wagener, K. B. *Adv. Synth. Catal.* **2002**, *344*, 597-613.

18. Smith, J. A.; Brzezinska, K. R.; Valenti, D. J.; Wagener, K. B. *Macromolecules* **2000**, *33*, 3781-3794.
19. Watson, M. D.; Wagener, K. B. *Macromolecules* **2000**, *33*, 8963-8970.
20. Ma, S. M.; Ni, B. K. *Org. Lett.* **2002**, *4*, 639-641.
21. Ashe, A. J.; Fang, X. D.; Kampf, J. W. *Organometallics* **2000**, *19*, 4935-4937.
22. Schuman, M.; Trevitt, M.; Redd, A.; Gouverneur, V. *Angew. Chem., Int. Ed.* **2000**, *39*, 2491.
23. Nicolaou, K. C.; Vourloumis, D.; Winssinger, N.; Baran, P. S. *Angew. Chem., Int. Ed.* **2000**, *39*, 44-122.
24. Arakawa, K.; Eguchi, T.; Kakinuma, K. *J. Org. Chem.* **1998**, *63*, 4741-4745.
25. Kirkland, T. A.; Lynn, D. M.; Grubbs, R. H. *J. Org. Chem.* **1998**, *63*, 9904-9909.
26. Nicolaou, K. C.; He, Y.; Vourloumis, D.; Vallberg, H.; Roschangar, F.; Sarabia, F.; Ninkovic, S.; Yang, Z.; Trujillo, J. I. *J. Am. Chem. Soc.* **1997**, *119*, 7960-7973.
27. Meng, D. F.; Su, D. S.; Balog, A.; Bertinato, P.; Sorensen, E. J.; Danishefsky, S. J.; Zheng, Y. H.; Chou, T. C.; He, L. F.; Horwitz, S. B. *J. Am. Chem. Soc.* **1997**, *119*, 2733-2734.
28. Cossy, J.; Willis, C.; Bellosta, V.; BouzBouz, S. *J. Org. Chem.* **2002**, *67*, 1982-1992.
29. Nicolaou, K. C.; Hughes, R.; Cho, S. Y.; Winssinger, N.; Labischinski, H.; Endermann, R. *Chem. Eur. J.* **2001**, *7*, 3824-3843.
30. O'Leary, D. J.; Blackwell, H. E.; Washenfelder, R. A.; Miura, K.; Grubbs, R. H. *Tetrahedron Lett.* **1999**, *40*, 1091-1094.
31. O'Leary, D. J.; Blackwell, H. E.; Washenfelder, R. A.; Grubbs, R. H. *Tetrahedron Lett.* **1998**, *39*, 7427-7430.

32. Diver, S. T.; Schreiber, S. L. *J. Am. Chem. Soc.* **1997**, *119*, 5106-5109.
33. Mohr, B.; Weck, M.; Sauvage, J. P.; Grubbs, R. H. *Angew. Chem., Int. Ed. Engl.* **1997**, *36*, 1308-1310.
34. Weck, M.; Mohr, B.; Sauvage, J. P.; Grubbs, R. H. *J. Org. Chem.* **1999**, *64*, 5463-5471.
35. Mortell, K. H.; Weatherman, R. V.; Kiessling, L. L. *J. Am. Chem. Soc.* **1996**, *118*, 2297-2298.
36. Kanai, M.; Mortell, K. H.; Kiessling, L. L. *J. Am. Chem. Soc.* **1997**, *119*, 9931-9932.
37. Arimoto, H.; Nishimura, K.; Kinumi, T.; Hayakawa, I.; Uemura, D. *J. Chem. Soc., Chem. Commun.* **1999**, 1361-1362.
38. Miller, S. J.; Grubbs, R. H. *J. Am. Chem. Soc.* **1995**, *117*, 5855-5856.
39. Miller, S. J.; Blackwell, H. E.; Grubbs, R. H. *J. Am. Chem. Soc.* **1996**, *118*, 9606-9614.
40. Blackwell, H. E.; Grubbs, R. H. *Angew. Chem., Int. Ed.* **1998**, *37*, 3281-3284.
41. Corey, E. J.; Cheng, X.-M. *The Logic of Chemical Synthesis*; Wiley: New York, 1995; Vol. 2.
42. Mori, K. *Biosci. Biotechnol. Biochem.* **1996**, *60*, 1925-1932.
43. *Natural Products Chemistry*; Academic Press: New York, 1975; Vol. 2.
44. Hubbard, R.; Kropf, A. *Proc. Natl. Acad. Sci. U. S. A.* **1958**, *44*, 130-139.
45. Jiang, H. L.; Kruger, N.; Lahiri, D. R.; Wang, D. R.; Vatele, J. M.; Balazy, M. *J. Biol. Chem.* **1999**, *274*, 16235-16241.
46. Ramwell, P. W. *The Prostaglandins*; Plenum: New York, 1973.
47. von Euler, U. S.; Eliasson, R. *Prostaglandins*; Academic Press: New York, 1967.

48. Benedetto, C., Ed. *Prostaglandins and Related Substances: A Practical Approach*; IRL Press: Washington, D. C., 1987.
49. Bergstrom, S. *Science* **1967**, *157*, 382.
50. Ivin, K. J.; Mol, J. C. *Olefin Metathesis and Metathesis Polymerization*; Academic Press: San Diego, 1997.
51. Dimonie, M.; Coca, S.; Dragutan, V. *J. Mol. Catal. A: Chem.* **1992**, *76*, 79-91.
52. Basset, J. M.; Leconte, M.; Lefebvre, F.; Hamilton, J. G.; Rooney, J. J. *Macromol. Chem. Phys.* **1997**, *198*, 3499-3506.
53. Mashima, K.; Kaidzu, M.; Tanaka, Y.; Nakayama, Y.; Nakamura, A.; Hamilton, J. G.; Rooney, J. J. *Organometallics* **1998**, *17*, 4183-4195.
54. McConville, D. H.; Wolf, J. R.; Schrock, R. R. *J. Am. Chem. Soc.* **1993**, *115*, 4413-4414.
55. Fujimura, O.; Grubbs, R. H. *J. Am. Chem. Soc.* **1996**, *118*, 2499-2500.
56. Fujimura, O.; Grubbs, R. H. *J. Org. Chem.* **1998**, *63*, 824-832.
57. Hoveyda, A. H.; Schrock, R. R. *Chem. Eur. J.* **2001**, *7*, 945-950.
58. Alexander, J. B.; La, D. S.; Cefalo, D. R.; Hoveyda, A. H.; Schrock, R. R. *J. Am. Chem. Soc.* **1998**, *120*, 4041-4042.
59. Zhu, S. S.; Cefalo, D. R.; La, D. S.; Jamieson, J. Y.; Davis, W. M.; Hoveyda, A. H.; Schrock, R. R. *J. Am. Chem. Soc.* **1999**, *121*, 8251-8259.
60. Aeilts, S. L.; Cefalo, D. R.; Bonitatebus, P. J.; Houser, J. H.; Hoveyda, A. H.; Schrock, R. R. *Angew. Chem., Int. Ed.* **2001**, *40*, 1452.
61. Cefalo, D. R.; Kiely, A. F.; Wuchrer, M.; Jamieson, J. Y.; Schrock, R. R.; Hoveyda, A. H. *J. Am. Chem. Soc.* **2001**, *123*, 3139-3140.

62. La, D. S.; Alexander, J. B.; Cefalo, D. R.; Graf, D. D.; Hoveyda, A. H.; Schrock, R. *J. Am. Chem. Soc.* **1998**, *120*, 9720-9721.
63. Weatherhead, G. S.; Houser, J. H.; Ford, J. G.; Jamieson, J. Y.; Schrock, R. R.; Hoveyda, A. H. *Tetrahedron Lett.* **2000**, *41*, 9553-9559.
64. Burke, S. D.; Muller, N.; Beaudry, C. M. *Org. Lett.* **1999**, *1*, 1827-1829.
65. Weatherhead, G. S.; Ford, J. G.; Alexanian, E. J.; Schrock, R. R.; Hoveyda, A. H. *J. Am. Chem. Soc.* **2000**, *122*, 1828-1829.
66. La, D. S.; Ford, J. G.; Sattely, E. S.; Bonitatebus, P. J.; Schrock, R. R.; Hoveyda, A. H. *J. Am. Chem. Soc.* **1999**, *121*, 11603-11604.
67. La, D. S.; Sattely, E. S.; Ford, J. G.; Schrock, R. R.; Hoveyda, A. H. *J. Am. Chem. Soc.* **2001**, *123*, 7767-7778.
68. Hultsch, K. C.; Jernelius, J. A.; Hoveyda, A. H.; Schrock, R. R. *Angew. Chem., Int. Ed.* **2002**, *41*, 589.
69. Grubbs, R. H. *J. Macromol. Sci. Pure Appl. Chem.* **1994**, *A31*, 1829-1833.
70. Bielawski, C. W.; Grubbs, R. H. *Angew. Chem., Int. Ed.* **2000**, *39*, 2903-2906.
71. Chatterjee, A. K.; Grubbs, R. H. *Org. Lett.* **1999**, *1*, 1751-1753.
72. Scholl, M.; Ding, S.; Lee, C. W.; Grubbs, R. H. *Org. Lett.* **1999**, *1*, 953-956.

**Chapter 2: Synthesis and Characterization of Chiral
Ruthenium-Based Olefin Metathesis Catalysts**

Abstract

The design of a series of novel chiral ruthenium-based olefin metathesis catalysts is described, and complexes **2.16-2.21** are synthesized using standard techniques. Overall yields are good, and purification of these catalysts is easily effected on the benchtop with standard flash chromatography. The rotational isomers of **3.16-3.21** are investigated through variable-temperature ^1H NMR spectroscopy with implications on the efficacy of these complexes in enantioselective olefin metathesis reactions. An X-ray crystal structure of bispyridine complex **3.23** (a close analogue to complex **3.20**) is obtained; the crystallographic data suggest that the design of the ligands in this series of catalysts is successful in transferring the chirality of the N-heterocyclic carbene ligands closer to the metal center.

Introduction

Over the past decade, olefin metathesis has emerged as a powerful method for the formation of carbon-carbon double bonds and is used widely in organic synthesis and polymer science.¹⁻⁵ A major advance in this field was the development of chiral molybdenum catalysts⁶ that exhibit high enantioselectivity in a variety of ring-closing⁷⁻¹⁰ and ring-opening^{8,11} metathesis reactions. However, these molybdenum-based systems require specific substrate-to-catalyst matching, necessitating reaction optimization and the availability of a number of catalysts. Additionally, the practicality of these systems remains a major challenge since they lack functional group tolerance and require the rigorous exclusion of air and moisture from reaction media. Furthermore, the control of cis/trans olefin geometry remains an important goal in natural product synthesis, including the industrially important synthesis of insect pheromones.¹² This Chapter details the synthesis and characterization of several ruthenium-based olefin metathesis catalysts¹³⁻²⁰ ligated with chiral *N*-heterocyclic carbenes (NHCs) employed in our studies of stereoselective ruthenium-catalyzed olefin metathesis.

Results and Discussion

Synthesis of chiral ruthenium-based olefin metathesis catalysts

In light of studies on the IMesH₂/ruthenium system **2.1** (IMesH₂ = 1,3-dimesityl-4,5-dihydroimidazol-2-ylidene) that suggest that the NHC ligand does not dissociate from ruthenium during metathesis,^{15,21,22} desymmetrization of the IMesH₂ ligand was effected in the development of chiral ruthenium metathesis catalysts. Although the mesityl rings of the NHC ligand are readily replaced with chiral substituents through synthesis from commercially available chiral alkylamines, preliminary investigations into the selectivity

and utility of these ruthenium complexes are not promising.²³ Alternatively, synthesis of the NHC from commercially available chiral diamines introduces chirality to the imidazole ring, but the stereocenters of the ligand are remote from the metal center. Furthermore, by replacing the mesityl substituents with mono-*o*-substituted aryl groups, a steric effect is expected more effectively to transfer the stereochemistry of the ligand nearer the metal center by placing the *o*-substituents of the aryl groups in an arrangement *anti* to the substituents on the imidazole ring (Figure 1).

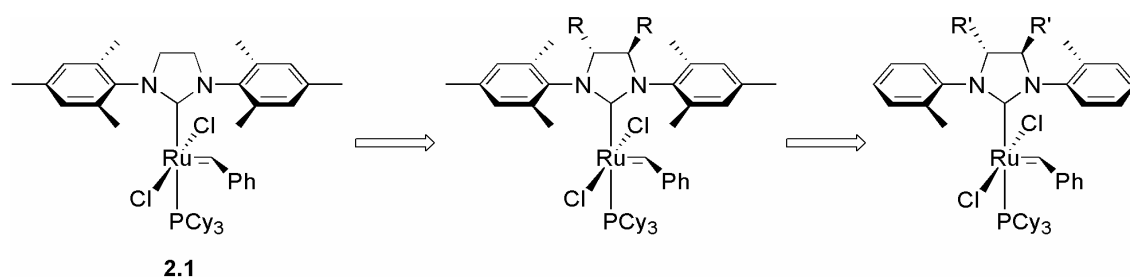
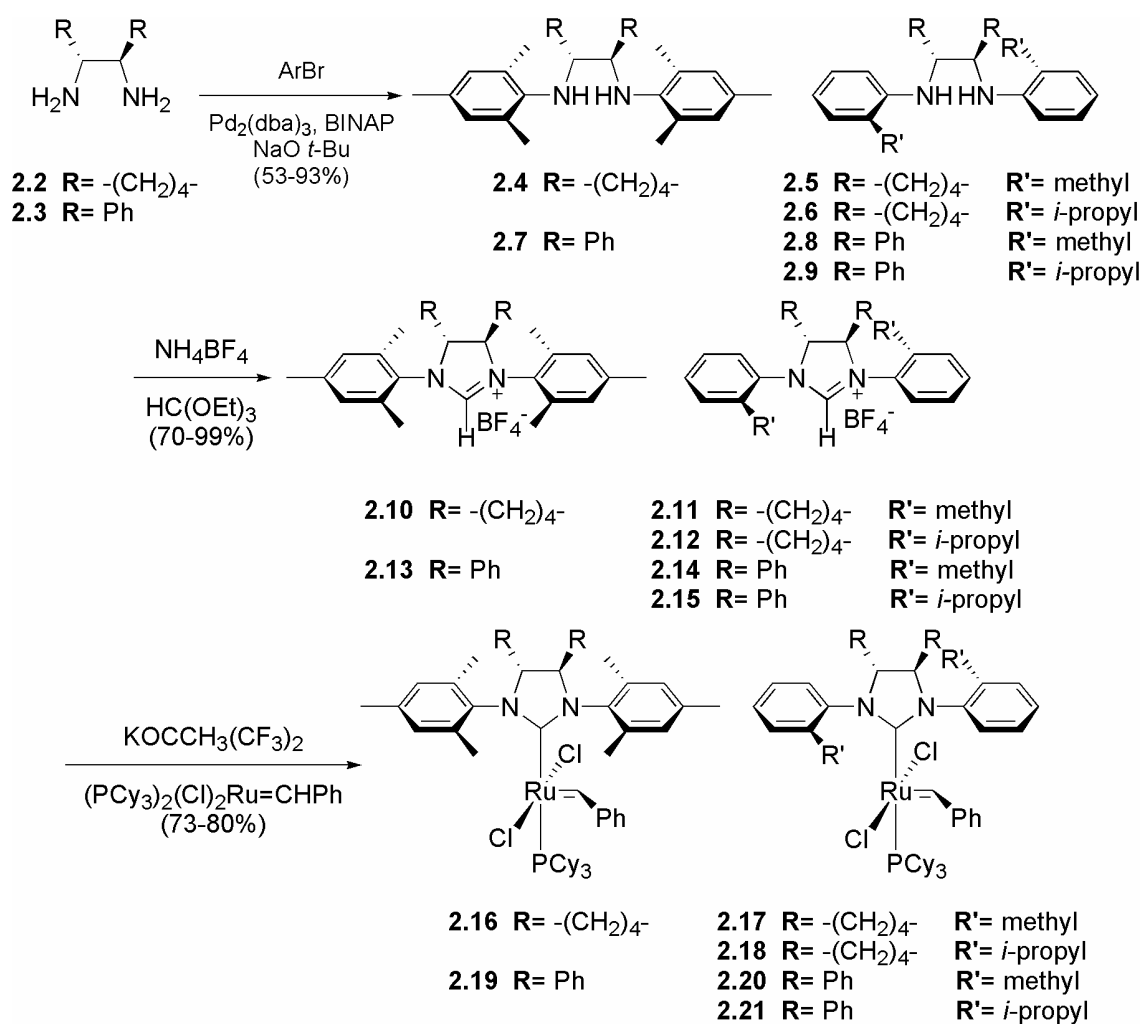


Figure 1. Desymmetrization of the IMesH₂/ruthenium system **2.1**.

The enantiomerically pure ruthenium complexes **2.16-2.21** are readily prepared in three steps from commercially available starting materials (Scheme 1). Diamines **2.4-2.6** and **2.7-2.9** are synthesized by palladium-catalyzed amination^{24,25} of the appropriate aryl bromides with (1*R*,2*R*)-1,2-diaminocyclohexane **2.2** or (1*R*,2*R*)-1,2-diphenylethylenediamine **2.3**, respectively. The resulting diamines are condensed with triethyl orthoformate and ammonium tetrafluoroborate to produce the corresponding imidazolium tetrafluoroborate salts **2.10-2.15**.²⁶ These salts are treated with potassium hexafluoro-*tert*-butoxide followed by (PCy₃)₂(Cl)₂Ru=CHPh to displace a single PCy₃ and generate the desired chiral complexes **2.16-2.21** in good yields. Although potassium *tert*-butoxide is an effective base in the synthesis of complexes **2.16** and **2.19**, if used in

the synthesis of **2.17-2.18** and **2.20-2.21** yields are dramatically reduced and formation of a *tert*-butoxide adduct of ruthenium is observed.²⁷ Complexes **2.16-2.21** are air-stable solids and are easily purified on the benchtop by column chromatography.²⁸ The bromide and iodide analogues of these complexes are generated *in situ* by the addition of excess LiBr or NaI, respectively.²²



Scheme 1. Synthesis of chiral catalysts.

Characterization of chiral ruthenium complexes by variable-temperature NMR spectroscopy

On account of the chirality of the *N*-heterocyclic carbene ligands of complexes **2.16-2.21**, the symmetry of these molecules is broken, and up to eight rotational isomers can be visualized for mono-*ortho*-substituted complexes at temperatures where alkylidene and NHC rotations are slow on the NMR time scale (Figure 2). Since a

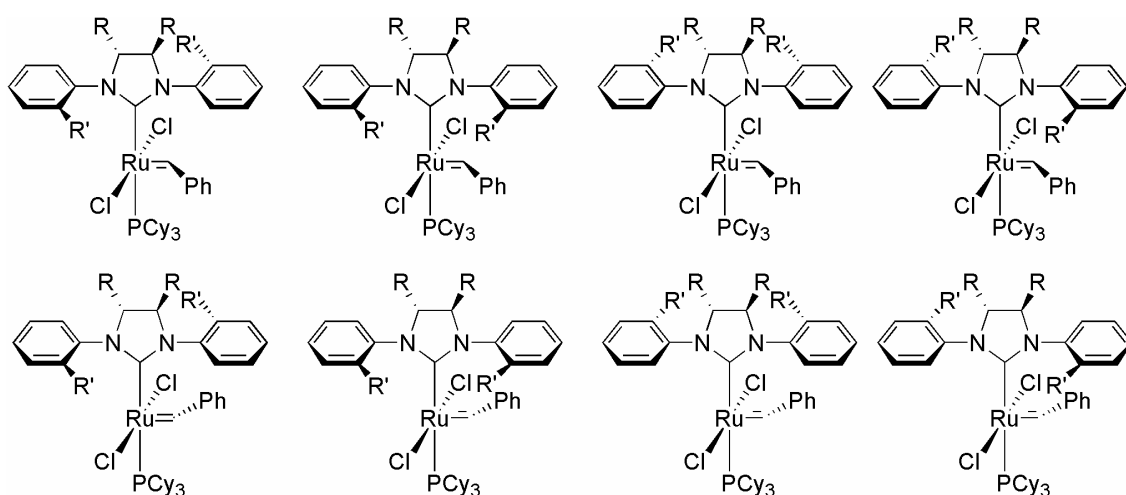


Figure 2. Possible rotational isomers of chiral mono-*o*-substituted complexes.

mixture of species in an enantioselective reaction is anticipated to complicate the reaction and lead to depressed enantiomeric excesses, it is of considerable interest to examine these complexes by variable temperature NMR spectroscopy. For example, in creating novel chiral olefin metathesis catalysts, *o*-methylnaphthyl complex **2.22** (Figure 3) was synthesized and examined at lower temperatures by ^1H NMR spectroscopy. In the alkylidene region of this complex, eight rotamers are detected, with two signals of equal intensity accounting for 10% of the species in solution, and six signals of equal intensity accounting for 90% of the species in solution. While the assignment of each of these

alkylidene signals to a specific rotamer is difficult to make, complexes of this design were abandoned in favor of mono-*ortho*-substituted ligands due to the relatively even distribution of these rotamers.

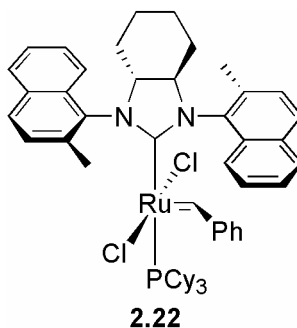


Figure 3. *Ortho*-methyl naphthyl complex **2.22**.

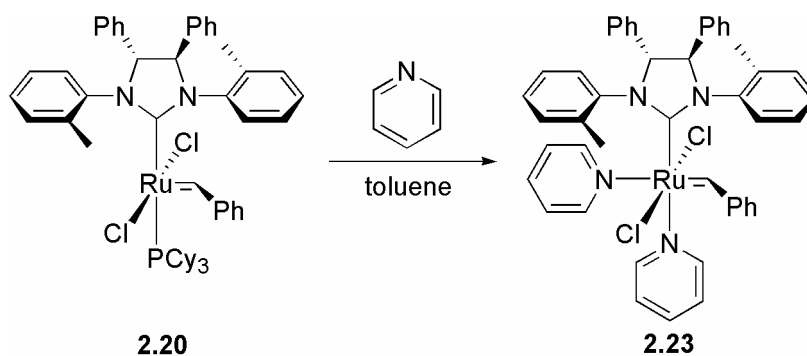
This type of analysis can be readily extended to complexes **2.16-2.21**. For example, at -30 °C, complex **2.16** shows two alkylidene species ($\delta = 19.47$ and 19.45 ppm) which integrate in a ratio of 1:1. Since the aryl side-groups of the NHC complex are symmetrical, these signals are attributable to the isomers arising from rotation around the alkylidene moiety; their occurrence in a 1:1 ratio suggests that the chiral ligand is not exerting a strong influence on alkylidene orientation. On the other hand, the rotational isomers of diphenyl-substituted complex **2.19** occur in a ratio of 1.1:1, suggesting that the phenyl moieties lead to a slightly stronger influence of the chiral ligand on alkylidene orientation.

This analysis can also be applied to the mono-*o*-substituted complexes: at -70 °C, *o*-methyl complex **2.17** shows seven alkylidene signals ($\delta = 19.60, 19.56, 19.52, 19.48, 19.45, 19.27, 19.22$ ppm) with 74% of the total integration attributable to three peaks of comparable intensity. By contrast, for *o*-isopropyl complex **2.18**, 75% of the alkylidene

integration is attributable to only two peaks (six total: $\delta = 19.89, 19.87, 19.78, 19.69, 19.51, 19.49$ ppm). This observation suggests that with the bulkier *o*-isopropyl groups, there is an increasing bias toward fewer species in greater proportion in solution. Some caution must be exercised in these assertions—since all of the eight possible alkylidene signals are not detected in these spectra, it is impossible to conclude that there is not any coincidental peak overlap. However, this trend is further carried out in the analysis of diphenyl *o*-substituted complexes **2.20** and **2.21**—increasing bias toward one major species in solution correlates with increasing steric bulk on the backbone and aryl side groups of the NHC ligand. As it turns out, this trend correlates well with the relative enantioselectivity of these complexes (see Chapter 3).

Characterization of chiral ruthenium complexes by X-ray crystallography

Although complexes **2.16-2.21** have proven to be difficult to crystallize, crystallographic evidence of the conformation of the chiral NHC ligands has been obtained by conversion of complex **2.20** to the bis(pyridine) adduct **2.23** (Scheme 2).



Scheme 2. Preparation of bis(pyridine) analogue to complex **2.20**.

Complex **2.23** is prepared by treatment of complex **2.20** with pyridine in toluene,²⁹ followed by precipitation by the addition of pentane, filtering, and washing. Complex **2.23** is more robust than its parent complex and also crystallizes more readily. The

crystal structure of **2.23** (Figure 4) shows that the NHC ligand is approximately C₂-symmetric with the *o*-methyl group oriented *anti* to the phenyl substituent of the imidazole ring. Additionally, the phenyl group of the benzylidene is oriented *anti* to the *o*-methyl substituent of the proximal aryl ring. This *anti-anti* arrangement suggests that the anticipated “gearing” of the ligand is occurring and that the stereochemistry of the phenyl substituents on the imidazole ring is effectively transferred closer to the metal center.

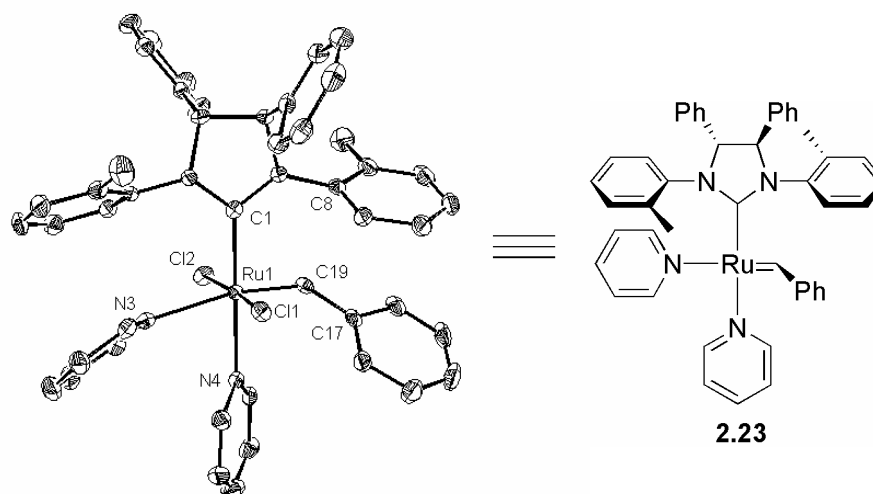


Figure 4. X-Ray crystal structure of complex **2.23** (50% probability ellipsoids). Selected bond lengths and angles for **2.23**: Ru(1)-C(19) 1.871 Å, Ru(1)-C(1) 2.031 Å, Ru(1)-N(3) 2.352 Å, Ru(1)-N(4) 2.187 Å, C(8)-C(19) 2.758 Å, Cl(1)-Ru(1)-Cl(2) 175°, C(19)-Ru(1)-N(3) 166°, C(1)-Ru(1)-N(4) 180°, Cl(1)-Ru(1)-C(19)-C(17) 46°.

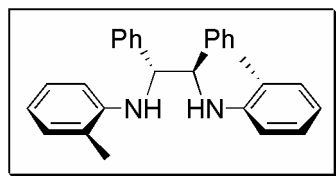
Experimental Section

General procedures

When specified, manipulation of organometallic compounds was performed using standard Schlenk techniques under an atmosphere of dry argon or in a nitrogen-filled Vacuum Atmospheres drybox ($O_2 < 2$ ppm). Argon was purified by passage through columns of BASF R3-11 catalyst (Chemalog) and 4Å molecular sieves (Linde). NMR Spectra were recorded on a Varian Inova (499.9 MHz for 1H ; 202.3 MHz for ^{31}P ; 125.7 MHz for ^{13}C) or a Varian Mercury 300 (299.8 for 1H ; 121.4 MHz for ^{31}P ; 74.5 MHz for ^{13}C). Chemical shifts are referenced to internal solvent resonances and are reported relative to tetramethylsilane. ^{31}P NMR Spectra were referenced using H_3PO_4 ($\delta = 0$ ppm) as an external standard.

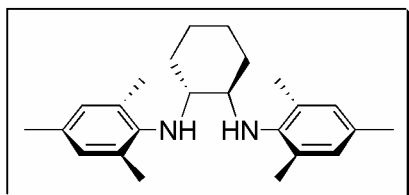
Materials and methods

Toluene, dichloromethane, tetrahydrofuran, and benzene were dried and degassed by passage through solvent purification columns containing activated alumina and copper. Silica gel used in organometallic complex purification was obtained from TSI. Ruthenium-based starting materials were used as received from Materia (Pasadena, CA). All others were purchased from Aldrich, and all liquids were purified by distillation.

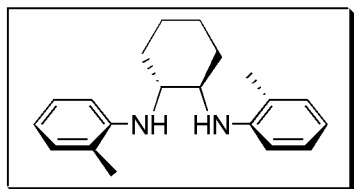


Representative preparation of compound 2.8. Under inert atmosphere, palladium acetate (0.016 g, 0.071 mmol), BINAP (0.088 g, 0.14 mmol), and sodium *t*-butoxide (0.410 g, 4.26 mmol) were added to toluene (25 mL) and stirred for 20 min. (R,R)-

diphenylethylenediamine (0.300 g, 1.42 mmol) and 2-bromotoluene (0.510 g, 2.98 mmol) were then added and the solution was heated to 100 °C for 16 hours. The solution was then cooled to ambient temperature, diluted with hexanes (75 mL), and filtered through a plug of silica. The silica was washed with methylene chloride to elute the product. The volatiles were removed *in vacuo* to yield a white solid (0.52 g, 93%). mp 49-51 °C. $[\alpha]_D^{22} +18.6^\circ$ (c = 0.5, CH₂Cl₂). ¹H NMR (300 MHz, CDCl₃): δ 2.15 (s, 6H), 4.73 (s, 2H), 6.33 (br s, 2H), 6.62 (t, *J* = 7.5 Hz, 2H), 6.91 (t, *J* = 7.8 Hz, 2H), 7.01 (d, *J* = 7.2 Hz, 2H), 7.25 (m, 10H). ¹³C NMR (125 MHz, CDCl₃): δ 17.7, 63.9, 111.8, 117.6, 122.9, 126.8, 127.0, 127.6, 128.5, 129.9, 139.7, 144.7. FAB HRMS [M+H] *m/z*: found 393.2319, calcd (C₂₈H₂₉N₂) 393.2331. Anal. Calcd for C₂₈H₂₈N₂: C, 85.67, H, 7.19, N, 7.14. Found C, 85.52, H, 7.31, N, 7.03.

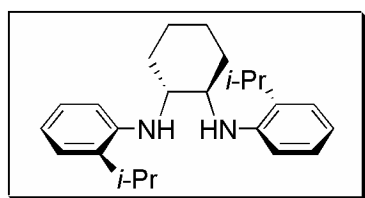


Compound **2.4**. (53%). mp 122 °C. $[\alpha]_D^{22} +37^\circ$ (c=1.05, CH₂Cl₂). ¹H NMR (300 MHz, CDCl₃): δ 1.17 (br, 4H), 1.62 (br, 2H), 1.83 (br, 2H), 2.24 (s, 6H), 2.31 (s, 12H), 3.06 (br, 2H), 3.40 (br, 2H), 6.82 (s, 4H). ¹³C NMR (125 MHz, CDCl₃): δ 19.34, 20.72, 25.03, 32.87, 62.26, 129.61, 130.85, 131.27, 142.13. IR (KBr, cm⁻¹) 584.3, 726.3, 753.2, 852.4, 1222.6, 1448.5, 1480.0, 2852.7, 2925.9, 3320.3, 3449.4. FAB HRMS [M+] *m/z*: found 350.2718, calcd (C₂₄H₃₄N₂) 350.2722.



Compound **2.5**. (67%) mp 84 °C. $[\alpha]_D^{22} = -27^\circ$ (c=0.94, CH₂Cl₂). ¹H NMR (300 MHz, CDCl₃): δ 1.2-1.6 (br m,

4H); 1.81 (br, 2H); 2.01(s, 6H); 2.38 (d, $J=12.3$ Hz, 2H); 3.35 (br, 2H); 3.7 (br, 2H); 6.68 (t, $J=7.2$ Hz, 1H); 6.75 (d, $J=6.6$ Hz, 1H); 7.05 (d, $J=7.2$ Hz, 1H); 7.14 (t, $J=8.1$ Hz, 1H). ^{13}C NMR (125 MHz, CDCl_3): δ 17.79, 24.93, 32.99, 57.85, 110.52, 117.27, 122.98, 127.21, 130.57, 145.99. IR (KBr, cm^{-1}) 745.3, 982.2, 1039.4, 1050.8, 1115.0, 1141.2, 1257.5, 1310.0, 1500.3, 1605.0, 2848.7, 2949.8, 3394.0. FAB HRMS $[\text{M}^+]$ m/z : found 294.2091 calcd ($\text{C}_{20}\text{H}_{26}\text{N}_2$) 294.2096. Anal. Calcd for $\text{C}_{20}\text{H}_{26}\text{N}_2$: C, 81.59; H, 8.90; N, 9.51. Found C, 81.71; H, 8.93; N, 9.38.



Compound **2.6**. (70%). $[\alpha]_{\text{D}}^{22} = -30.0^\circ$ ($c=0.59$, CH_2Cl_2).

^1H NMR (300 MHz, CDCl_3): δ 1.10 (d, $J=6.9$ Hz, 6H);

1.19 (d, $J=6.6$ Hz, 6H); 1.2-1.5 (br m, 4H); 1.81 (br m,

2H); 2.40 (d, $J=12.9$ Hz, 2H); 2.72 (m, $J=6.6$ Hz, 2H); 3.36 (d, $J=8.1$ Hz, 2H); 3.89 (br s,

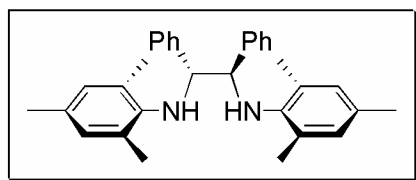
2H); 6.76 (br s, 4H); 7.13 (br m, 4H) ^{13}C NMR (125 MHz, CDCl_3): δ 22.43, 22.56,

24.95, 27.12, 32.83, 57.84, 111.25, 117.62, 125.42, 126.75, 133.28, 144.53. IR (neat, cm^{-1})

745.3, 1038.7, 1162.0, 1254.4, 1302.1, 1359.6, 1453.8, 1513.7, 1583.0, 1602.5,

2860.1, 2959.6, 3036.4, 3064.4, 3424.7. FAB HRMS $[\text{M}^+]$ m/z : found 350.2714 calcd

($\text{C}_{24}\text{H}_{34}\text{N}_2$) 350.2722.

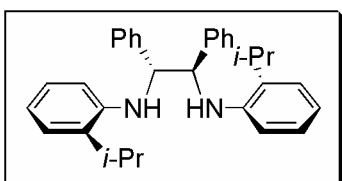


Compound **2.7**. (80 %). mp 65-67 $^\circ\text{C}$. $[\alpha]_{\text{D}}^{22} = -7.5^\circ$ (c

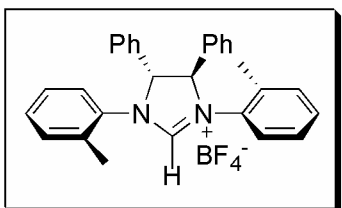
0.5, CH_2Cl_2). ^1H NMR (300 MHz, CDCl_3): δ 2.10 (s,

12H), 2.15 (s, 6H), 3.99 (s, 2H), 4.78 (s, 2H), 6.69 (s,

4H), 6.84 (m, 4H), 7.12 (m, 6H). ^{13}C NMR (125 MHz, CDCl_3): δ 19.5, 20.5, 66.5, 127.0, 127.6, 128.3, 128.6, 129.6, 130.3, 140.5, 141.5. FAB HRMS $[\text{M}+\text{H}]$ m/z : found 449.2969, calcd ($\text{C}_{32}\text{H}_{37}\text{N}_2$) 449.2957.

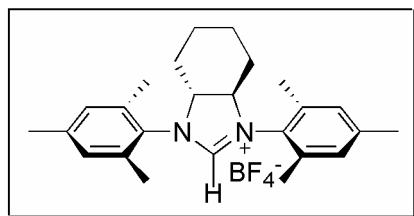


Compound **2.9**. (70 %). mp 86-88 °C. $[\alpha]_{\text{D}}^{22} +16.9$ ° (c 0.5, CH_2Cl_2). ^1H NMR (300 MHz, CDCl_3): δ 1.15 (d, $J=6.9$ Hz, 6H), 1.28 (d, $J=6.9$ Hz, 6H), 2.88 (m, 2H), 4.74 (s, 2H), 6.29 (d, $J=8.1$ Hz, 2H), 6.69 (t, $J=7.2$ Hz, 2H), 6.88 (d, $J=7.2$ Hz, 2H), 7.11 (d, $J=7.5$ Hz, 2H), 7.2-7.3 (m, 10H). ^{13}C NMR (125 MHz, CDCl_3): δ 22.5, 23.4, 27.5, 63.9, 112.4, 117.8, 124.7, 126.3, 126.9, 127.6, 128.6, 133.0, 139.9, 143.3. FAB HRMS $[\text{M}+\text{H}]$ m/z : found 449.2962, calcd ($\text{C}_{32}\text{H}_{37}\text{N}_2$) 449.2957.

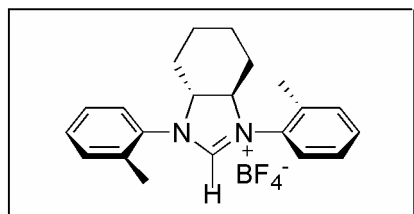


Representative preparation of compound 2.14. Diamine **2.8** (0.290 g, 0.74 mmol), ammonium tetrafluoroborate (0.093 g, 0.89 mmol), and triethyl orthoformate (1 mL) were heated to 120 °C for 5 hours. The solution was then allowed to cool to ambient temperature, and the volatiles removed *in vacuo*. The solids were then dissolved in a minimal quantity of methylene chloride and precipitated and washed with diethyl ether (3 X 10 mL). The resulting solids were then purified by flash chromatography (5% methanol in methylene chloride) to yield a white solid (0.360 g, 99%). mp 188-191°C. $[\alpha]_{\text{D}}^{22} +32.2$ ° (c 0.5, CH_2Cl_2). ^1H NMR (300 MHz, CDCl_3): δ 2.45 (s, 6H), 5.78 (s, 2H), 7.17 (m, 6H), 7.39 (m, 12H), 8.32 (s, 1H). ^{13}C NMR (125 MHz, CDCl_3): δ 18.5, 76.1, 127.6, 127.7, 128.0,

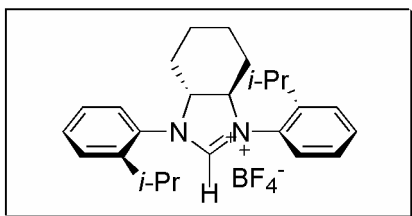
129.6, 130.0, 130.2, 131.6, 132.5, 133.3, 133.4, 157.3. FAB HRMS $[M+(-BF_4)]$ m/z : found 403.2159, calcd ($C_{29}H_{27}N_2$) 403.2174.



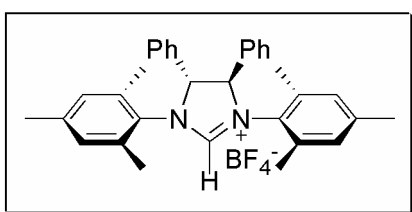
Compound **2.10**. (99%) mp 187 °C. $[\alpha]_D^{22} +29.7$ ° (c 1.04, CH_2Cl_2). 1H NMR (300 MHz, CD_2Cl_2): δ 1.33-1.44 (br m, 2H); 1.66-1.84 (br m, 2H); 1.94-2.10 (br m, 4H); 2.30 (s, 6H); 2.35 (s, 6H); 2.37 (s, 6H); 4.10 (br m, 2H); 7.04 (s, 2H); 7.08 (s, 2H); 8.24 (s, 1H). ^{13}C NMR (125 MHz, CD_2Cl_2): δ 18.17, 18.85, 21.33, 24.20, 27.94, 71.50, 129.42, 130.56, 130.71, 135.17, 136.68, 141.45, 161.20. IR (KBr, cm^{-1}): 519.2, 578.2, 742.5, 848.0, 939.3, 1063.6, 1168.8, 1235.3, 1251.7, 1272.6, 1388.4, 1451.6, 1482.3, 1578.8, 1613.5, 2951.9, 3049.1, 3422.9. FAB HRMS $[M+(-BF_4)]$ m/z : found 361.2641, calcd ($C_{25}H_{33}N_2$) 361.2644.



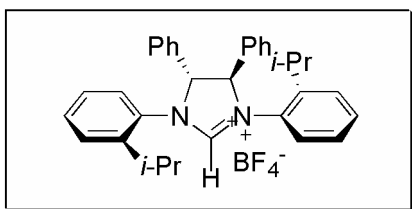
Compound **2.11**. (90%) mp 213 °C. $[\alpha]_D^{22} +33.5$ ° (c 0.97, CH_2Cl_2). 1H NMR (300 MHz, CD_2Cl_2): δ 1.41 (br m, 2H); 1.79 (br m, 2H); 1.99 (br m, 2H); 2.12 (br d, $J=11.1$ Hz, 2H); 2.41 (s, 6H); 4.21 (br m, 2H); 7.42 (m, 8H); 8.16 (s, 1H). ^{13}C NMR (125 MHz, CD_2Cl_2): δ 18.11, 24.15, 27.87, 71.77, 127.36, 128.29, 130.92, 132.42, 133.39, 134.99, 159.72. IR (KBr, cm^{-1}): 524.0, 766.7, 1066.6, 1162.5, 1256.0, 1303.0, 1450.2, 1496.6, 1573.6, 1595.4, 2874.5, 2961.9, 3072.2, 3441.3. FAB HRMS $[M+(-BF_4)]$ m/z : found 305.2018, calcd ($C_{21}H_{25}N_2$) 305.2018.



Compound **2.12**. (93%). mp 205 °C. $[\alpha]_D^{22} +20.4$ ° (c 1.0, CH₂Cl₂). ¹H NMR (300 MHz, CD₂Cl₂): δ 1.23-1.46 (br m, 16H); 1.92-2.18 (br m, 4H); 2.6-3.5 (br m, 2H); 3.7-4.6 (br m, 2H); 7.37-7.44 (br m, 3H); 7.44-7.60 (br m, 5H); 8.00 (s, 1H). ¹³C NMR (125 MHz, CD₂Cl₂): spectrum is broad, 23.49, 24.10, 24.85, 27.72, 28.86, 72.38, 126.81, 127.86, 128.17, 129.86, 131.53, 146.22, 159.72. IR (KBr, cm⁻¹) 498.6, 557.1, 598.3, 768.5, 1050.1, 1162.6, 1248.1, 1449.2, 1491.5, 1574.2, 1596.6, 2870.2, 2965.9, 3066.8, 3422.8. FAB HRMS [M+(-BF₄)] *m/z*: found 361.2647; calcd (C₂₅H₃₃N₂) 361.2644.

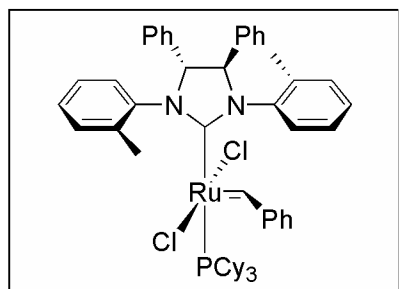


Compound **2.13**. (70%). mp 127-130°C. $[\alpha]_D^{22} +23.7$ ° (c 0.5, CH₂Cl₂). ¹H NMR (300 MHz, CDCl₃): δ 1.93 (s, 6H), 2.23 (s, 6H), 2.67 (s, 6H), 5.98 (s, 2H), 6.75 (s, 2H), 6.98 (s, 2H), 7.37 (m, 10H), 7.39, 8.65 (s, 1H). ¹³C NMR (125 MHz, CDCl₃): δ 18.3, 19.1, 21.1, 72.9, 128.5, 128.8, 129.4, 130.1, 130.7 (2), 131.5, 134.0, 136.1, 140.3, 158.2. FAB HRMS [M+ (-BF₄)] *m/z*: found 459.2812, calcd (C₃₃H₃₅N₂) 459.2800.

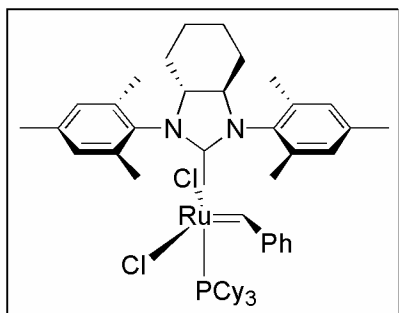


Compound **2.15**. (73%). mp 115-118 °C. $[\alpha]_D^{22} +27.8$ ° (c 0.5, CH₂Cl₂). ¹H NMR (300 MHz, CDCl₃): δ 1.18 (d, *J* = 6.6 Hz, 6H), 1.33 (d, *J* = 7.2 Hz, 6H), 3.13 (sept, *J* = 6.9 Hz, 2H), 5.79 (s, 2H), 7.2-7.5 (m, 16H), 7.58 (d, *J* = 8.1 Hz, 2H), 8.25 (s, 1H). ¹³C NMR (125 MHz, CDCl₃): δ 24.1, 24.7, 28.7, 77.1, 126.7, 127.7, 128.3, 128.5,

129.6, 130.3 (2), 130.7, 132.7, 144.4, 157.3. FAB HRMS $[M+(-BF_4)]$ m/z : found 459.2800, calcd ($C_{33}H_{35}N_2$) 459.2800.

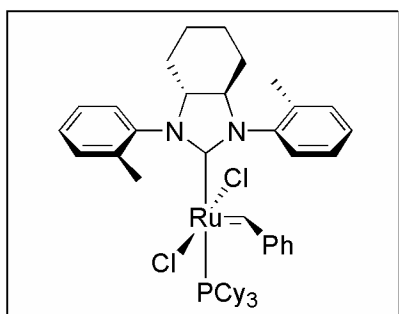


Representative preparation of complex 2.20. In a glove box, imidazolium salt **2.14** (0.200 g, 0.408 mmol) and potassium hexafluoro-*t*-butoxide (0.108 g, 0.490 mmol) were dissolved in tetrahydrofuran (4 mL), added to a solution of bis(tricyclohexylphosphine)-benzylidene ruthenium dichloride (0.403 g, 0.490 mmol) in toluene (10 mL), and transferred to a schlenk flask. The flask was removed from the glove box and heated to 80 °C under argon (closed) for 1-1.5 hours. The solution was cooled to ambient temperature and the volatiles were removed *in vacuo*. The product was purified by column chromatography (SiO_2 , 7:1 pentane:Et₂O) to yield a brown microcrystalline solid (0.300 g, 78%). mp 142-144 °C (dec.). $[\alpha]_D^{22} +6.0$ ° (c 0.005, CH₂Cl₂). ¹H NMR (500 MHz, CDCl₃) exists as a mixture of atropisomers (3.2:1): δ 0.9-2.9 (m, ArCH(CH₃)₂ + PCy₃), 5.01 (bs, NCHPh), 5.17 bs, NCHPh), 6.5-7.6 (m, ArH), 8.15 (bs, *o*-ArH of benzylidene), 19.41 (s, Ru=CHPh), 19.46 (s, Ru=CHPh). ¹³C NMR (125 MHz, C₆D₆): δ 221.0 (NCN), 297.3 (NCN Ru=CHPh). ³¹P NMR (121 MHz, C₆D₆): δ 26.96. IR (KBr, cm⁻¹) 3059, 3030, 2925 (s), 2849 (s), 1493 (s), 1446 (s), 1419 (s), 762, 743, 721, 710. ES HRMS $[M-Cl]^+$ m/z : found 909.3647, calcd ($C_{54}H_{65}ClN_2PRu$) 909.3647. Anal. Calcd for $C_{54}H_{65}Cl_2N_2PRu$: C, 68.63, H, 6.93, N, 2.96. Found C, 69.19, H, 7.01, N, 3.03.



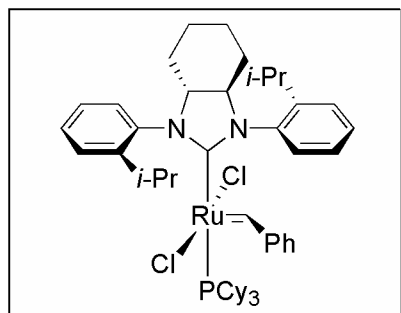
Complex **2.16**. (80%). $[\alpha]_D^{22} = +100.5^\circ$ ($c = 0.19$, CH_2Cl_2). $^1\text{H NMR}$ (500 MHz, CD_2Cl_2 (27:1)): δ 0.60-1.52 (br m, 34 H); 1.53 (d, $J = 1\text{ Hz}$, 6H); 1.62-1.80 (br m, 3H); 1.90 (s, 3H); 1.91-2.25 (br m, 4H); 2.30 (s, 3H); 2.33-2.78 (br m, 6H); 3.47-4 (br m, 2H); 5.77 (br s, 1H);

6.62-7.45 (br m, 7H); 8.97 (br s, 1H); 19.00 (s, 1H);. $^{13}\text{C NMR}$ (125 MHz, C_6D_6): δ 225.52 (br, NCN); 294.07, 294.35 (Ru=CHPh). $^{31}\text{P NMR}$ (121 MHz, CD_2Cl_2): δ 30.02. IR (KBr, cm^{-1}) 687.0, 848.2, 897.6, 1135.8, 1257.7, 1360.0, 1384.5, 1445.4, 1480.1, 2850.8, 2925.1, 3437.8. ES HRMS $[\text{M}-\text{Cl}]^+$ m/z : found 867.4092, calcd ($\text{C}_{50}\text{H}_{71}\text{ClN}_2\text{PRu}$) 867.4098.



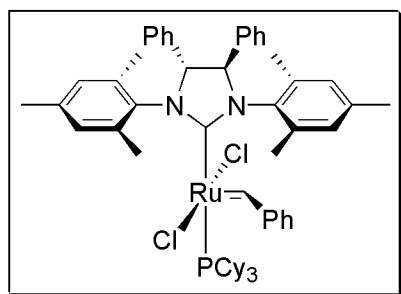
Complex **2.17**. (73%). $[\alpha]_D^{22} = -68^\circ$ ($c = 0.05$, CH_2Cl_2). $^1\text{H NMR}$ (500 MHz, CD_2Cl_2) exists as a mixture of atropisomers: δ 0.72-2.29 (br m, 45 H); 2.49-2.78 (br m, 2H); 3.35-4.05 (br m, 2H); 5.92-8.33 (br m, 13 H); 18.93-19.03 (br m, 1H). $^{13}\text{C NMR}$ (125 MHz, CD_2Cl_2):

δ 227.61 (d, $J = 73\text{ Hz}$, NCN); 296.40 (br s, Ru=CHPh). $^{31}\text{P NMR}$ (121 MHz, CD_2Cl_2): δ 25.60, 27.95, 28.83. IR (KBr, cm^{-1}) 678.5, 721.7, 1147.4, 1261.9, 1446.2, 1491.8, 1636.6, 2849.6, 2925.7, 3447.9. ES HRMS $[\text{M}-\text{Cl}]^+$ m/z : found 811.3456, calcd ($\text{C}_{46}\text{H}_{63}\text{ClN}_2\text{PRu}$) 811.3470.



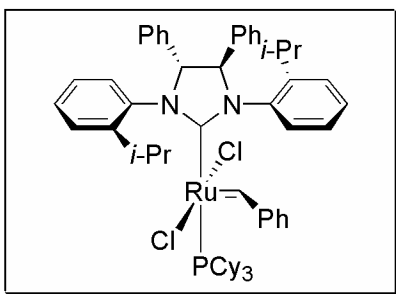
Complex **2.18**. (75%). $[\alpha]_D^{22} = -120^\circ$ ($c = 0.05$, CH_2Cl_2). ^1H NMR (500 MHz, CD_2Cl_2) exists as a mixture of atropisomers (4.9:1): δ 0.80-2.01 (br m, 53 H); 3.07-4.00 (br m, 4H); 6.04-8.48 (m, 13H); 19.04 (s, 0.83 H); 19.21 (s, 0.17 H). ^{13}C NMR (125 MHz,

CD_2Cl_2): δ 274.00 (d, $J = 78$ Hz, NCN); 298.51 (br s, Ru=CHPh). ^{31}P NMR (121 MHz, CD_2Cl_2): δ 23.85, 25.70, 29.65. IR (KBr, cm^{-1}) 678.1, 756.0, 848.6, 897.1, 1259.7, 1447.4, 1489.6, 1559.4, 1653.8, 2849.5, 2925.1, 3447.4. ES HRMS $[\text{M}-\text{Cl}]^+$ m/z : found 867.4080, calcd ($\text{C}_{50}\text{H}_{71}\text{ClN}_2\text{PRu}$) 867.4098.

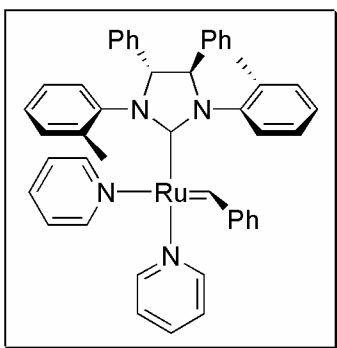


Complex **2.19**. (0.300 g, 78%). mp 140-142 $^\circ\text{C}$ (dec.). $[\alpha]_D^{22} -0.6^\circ$ ($c = 0.005$, CH_2Cl_2). ^1H NMR (500 MHz, CD_2Cl_2) exists as a mixture of atropisomers (1.1:1): δ 0.9-3.1 (broad multiplets, $\text{ArCH}(\text{CH}_3)_2 + \text{PCy}_3$), 5.5-7.5

(broad multiplets, ArH), 9.0 (broad singlet), 19.10 (s, Ru=CHPh), 19.25 (s, Ru=CHPh). ^{13}C NMR (125 MHz, C_6D_6): δ 223.7 (bs, NCN), 295.6 (Ru=CHPh), 296.6 (Ru=CHPh). ^{31}P NMR (121 MHz, C_6D_6): δ 29.16. IR (KBr, cm^{-1}) 2924 (s), 2850 (s), 1446 (s), 1401, 1378, 1237 (s), 736, 697. ES HRMS $[\text{M}-\text{Cl}]^+$ m/z : found 965.4232, calcd ($\text{C}_{58}\text{H}_{73}\text{ClN}_2\text{PRu}$) 965.4257. Anal. Calcd for $\text{C}_{58}\text{H}_{73}\text{Cl}_2\text{N}_2\text{PRu}$: C, 69.58, H, 7.35, N, 2.80. Found C, 69.79, H, 7.61, N, 2.59.



Complex **2.21**. (0.300 g, 78%). mp 150-155 °C (dec.). $[\alpha]_D^{22} +21.0^\circ$ (c 0.005, CH₂Cl₂). ¹H NMR (500 MHz, CD₂Cl₂) exists as a mixture of atropisomers (27:1): δ 0.9-1.9 (m, ArCH(CH₃)₂ + PCy₃), 3.53 (m, ArCH(CH₃)₂), 3.76 (m, ArCH(CH₃)₂), 4.92 (d, $J=4$ Hz, NCHPh), 5.23 (d, $J=4$ Hz, NCHPh), 6.6-7.6 (m, ArH), 8.59 (d, $J=7$ Hz), 19.25 (s, Ru=CHPh), 19.34 (s, Ru=CHPh). ¹³C NMR (125 MHz, C₆D₆): δ 220.2 (d, $J=75.6$ Hz, NCN), 298.2 (NCN Ru=CHPh). ³¹P NMR (121 MHz, CD₂Cl₂): δ 24.9. IR (KBr, cm⁻¹) 3060, 2926 (s), 2849 (s), 1489 (s), 1448 (s), 1417 (s), 758 (s), 702 (s). ES HRMS [M-Cl]⁺ m/z : found 965.4283, calcd (C₅₈H₇₃ClN₂PRu) 965.4257. Anal. Calcd for C₅₈H₇₃Cl₂N₂PRu: C, 69.58, H, 7.35, N, 2.80. Found C, 70.27, H, 7.64, N, 2.61.



Preparation of 2.23. Pyridine (0.20 mL) was added to a solution of **2.20** (0.050 g, 0.053 mmol) in toluene (0.5 mL). The solution was stirred at ambient temperature for 15 minutes during which time the color changed from red-brown to bright green. After ~ 30 minutes a green precipitate formed. Pentane was added to further precipitate the product. The mother liquor was decanted and the green solid was washed 3 times with pentane (2 mL) and dried *in vacuo* (0.040 g, 92%). $[\alpha]_D^{22} -45.0^\circ$ (c 0.005, CH₂Cl₂). ¹H NMR (300 MHz, CDCl₃) exists as a mixture of atropisomers (2.5:1): δ 1.73 (s, ArCH₃, 3H), 2.66 (s, ArCH₃, 3H), 2.78 (s, ArCH₃, 3H), 2.97 (s, ArCH₃, 3H), 5.29 (d, $J=4$ Hz, NCHPh, 1H), 2.40 (d, $J=7$ Hz, NCHPh, 1H), 5.53 (d, $J=4$ Hz, NCHPh, 1H), 5.74 (d, $J=7$ Hz, NCHPh,

1H), 6.2-8.6 (*ArH*, 31H), 9.81 (dd, $J=7.5, 1.5$, 2H), 9.97 (m, 2H), 19.33 (s, 1H), 19.35 (1H). ^{13}C NMR (125 MHz, C_6D_6): δ 219.5 (NCN), 220.5 (NCN), 317.3 (Ru=CHPh), 318.3 (Ru=CHPh). IR (KBr, cm^{-1}) 3136, 3107, 3060, 3028, 2934, 2876, 1492 (s), 1445 (s), 1378 (s), 1249 (s), 1220 (s), 756 (s), 706 (s). Anal. Calcd for $\text{C}_{46}\text{H}_{42}\text{Cl}_2\text{N}_4\text{Ru}$: C, 67.15, H, 5.14, N, 6.81. Found C, 67.24, H, 5.29, N, 6.80.

References and Notes

1. Trnka, T. M.; Grubbs, R. H. *Acc. Chem. Res.* **2001**, *34*, 18-29.
2. Furstner, A.; Thiel, O.; Ackermann, L.; Schanz, H.; Nolan, S. *J. Org. Chem.* **2000**, *65*, 2204-2207.
3. Ivin, K. J. *J. Mol. Catal. A: Chem.* **1998**, *133*, 1-16.
4. Randall, M. L.; Snapper, M. L. *J. Mol. Catal. A: Chem.* **1998**, *133*, 29-40.
5. Grubbs, R. H.; Chang, S. *Tetrahedron* **1998**, *54*, 4413-4450.
6. Hoveyda, A.; Schrock, R. *Chem. Eur. J.* **2001**, *7*, 945-950.
7. Alexander, J. B.; La, D. S.; Cefalo, D. R.; Hoveyda, A. H.; Schrock, R. R. *J. Am. Chem. Soc.* **1998**, *120*, 4041-4042.
8. La, D. S.; Alexander, J. B.; Cefalo, D. R.; Graf, D. D.; Hoveyda, A. H.; Schrock, R. R. *J. Am. Chem. Soc.* **1998**, *120*, 9720-9721.
9. Cefalo, D. R.; Kiely, A. F.; Wuchrer, M.; Jamieson, J. Y.; Schrock, R. R.; Hoveyda, A. H. *J. Am. Chem. Soc.* **2001**, *123*, 3139-3140.
10. Zhu, S. S.; Cefalo, D. R.; La, D. S.; Jamieson, J. Y.; Davis, W. M.; Hoveyda, A. H.; Schrock, R. R. *J. Am. Chem. Soc.* **1999**, *121*, 8251-8259.
11. Weatherhead, G. S.; Ford, J. G.; Alexanian, E. J.; Schrock, R. R.; Hoveyda, A. H. *J. Am. Chem. Soc.* **2000**, *122*, 1828-1829.
12. Rouhi, A. M. *Chem. Eng. News* **2002**, *80*, 29-33.
13. Scholl, M.; Ding, S.; Lee, C. W.; Grubbs, R. H. *Org. Lett.* **1999**, *1*, 953-956.
14. Scholl, M.; Trnka, T. M.; Morgan, J. P.; Grubbs, R. H. *Tetrahedron Lett.* **1999**, *40*, 2247-2250.

15. Huang, J.; Stevens, E.; Nolan, S.; Petersen, J. *J. Am. Chem. Soc.* **1999**, *121*, 2674-2678.
16. Jafarpour, L.; Nolan, S. *J. Organomet. Chem.* **2001**, *617*, 17-27.
17. Weskamp, T.; Kohl, F. J.; Gleich, D.; Herrmann, W. A. *Angew. Chem., Int. Ed.* **1999**, *38*, 2416-2419.
18. Bielawski, C. W.; Grubbs, R. H. *Angew. Chem., Int. Ed.* **2000**, *39*, 2903-2906.
19. Chatterjee, A.; Morgan, J.; Scholl, M.; Grubbs, R. *J. Am. Chem. Soc.* **2000**, *122*, 3783-3784.
20. Choi, T.; Chatterjee, A.; Grubbs, R. *Angew. Chem., Int. Ed.* **2001**, *40*, 1277.
21. Herrmann, W. A.; Kocher, C. *Angew. Chem., Int. Ed.* **1997**, *36*, 2163-2187.
22. Sanford, M.; Ulman, M.; Grubbs, R. *J. Am. Chem. Soc.* **2001**, *123*, 749-750.
23. See Chapter 3 of this thesis.
24. Wolfe, J.; Wagaw, S.; Marcoux, J.; Buchwald, S. *Acc. Chem. Res.* **1998**, *31*, 805-818.
25. Yang, B.; Buchwald, S. *J. Organomet. Chem.* **1999**, *576*, 125-146.
26. Saba, S.; Brescia, A.-M.; Kaloustain, M. K. *Tetrahedron Lett.* **1991**, *32*, 5031-5034.
27. Sanford, M.; Henling, L.; Day, M.; Grubbs, R. *Angew. Chem., Int. Ed.* **2000**, *39*, 3451.
28. Kingsbury, J. S.; Harrity, J. P. A.; Bonitatebus, P. J.; Hoveyda, A. H. *J. Am. Chem. Soc.* **1999**, *121*, 791-799.
29. Sanford, M. S.; Love, J. A.; Grubbs, R. H. *Organometallics* **2001**, *20*, 5314-5318.

**Chapter 3: Enantioselective Ruthenium-Catalyzed Ring-
Closing Metathesis**

Abstract

The enantioselective desymmetrization of a series of achiral trienes was effected using a variety of chiral ruthenium complexes. Trends for achieving higher enantioselectivity are described and correlate with increasing steric bulk on the organometallic complexes. The best reaction observed to date is the desymmetrization of triene **3.9** in 90% enantiomeric excess with complexes **3.6** or **3.13**; the addition of NaI is essential to achieving high enantioselectivity. A stereochemical model has been developed involving olefin-binding *cis* to the *N*-heterocyclic carbene ligand with rearrangement of one of the halide ligands *trans* to the *N*-heterocyclic carbene in the ring-closing event.

Introduction

As described in Chapter 2 of this thesis, we have prepared and characterized a series of ruthenium-based olefin metathesis catalysts **3.1-3.6** ligated with chiral *N*-heterocyclic carbene (NHC) ligands synthesized from chiral diamine starting materials (Figure 1). X-Ray crystallography and variable-temperature NMR spectroscopy have provided insight into the efficiency of the “gearing” of these chiral ligands, and it remains of interest to examine the possible correlation between these phenomena and the enantioselectivity of these catalysts.

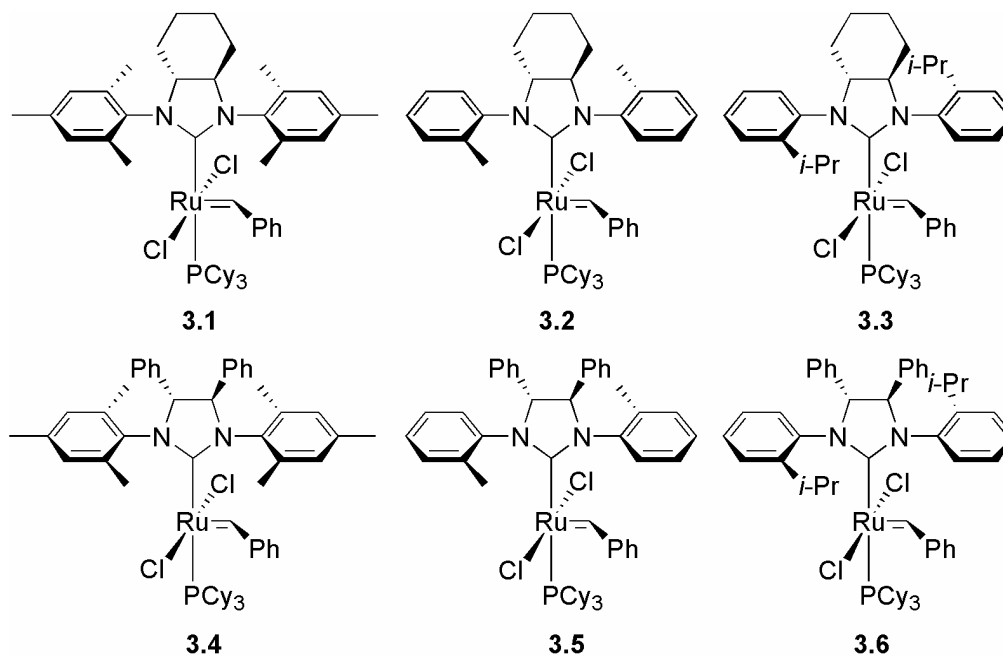
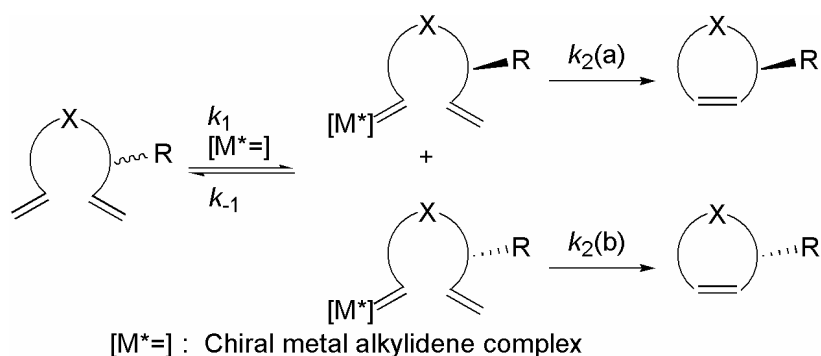


Figure 1. Chiral olefin metathesis catalysts.

Initially, we tested the ability of these catalysts to effect the kinetic resolution of chiral dienes via ring-closing metathesis. As described in Chapter 1, chiral molybdenum alkylidenes are highly selective catalysts for this class of reactions. The mechanism of the molybdenum-catalyzed kinetic resolution involves two discrete steps (Scheme 1):¹

First, the metal-alkylidene species “crosses onto” the substrate in a highly reversible metathesis step, establishing a rapidly exchanging equilibrium of diastereomeric intermediates. Second, a slower, rate-determining ring-closing metathesis step occurs in order to provide a cyclic product. The high selectivity of these reactions depends on both the rapid equilibrium of the first step and a large difference between $k_2(a)$ and $k_2(b)$.



Scheme 1. Presumed mechanism of kinetic resolution via enantioselective ring-closing metathesis.

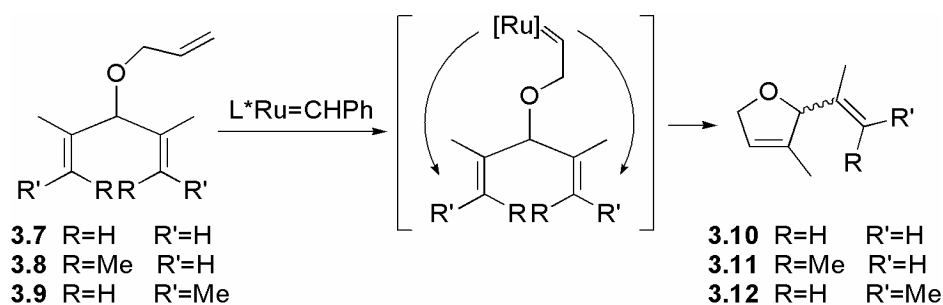
With the NHC-ruthenium systems, however, the product-forming second step is expected to be fast compared to the initial metathetical step between catalyst and substrate. In this case, even if the difference between $k_2(a)$ and $k_2(b)$ is large, an enantioselective reaction is not observed. In fact, consistent with the predicted outcome, catalysts **3.1-3.6** do not effect the kinetic resolution of chiral dienes efficiently.

Results

Asymmetric desymmetrization of achiral trienes

To overcome the limitations of kinetic resolution, we turn our attention to enantioselective desymmetrization, a reaction in which an achiral molecule is desymmetrized by a chiral catalyst in order to give enantioenriched product. Unlike kinetic resolution, these reactions do not require the establishment of a rapid equilibrium

prior to the productive ring-closing metathesis step. Furthermore, this type of reaction remains one of the most attractive types of reactions for olefin metathesis because of the theoretical possibility of achieving complete conversion of starting material to enantiopure product. By comparison, kinetic resolution offers a theoretical maximum of only 50 percent conversion to an enantiopure product. With catalysts **3.1-3.6** in hand, the enantioselective desymmetrization of substrates **3.7-3.9** to dihydrofurans **3.10-3.12** is effected.² Substrates **3.7-3.9** feature a monosubstituted central olefin with which the catalyst reacts in the initial metathesis reaction, and two di- or trisubstituted pendant olefins with which the stereochemically defining cyclization step occurs (Scheme 2).³

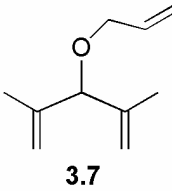
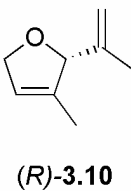
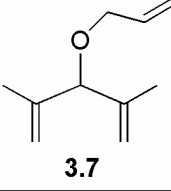
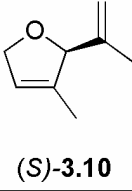


Scheme 2. Desymmetrization of achiral triene substrates **3.7-3.9**.

A preliminary series of reactions, the desymmetrization of substrate **3.7**, reveals three distinct trends in catalyst selectivity (Table 1). First, catalysts prepared from (1*R*,2*R*)-1,2-diaminocyclohexane (**3.1-3.3**) are effectively nonselective (<9% *ee*, entries 1-6) and do not improve in selectivity with NHC variation as is observed with catalysts prepared from (1*R*,2*R*)-diphenylethylenediamine (**3.4-3.6**) (up to 39% *ee*, entries 7-12). Interestingly, catalysts **3.1-3.3** favor formation of the opposite enantiomer as catalysts **3.4-3.6**, perhaps suggesting that the restricted conformation of the cyclohexyl backbone in the NHC ligand is causing the protons of the NHC five-membered ring to exert the

predominant steric influence in the catalytic reaction. Second, replacement of the mesityl groups (**3.4**, 15% *ee*, entry 7) with *o*-methyl- (**3.5**, 23% *ee*, entry 8) or *o*-isopropylaryl groups (**3.6**, 23% *ee*, entry 9) increases the enantioselectivity. Third, changing the halide ligands of catalyst **3.6** from Cl⁻ (23% *ee*, entry 9) to I⁻ (39% *ee*, entry 12) further improves the enantioselectivity. Importantly, although the enantioselectivity increases upon changing to iodide, a marked reduction in the conversion of **3.7** is observed, presumably due to the instability of the diiodoruthenium methylenide complex⁴ generated in the course of this reaction.

Table 1. Enantioselective desymmetrization of triene **3.7** by catalysts **3.1-3.6**.^a

entry	substrate	catalyst	product	ee(%) ^b	<i>k</i> _{rel}	convn(%) ^c
1	 3.7	3.1	 (<i>R</i>)- 3.10	8	1.2	93
2		3.2		3	1.1	>95
3		3.3		5	1.1	>95
4		3.1+Nal		5	1.1	20
5		3.2+Nal		5	1.1	46
6		3.3+Nal		5	1.1	42
7	 3.7	3.4	 (<i>S</i>)- 3.10	13	1.3	57
8		3.5		23	1.6	95
9		3.6		23	1.6	96
10		3.4+Nal		5	1.1	28
11		3.5+Nal		38	2.2	18
12		3.6+Nal		39	2.2	20

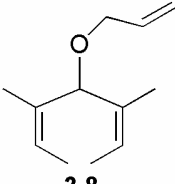
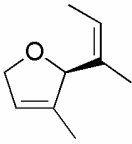
^a Conditions: 2.5 mol % of catalyst, 55 mM substrate in CH₂Cl₂, 38° C. When halide salt is added: 5 mol % of catalyst, 100 mol % of halide salt, 55 mM substrate in THF, 38° C.

^b Absolute stereochemistry determined by comparison with GLC chromatograms reported in ref 2. ^c Measured by chiral GLC (Chiraldex GTA Alltech) with toluene as an internal standard.

To prevent the generation of the methylenide complex and to further explore the substrate requirements for high enantioselectivity, trisubstituted substrates **3.8** and **3.9** are tested. In the case of the (*Z*)-trisubstituted olefin **3.8**, conversions improve markedly (Table 2). Also, the trends observed with substrate **3.7** still hold true. For example, the

mesityl substituted complex **3.4** exhibits very low enantioselectivity, even when the Cl⁻ ligands are replaced with I⁻ (<2% *ee*, entries 1 and 4). Furthermore, in the case of the *ortho*-monosubstituted catalysts **3.5** and **3.6**, the replacement of the Cl⁻ ligands with I⁻ results in a noteworthy improvement in enantioselectivity (from <2% *ee* to 17% *ee* with **3.5**, entries 2 and 5; from 12% *ee* to 35% *ee* with **3.6**, entries 3 and 6). From these data, a trend is emerging that correlates greater enantioselectivity with bulkier ligands on the catalyst: in the backbone of the NHC ligand, phenyl groups are superior to a bridging cyclohexyl; *o*-isopropylaryl-substituted catalysts performs as well or better than *o*-methylaryl-substituted catalysts; and the results with iodide ligands are superior to those with chloride ligands. Nonetheless, the highest enantiomeric excess observed in these data is still not practical.

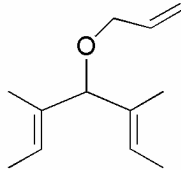
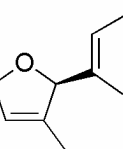
Table 2. Enantioselective desymmetrization of triene **3.8** by catalysts **3.4-3.6**.

entry	substrate	catalyst	product	ee(%)	<i>k</i> _{rel}	convn(%)
1	 3.8	3.4	 (S)-3.11	<2	1.0	65
2		3.5		<2	1.0	80
3		3.6		12	1.3	97
4		3.4+NaI		<2	1.0	43
5		3.5+NaI		17	1.4	78
6		3.6+NaI		35	2.1	90

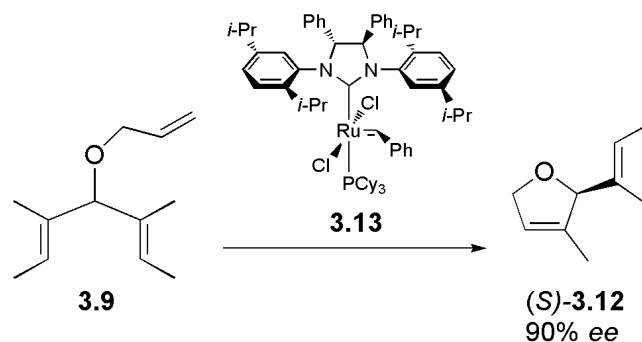
However, in the case of (*E*)-trisubstituted olefin **3.9**, high enantioselectivity and high conversion are achieved (90% *ee*, Table 3, entry 6). The results with this substrate again bear out the observed trends. The *o*-isopropylaryl-substituted catalyst **3.6** is in all comparable instances a superior catalyst to *o*-methylaryl-substituted catalyst **3.5** (entries 1-6). Also, varying the halide ligand from Cl⁻ to Br⁻ to I⁻ improves the enantioselectivity of the reaction. Specifically, complex **3.6** gives the highest enantiomeric excess with I⁻ ligands (90% *ee*, entry 6), the lowest enantiomeric excess with Cl⁻ ligands (35% *ee*, entry

2), and an intermediate enantiomeric excess with Br⁻ ligands (69% *ee*, entry 4). Significantly, neither solvent (THF, dichloromethane, benzene) nor temperature (-15 °C, 0 °C, 38 °C) has an effect on the enantioselectivity of these systems. Additionally, the activity and stability of catalysts **3.1-3.6** are similar to those of the regularly employed IMesH₂/ruthenium system (rigorous exclusion of air and moisture is not required).

Table 3. Enantioselective desymmetrization of triene **3.9** by catalysts **3.5** and **3.6**.

entry	substrate	catalyst	product	ee(%)	<i>k</i> _{rel}	convn(%)
1	 3.9	3.5	 (<i>S</i>)- 3.12	28	1.8	64
2		3.6		35	2.1	82
3		3.5+LiBr		63	4.4	90
4		3.6+LiBr		69	5.5	90
5		3.5+Nal		85	12.3	91
6		3.6+Nal		90	19.0	82

Interestingly, varying the *meta*-substituent of the aryl-side group of complex **3.6** from a proton to *i*-propyl to give complex **3.13**⁵ does not change the outcome of this reaction (Scheme 3).

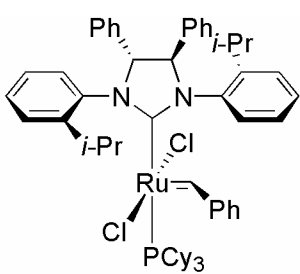


Scheme 3. Enantioselective desymmetrization of achiral triene **3.9** by catalyst **3.13**.

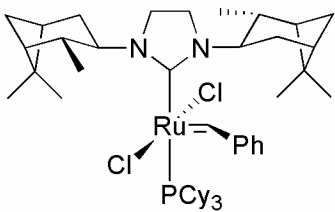
Although these reactions demonstrate that the described ligand design motif is viable for the development of enantioselective ruthenium-based olefin metathesis

catlaysts, the synthesis of catalysts like **3.1-3.6** utilizes costly materials and is tedious. By contrast, an attractive approach to catalyst development has been the synthesis of chiral NHCs from inexpensive and readily available chiral alkylamines. To this end, experiments were conducted to test the enantioselectivity of ruthenium-based olefin metathesis catalyst **3.14**^{6,7} ligated with 1,3-diisopinocampheol-4,5-dihydroimidazol-2-ylidene. The basic design of this catalyst differs from that of **3.1-3.6** in that the chirality of the ligand lies not in the backbone of the five-membered ring of the NHC, but instead lies in the side groups of the NHC. Interestingly, in the enantioselective ring-closing metathesis of achiral triene **3.9**, complex **3.14** (38% *ee*, Table 4, entry 2) appears potentially to be as enantioselective as complex **3.6** (35% *ee*, entry 1). However, upon treating **3.14** with NaI, the enantiomeric excess exhibited by the catalyst drops precipitously to 20% *ee* (entry 4), which compares unfavorably with the 90% *ee* (entry 3)

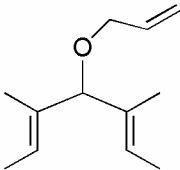
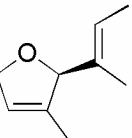
Table 4. Enantioselective desymmetrization of triene **3.9** by catalysts **3.6** and **3.14**.



3.6



3.14

entry	substrate	catalyst	product	ee(%)	<i>k</i> _{rel}	convn(%)
1	 <p>3.9</p>	3.6	 <p>(S)-3.12</p>	35	2.1	82
2		3.14		38	2.2	82
3		3.6+NaI		90	19.0	100
4		3.14+NaI		20	1.5	100

exhibited by catalyst **3.6**. It was observed in this reaction that catalyst **3.14** is extremely unstable as the diiodide species, and although conversion is high (100%), the catalyst is probably decomposing to achiral species that are active for olefin metathesis. In fact, catalyst **3.14** is itself so unstable that the isopinocampheol NHC ligand dissociates from the metal even when the compound is being stored as a solid. Based on these results, it is feasible that more stable complexes based on chiral alkylamines could merit further exploration as enantioselective olefin metathesis catalysts.

Discussion

Stereochemical model for molybdenum-catalyzed enantioselective olefin metathesis

With these enantioselective desymmetrization data in hand, it is important to devise a stereochemical model consistent with the observed results in order to understand our systems better and to provide future direction for catalyst development. Since we report the first enantioselective ruthenium-based olefin metathesis catalysts, the most closely related systems with which to compare our results are the molybdenum-based systems. With the first report of enantioselective olefin metathesis, Fujimura and Grubbs

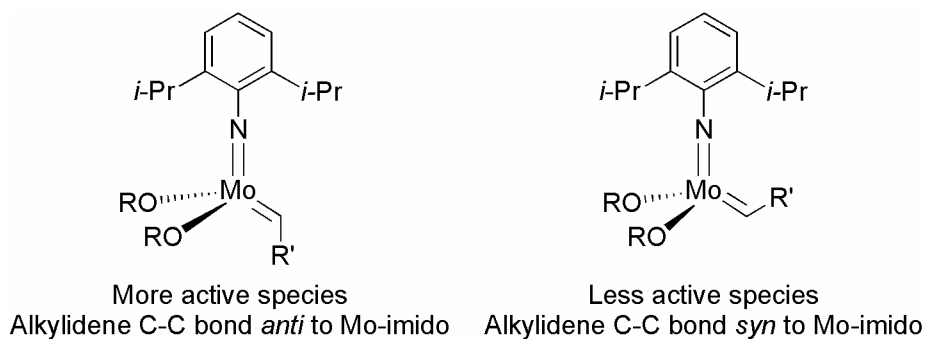


Figure 2. Relative activity of molybdenum-alkylidene isomers.

suggest a stereochemical model to explain the outcome of the kinetic resolution of a series of chiral dienes.¹ Since then, the Schrock and Hoveyda groups have described a modified version of this model and have shown it to be consistent with their results.^{8,9}

This model comprises three features that define the likely intermediate of the enantioselective olefin metathesis reaction. First, based on mechanistic and modelling studies, the molybdenum-alkylidene species possesses much higher reactivity when the carbon-carbon bond of its alkylidene moiety is oriented *anti* to its molybdenum-imido moiety (Figure 2).¹⁰ Second, the olefin is expected to complex *cis* to the imido ligand on the alkylidene face,^{11,12} which is not blocked by the chiral bisalkoxide ligand (Figure 3).

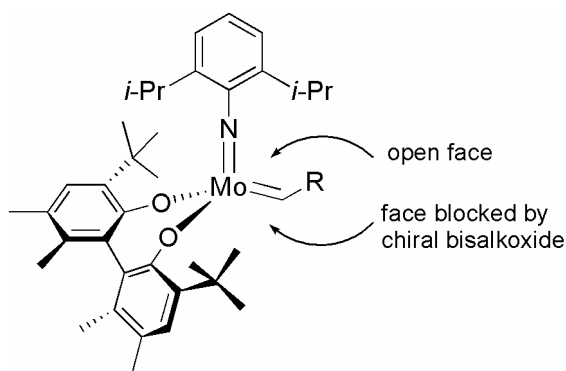


Figure 3. Effect of chiral bisalkoxide ligand.

Third, a substituent on the substrate is proposed to prefer a pseudo-equatorial orientation over a pseudo-axial orientation in the transition state during ring-closing. For example, in the kinetic resolution of substrate **3.16** through ring-closing metathesis with catalyst **3.15**, it is observed experimentally that (*S*)-**3.16** undergoes RCM with the catalyst than (*R*)-**3.16**.¹³ In this example, the siloxy substituent is expected to occupy a pseudoequatorial position in the case of the faster-reacting (*S*)-enantiomer (**3.15a**), and a pseudoaxial position in the case of the slower-reacting (*R*)-enantiomer (**3.15b**) (Figure 4).

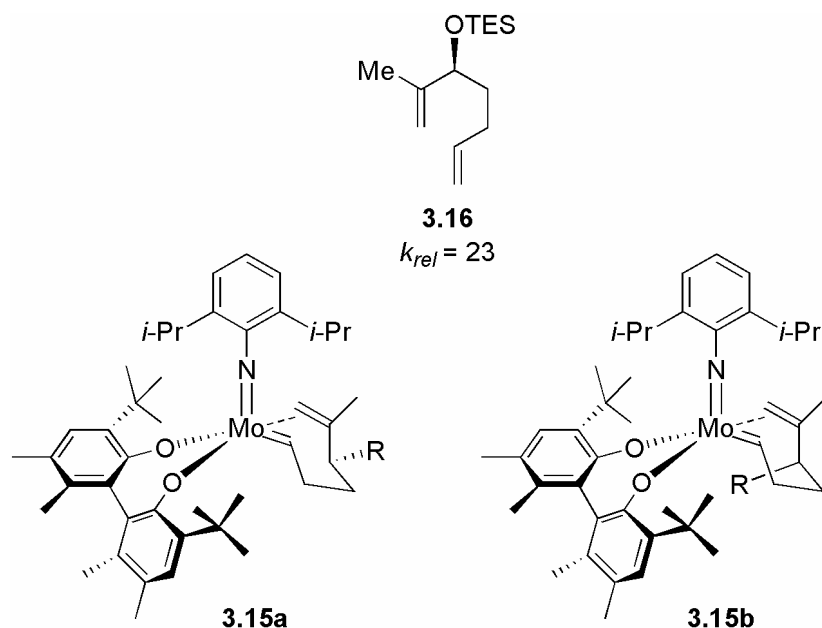
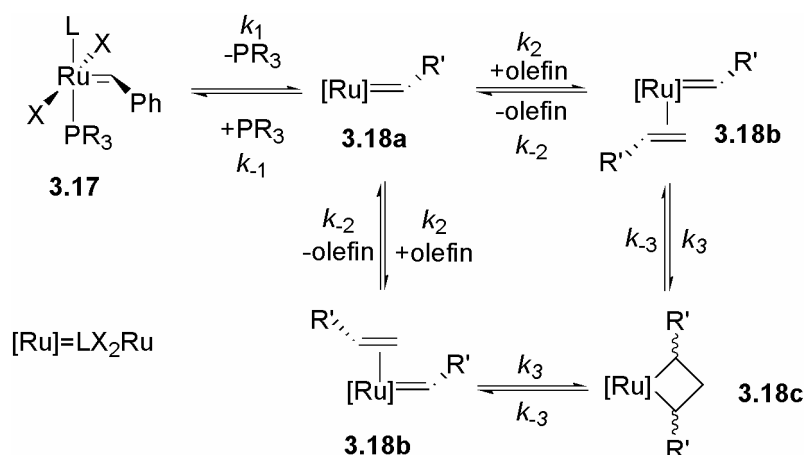


Figure 4. Molybdenum-catalyzed enantioselective metathesis stereochemical model.

Possible geometries of olefin-complex intermediates for ruthenium-based systems

The most current model^{14,15} for the mechanism of the olefin metathesis reactions catalyzed by complexes of the type $(L)(X)_2(PR_3)Ru=CHR'$ (**3.17**) involves as a first step the dissociation of the phosphine ligand in order to produce 14-e⁻ intermediate **3.18a** (Scheme 4). This intermediate is, in turn, expected to complex an olefin to afford the ruthenium-olefin adduct **3.18b**. Olefin adduct **3.18b** then undergoes carbon-carbon and carbon-ruthenium bond formation in order to produce metallacyclobutane species **3.18c** as either a transition state or a discrete intermediate. Bond cleavage in metallacyclobutane **3.18c** again produces an olefin adduct in the catalytic cycle. High metathesis activity is generally observed for complexes for which k_1 is large and k_{-1}/k_2 is relatively small (both of these values can be determined experimentally).



Scheme 4. Mechanism of ruthenium-catalyzed olefin metathesis.

Beyond showing that the NHC ligand does not dissociate from the metal during the course of the reaction, the current mechanistic understanding for ruthenium-based olefin metathesis is very limited in helping to design efficient enantioselective catalysts because very little is understood about the stereochemistry of the involved intermediates. In the literature, three different conformations of the intermediate olefin complex have been proposed (Figure 5): **A**, in which one halide ligand is bound trans to the L-type

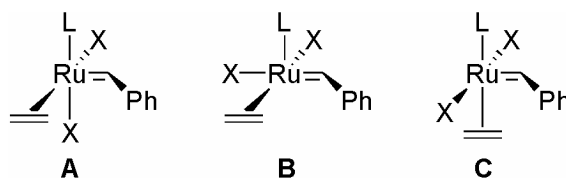


Figure 5. Possible geometries of olefin-complex intermediate.

ligand and the olefin binds cis to the L-type ligand; **B**, in which the halide ligands adopt a cis arrangement to the L-type ligand in the alkylidene-halide-olefin plane and the olefin binds cis to the L-type ligand; and **C**, in which the olefin binds trans to the L-type ligand.

Intermediate olefin-complex conformation **A** has been suggested in the literature recently based on both physical and computational studies. The trans/cis isomerization of chlorides on a related ruthenium complex has been observed.¹⁶ Furthermore, the Chen group has performed density functional calculations on $\text{Cl}_2(\text{PH}_3)\text{Ru}(-\text{CH}_2\text{CH}_2\text{CH}_2-)$, an

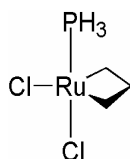
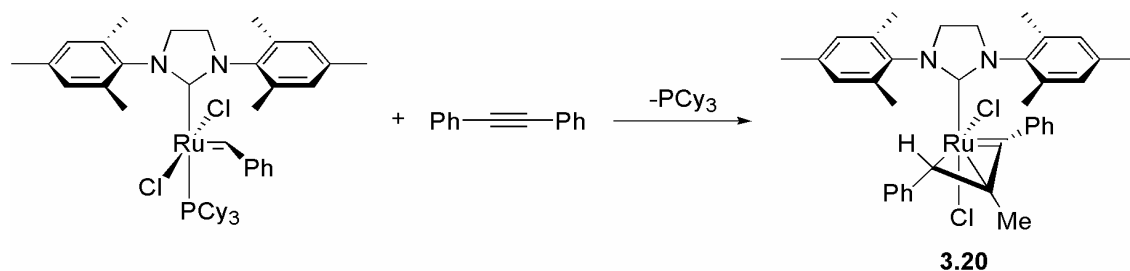


Figure 6. Lowest-energy metallacyclobutane according to computation.

analogue to the proposed metallacyclobutane transition state for the olefin metathesis catalytic cycle.¹⁷ Full geometric optimization suggests that the lowest-energy conformation for this transition state contains a Cl^- ligand trans to the L-type donor, PH_3 (Figure 6). Finally, intermediate olefin complex **A** is suggested by the isolation and crystallographic characterization of complex **3.20** (Scheme 5).¹⁸ However, as with any isolable complex, it is speculative to compare this complex to the intermediate complex in question; in fact, complex **3.20** exhibits poor metathesis activity.



Scheme 5. Reaction of IMesH_2 /ruthenium system with diphenylacetylene.

Intermediate complex **B** has been suggested in a computational study that reports that trans to cis chloride rearrangement is facile at room temperature and that the olefin complexes to ruthenium cis to the L-type donor ligand.¹⁹ In an initial study of the mechanism of ruthenium-catalyzed olefin metathesis, Dias *et al.* favored intermediate olefin complex **B** based on arguments of microreversibility.²⁰ Furthermore, the authors supported the plausibility of olefin-complex intermediate **B** based on olefin complexes of $(\text{PCy}_3)_2\text{Cl}_2\text{Ru}(\text{CO})$ (**3.21** and **3.22**, Figure 7).²¹ The carbon monoxide ligand in **3.21** and **3.22** is expected to engage in substantial π -bonding and to interact with the same

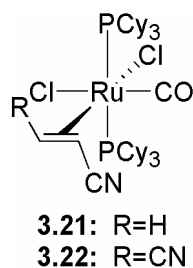
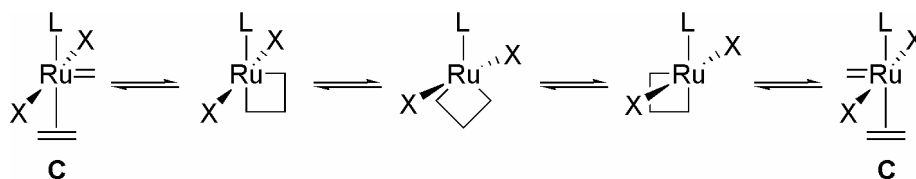


Figure 7. Olefin complexes of ruthenium.

ruthenium orbitals as the alkylidene ligand, thus serving as a reasonable analogue of **B**. The stereochemistry of **3.21** and **3.22** has been determined by ^{31}P NMR spectroscopy, and a crystal structure has been obtained for a closely analogous compound.²² Of course, compounds **3.21** and **3.22** each contain one more L-type ligand than intermediate **B**, and any inference drawn from the model compounds is speculative.

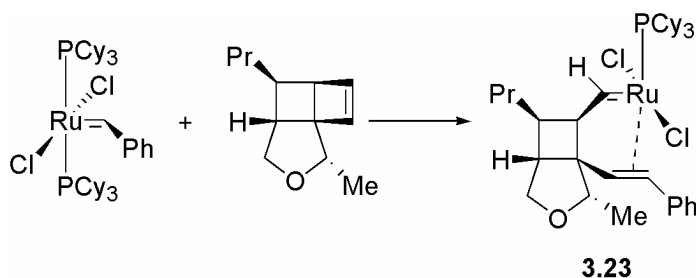
Intermediate complex **C**, in which olefin binds trans to the L-type ligand, has also been suggested as a low-energy intermediate in computational studies by the Chen group.¹⁷ Although intermediate **C** was mostly discounted by Dias *et al.* based on arguments of microreversibility, a plausible mechanism has been proposed in which the

metallacyclobutane moiety rotates relative to the L-type and chloride ligands in order to maintain a symmetric reaction profile for a degenerate metathesis reaction (Scheme 6).



Scheme 6. Reaction mechanism featuring “swinging” metallacyclobutane moiety.

Physical evidence for intermediate **C** arises from complex **3.23**, the only ruthenium-alkylidene olefin complex reported in the literature (Scheme 7).²³ With the olefin moiety appended to the ruthenium metal center trans to the L-type ligand, complex **3.23** is readily compared to intermediate **C**. Although complex **3.23** is slow to initiate, it exhibits reasonable activity in metathesis reactions.



Scheme 7. Synthesis of ruthenium-olefin complex **3.23**.

Stereochemical model for ruthenium-catalyzed enantioselective olefin metathesis

In light of the three distinct olefin-complex intermediate geometries reported in the literature, it is of considerable interest for us to compare these geometries to the stereochemical outcome of the enantioselective desymmetrization reactions and to devise

a stereochemical model that is consistent with our data. Of the three conformations of the intermediate olefin complex that have been proposed, only **C** is inconsistent with the observed stereochemical outcome of the desymmetrization of substrates **3.7-3.9**; and although geometry **B** cannot be discounted, geometry **A** appears to be most consistent with the observed ligand effects and stereochemical outcome of these reactions.

The stereochemical model for our favored geometry, olefin-complex **A**, is very similar to the model proposed by the Schrock and Hoveyda groups for molybdenum alkylidene species (see above). Three key features of this model are consistent with the observed selectivity. First, the alkylidene substituent is oriented *anti* to the bulky NHC ligand (Figure 8). Second, the tethered olefin binds to the front face of the complex to

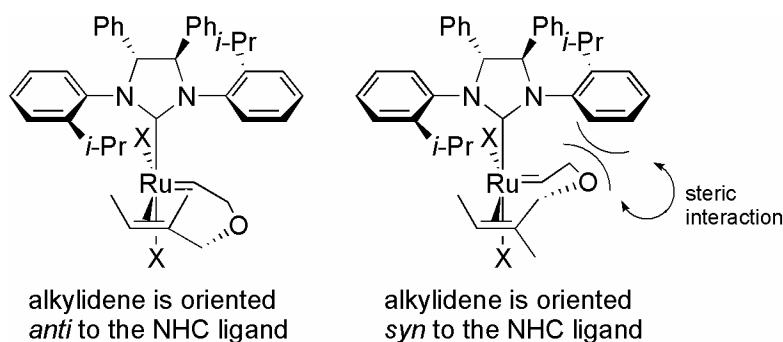


Figure 8. Steric interaction between alkylidene and NHC ligands.

avoid a steric interaction with the bulky *o*-isopropyl groups of the NHC ligand. Third, a steric interaction favors the olefin complex in which the unbound olefin (R in Figure 9) occupies the distal position relative to the apical halide; the energetic favorability of this geometry is reinforced by the pseudo-equatorial nature of this orientation. The proposed steric interaction between the unbound olefin and apical halide is consistent with the

dramatic increase in enantioselectivity observed upon changing the halide from Cl^- to Br^- to I^- .

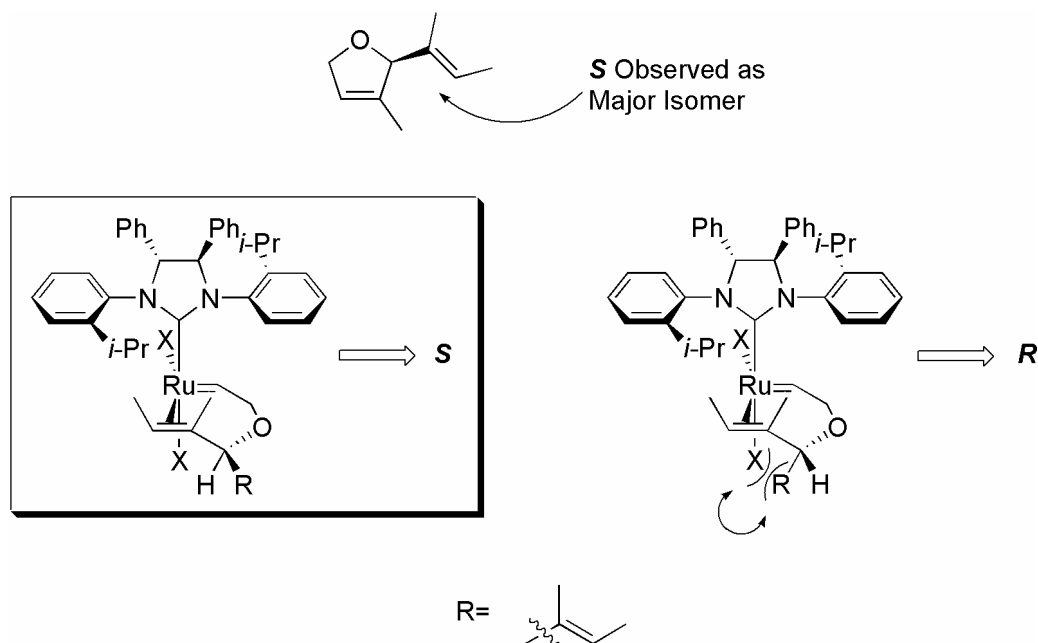


Figure 9. Stereochemical model **A**.

The stereochemical model based on olefin-complex geometry **B** is very similar to the model based on geometry **A**. The first two features of the model are exactly the same: the allylidene substituent is oriented *anti* to the bulky NHC ligand, and the tethered olefin binds to the front face of the complex to avoid a steric interaction with the chiral NHC ligand. For the third feature of the model, however, the energetic favorability of the geometry occupied by the unbound olefin depends entirely on the pseudoequatorial nature of this orientation (Figure 10). Furthermore, the dramatic increase in enantioselectivity observed upon changing the halide from Cl^- to Br^- to I^- is attributed entirely to a change in the electronics of the complex. Perhaps when ligated with iodide

ligands, the chiral catalyst is slower to form a metallacyclobutane with the olefin and conclude the catalytic cycle, thus allowing the system a greater chance to reach equilibrium in the enantiodetermining formation of olefin complex.

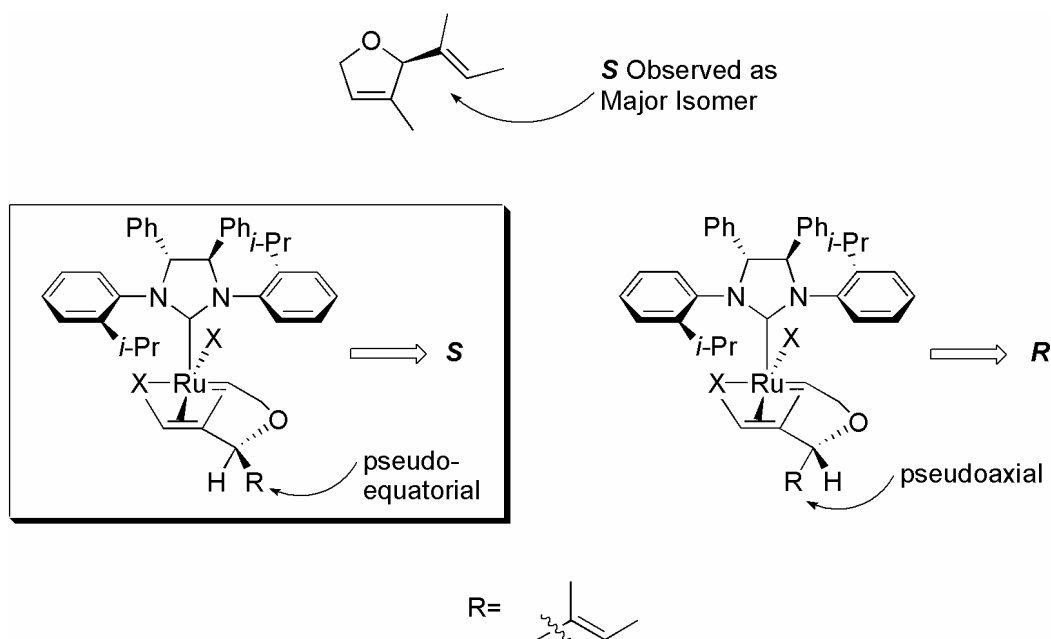


Figure 10. Stereochemical model **B**.

Finally, a stereochemical model based on olefin-complex geometry **C** is inconsistent with the observed results from the enantioselective desymmetrization of achiral trienes **3.7-3.9**. Even upon cursory consideration, this model seems doubtful because, in binding trans to the NHC ligand, the substrate is quite far removed from the metal center, making the achievement of high enantiomeric excesses unlikely. Furthermore, with closer consideration, the most plausible stereochemical model based upon olefin-complex geometry **C** is inconsistent with the observed data. This model has two main features: First, the alkylidene moiety is oriented in such a manner as to minimize steric interaction with the *o*-isopropyl groups of the chiral NHC ligand.

Second, the unbound olefin (R in Figure 11) is expected to be oriented in a pseudoequatorial position, away from a possible steric interaction with the complex's halide ligand. Only with placement of the unbound olefin into an unfavorable pseudoaxial conformation with proximity to the bulky halide ligand could the observed outcome (the *S* enantiomer) be achieved (Figure 11).

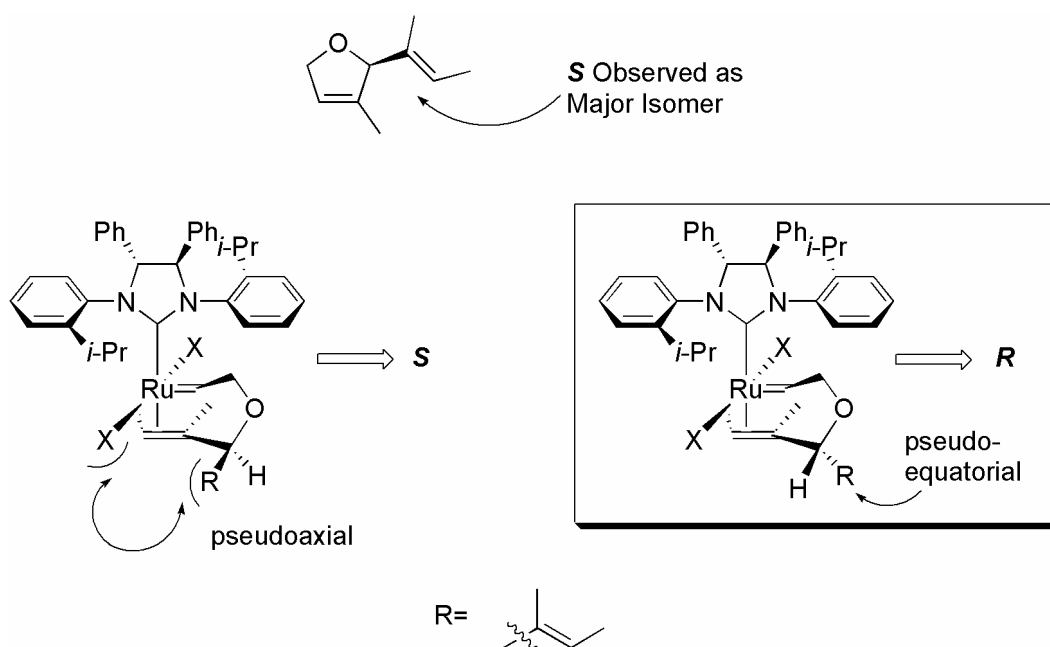


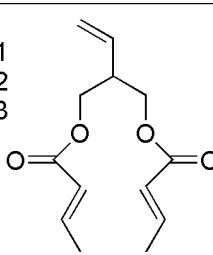
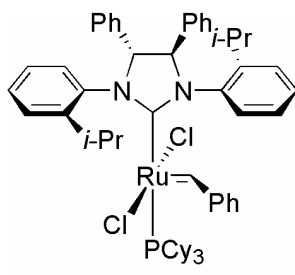
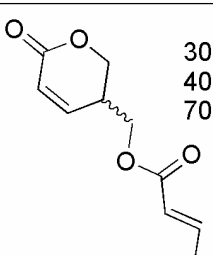
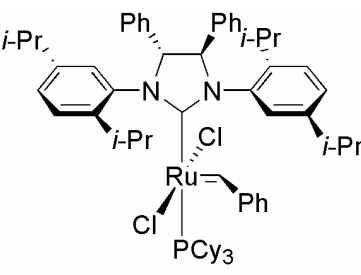
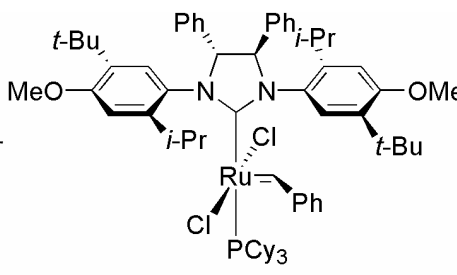
Figure 11. Stereochemical model C.

Ring-closing substrates inaccessible for molybdenum catalysts

An important motivation for the development of enantioselective ruthenium-based olefin metathesis catalysts has been the anticipated functional-group compatibility and activity exhibited by these late-metal complexes. Ruthenium-based catalysts of the described motif (**3.6**, **3.13**, and **3.24**) have been employed in the ring-closing of bisacrylate **3.25**, a substrate inaccessible to the molybdenum-alkylidene species (Table 5).²⁴ Although the enantioselective desymmetrization of **3.25** proceeds with only modest

selectivity when effected by catalyst **3.6** (30% *ee*, entry 1), the selectivity improves remarkably with larger substitution in the *meta*-position on the aryl groups of the NHC ligand. With *meta*-isopropyl substitution in complex **3.13**, the enantiomeric excess of product **3.26** increases to 40% (entry 2, $k_{\text{rel}} = 2.3$), and *meta*-*t*-butyl substitution in complex **3.24** further increases the enantiomeric excess to 70% (entry 3, $k_{\text{rel}} = 5.7$). Although the exact role played by the *meta*-substituent in these reactions is unknown, these results are important in demonstrating that this class of chiral metathesis catalysts is able to effect new reactions inaccessible to molybdenum systems.

Table 5. Enantioselective desymmetrization of achiral triene **3.25**.

entry	substrate	catalyst	product	ee(%)	k_{rel}	convn(%)
1	 3.25	 3.6	 3.26	30	1.9	~20
2		 3.13		40	2.3	~20
3		 3.24		70	5.7	~20

Experimental Section

General procedures

When specified, manipulation of organometallic compounds was performed using standard Schlenk techniques under an atmosphere of dry argon or in a nitrogen-filled Vacuum Atmospheres drybox ($O_2 < 2$ ppm). Argon was purified by passage through columns of BASF R3-11 catalyst (Chemalog) and 4Å molecular sieves (Linde). Chiral GC assays were effected using a Chiraldex-GTA column from Alltech.

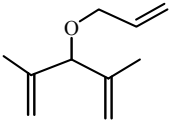
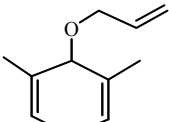
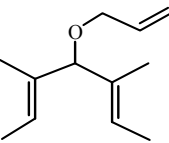
Materials and methods

Dichloromethane, tetrahydrofuran, and benzene were dried by passage through solvent purification columns.

Representative procedure for the enantioselective desymmetrization of achiral trienes

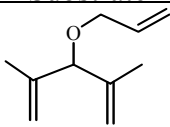
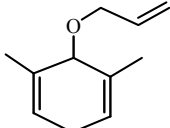
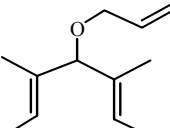
In a 10 mL schlenk flask on the bench top, tetrahydrofuran (2.0 mL) was added to catalyst **3.6** (0.0050 g, 0.0050 mmol). Sodium iodide (0.015 g, 0.100 mmol) was added and the solution was stirred at ambient temperature for 1 hour. All of the salts were observed to dissolve and the color turned from reddish-brown to brown. Substrate **3.8** (0.020 g, 0.11 mmol) and toluene (10 μ L internal standard) were added via syringe and the solution was heated at 35 °C for 2 hours after which time the solution darkened considerably. An aliquot was collected and analyzed by chiral GC for enantiomeric excess and conversion.

Desymmetrization of achiral trienes 3.8-3.10 by catalysts 3.1-3.3

Substrate	Catalyst	Additive	ee % ^a	Conversion %
 3.8	3.1	none	8	93
	3.2	none	3	>95
	3.3	none	5	>95
	3.1	NaI	5	20
	3.2	NaI	5	46
	3.3	NaI	5	42
 3.9	3.1	none	4	>95
	3.2	none	5	44
	3.3	none	6	94
	3.1	NaI	1	>95
	3.2	NaI	5	>95
	3.3	NaI	10	>95
 3.10	3.1	none	9	>95
	3.2	none	0	>95
	3.3	none	11	>95
	3.1	NaI	13	20
	3.2	NaI	13	>95
	3.3	NaI	3	>95

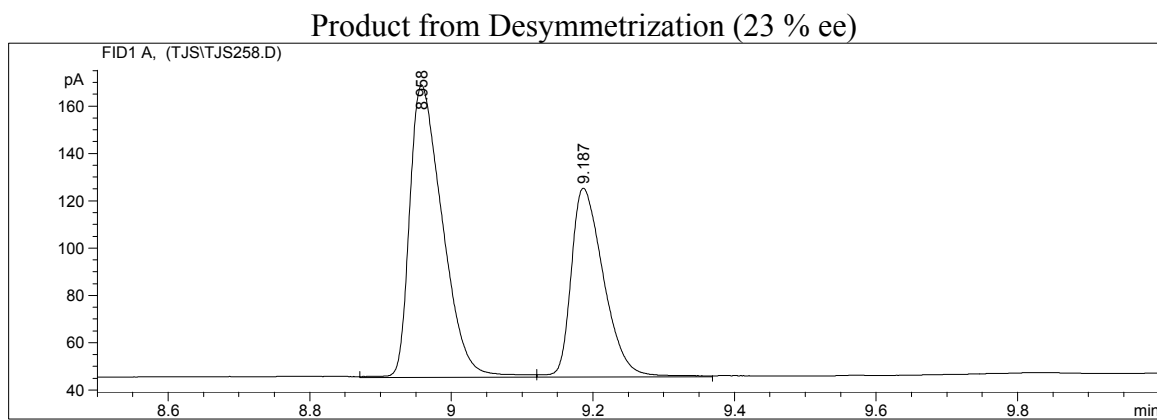
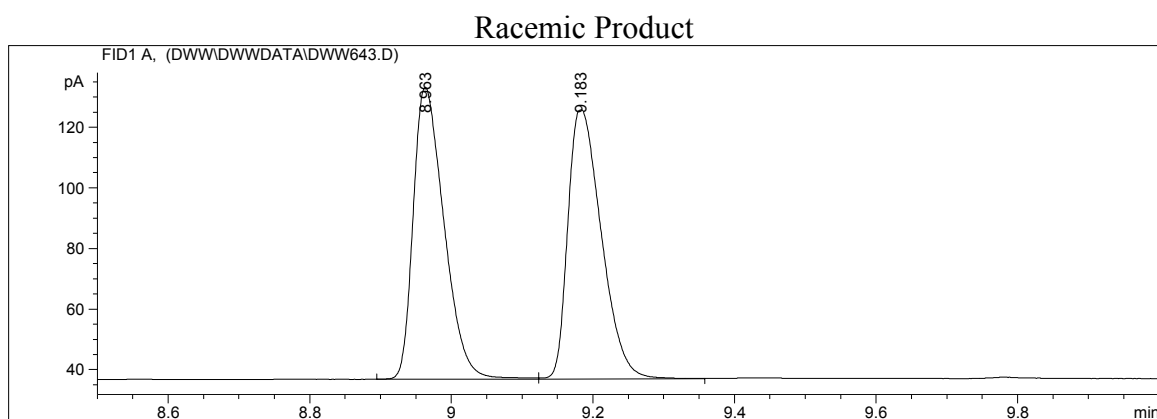
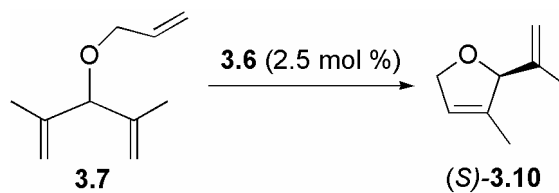
^aThe **R** enantiomer is the major product in all entries exhibiting significant enantiomeric excesses.

Desymmetrization of achiral trienes **3.8-3.10** by catalyst **3.4-3.6**

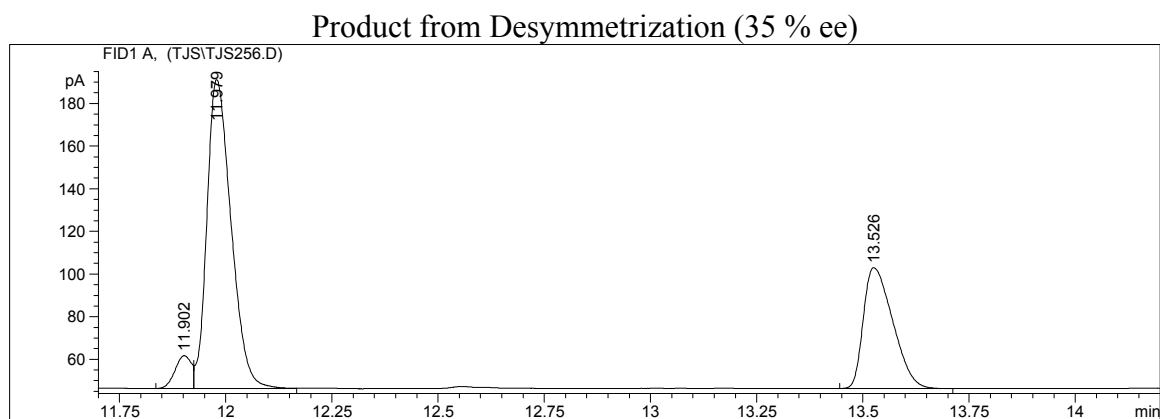
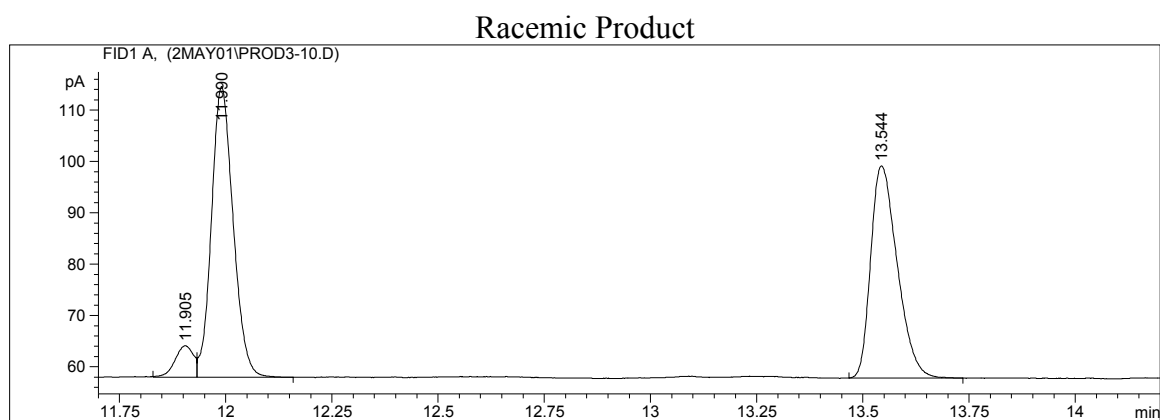
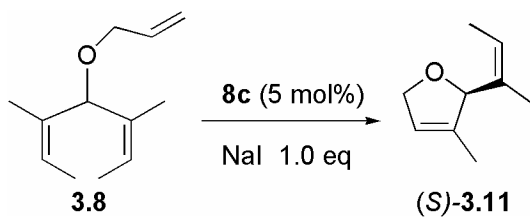
Substrate	Catalyst	Additive	ee % ^a	Conversion %
 3.8	3.4	none	13	57
	3.5	none	23	95
	3.6	none	23	96
	3.4	NaI	5	28
	3.5	NaI	38	18
	3.6	NaI	39	20
 3.9	3.4	none	<2	65
	3.5	none	<2	80
	3.6	none	12	97
	3.4	NaI	<2	43
	3.5	NaI	17	78
	3.6	NaI	35	90
 3.10	3.4	none	15	67
	3.5	none	28	64
	3.6	none	35	82
	3.4	NaI	17	39
	3.5	LiBr	63	90
	3.5	NaI	85	91
	3.6	LiBr	69	90
	3.6	NaI	90	82

^a The **S** enantiomer is the major product in all entries exhibiting significant enantiomeric excesses.

Enantioselective desymmetrization product **3.10** assay by chiral GC

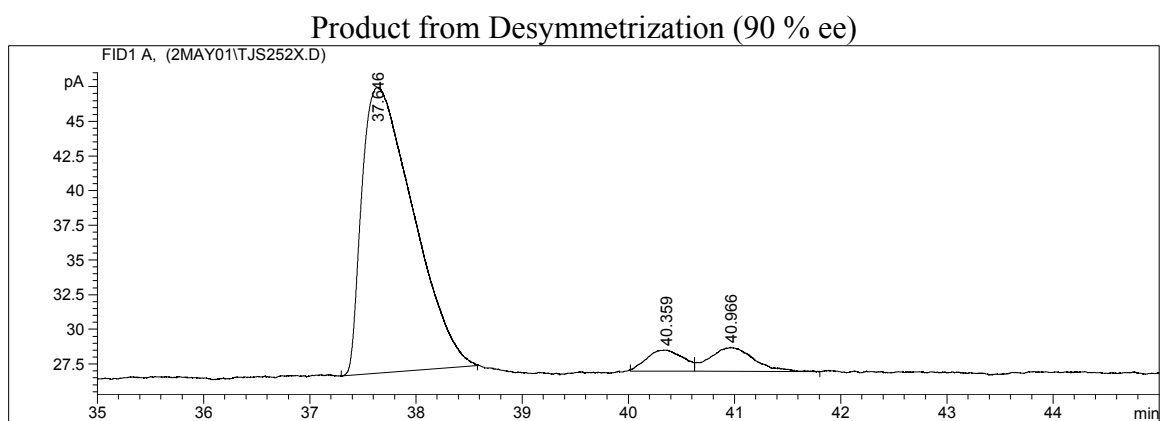
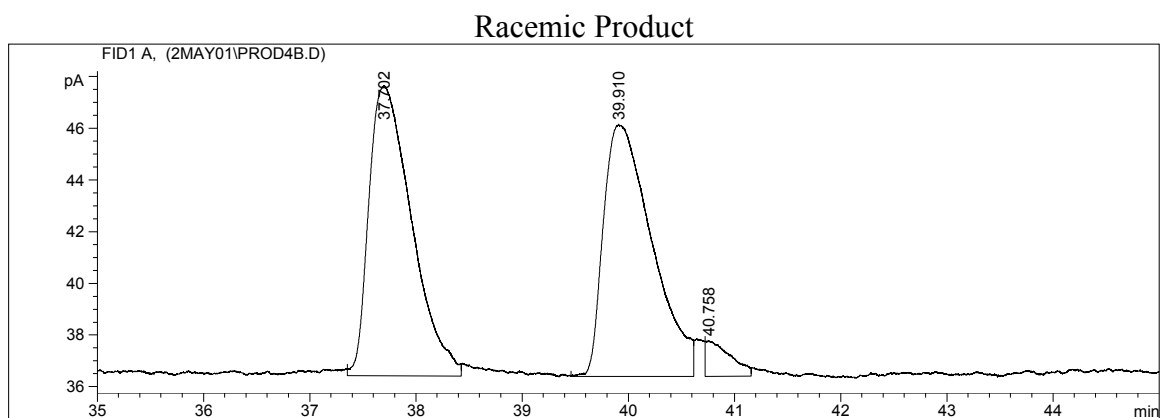
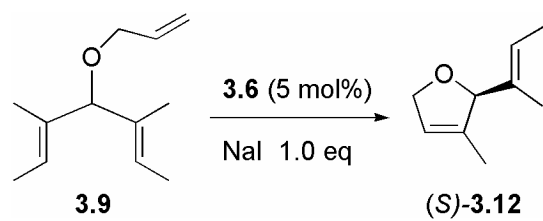


Conditions: 50 to 100 °C, 5 °C/min, 1mL/min flow rate, Chiraldex-GTA column from Alltech.

Enantioselective desymmetrization product 3.11 assay by chiral GC

Conditions: 45 to 110 °C, 2 °C/min, 1mL/min flow rate, Chiraldex-GTA column from Alltech.

Enantioselective desymmetrization product 3.12 assay by chiral GC



Conditions: 60 °C, 1mL/min flow rate, Chiraldex-GTA column from Alltech.

References and Notes

1. Fujimura, O.; Grubbs, R. H. *J. Am. Chem. Soc.* **1996**, *118*, 2499-2500.
2. La, D. S.; Alexander, J. B.; Cefalo, D. R.; Graf, D. D.; Hoveyda, A. H.; Schrock, R. R. *J. Am. Chem. Soc.* **1998**, *120*, 9720-9721.
3. Ulman, M.; Grubbs, R. H. *Organometallics* **1998**, *17*, 2484-2489.
4. Ulman, M.; Grubbs, R. H. *J. Org. Chem.* **1999**, *64*, 7202-7207.
5. This complex was provided by Steve Goldberg, who has employed it in enantioselective cross metathesis.
6. Trnka, T. M. Thesis. California Institute of Technology: Pasadena, 2002.
7. Complex 3.14 prepared by Tina Trnka.
8. Hoveyda, A. H.; Schrock, R. R. *Chem. Eur. J.* **2001**, *7*, 945-950.
9. Weatherhead, G. S.; Houser, J. H.; Ford, J. G.; Jamieson, J. Y.; Schrock, R. R.; Hoveyda, A. H. *Tetrahedron Lett.* **2000**, *41*, 9553-9559.
10. Fox, H. H.; Schofield, M. H.; Schrock, R. R. *Organometallics* **1994**, *13*, 2804-2815.
11. Schrock, R. R. *Polyhedron* **1995**, *14*, 3177-3195.
12. Wu, Y. D.; Peng, Z. H. *J. Am. Chem. Soc.* **1997**, *119*, 8043-8049.
13. Alexander, J. B.; La, D. S.; Cefalo, D. R.; Hoveyda, A. H.; Schrock, R. R. *J. Am. Chem. Soc.* **1998**, *120*, 4041-4042.
14. Sanford, M.; Ulman, M.; Grubbs, R. *J. Am. Chem. Soc.* **2001**, *123*, 749-750.
15. Sanford, M. S.; Love, J. A.; Grubbs, R. H. *J. Am. Chem. Soc.* **2001**, *123*, 6543-6554.
16. Bianchini, C.; Lee, H. M. *Organometallics* **2000**, *19*, 1833-1840.
17. Adlhart, C.; Hinderling, C.; Baumann, H.; Chen, P. *J. Am. Chem. Soc.* **2000**, *122*, 8204-8214.

18. Trnka, T. M.; Day, M. W.; Grubbs, R. H. *Organometallics* **2001**, *20*, 3845-3847.
19. Aagaard, O. M.; Meier, R. J.; Buda, F. *J. Am. Chem. Soc.* **1998**, *120*, 7174-7182.
20. Dias, E. L.; Nguyen, S. T.; Grubbs, R. H. *J. Am. Chem. Soc.* **1997**, *119*, 3887-3897.
21. Moers, F. G.; Langhout, L. P. *J. Inor. Nucl. Chem.* **1977**, *39*, 591-593.
22. Brown, L. D.; Barnard, C. F. J.; Daniels, J. A.; Mawby, R. J.; Ibers, J. A. *Inorg. Chem.* **1978**, *17*, 2932-2935.
23. Tallarico, J. A.; Bonitatebus, P. J.; Snapper, M. L. *J. Am. Chem. Soc.* **1997**, *119*, 7157.
24. Complex 3.24 synthesized by Jacob Berlin. Reaction results provided by Steve Goldberg.

**Chapter 4: Testing the Inherent Stereoselectivity of
Ruthenium-Based Olefin Metathesis Catalysts**

Abstract

In order to determine the inherent cis/trans selectivity of ruthenium-based olefin metathesis catalysts, complexes are utilized in a single-turnover reaction with dihydrofuran and analyzed by NMR spectroscopy. The complexes tested exhibit E:Z selectivities ranging from 2:1 to greater than 19:1, and the results of these reactions correlate to observations in the formation of macrocycles through ring-closing metathesis. Several trends in the data are discussed, and a stereochemical model consistent with the observed stereochemical outcomes of these reactions is described.

Introduction

A major goal in the development of useful olefin metathesis catalysts centers around the ability to control the cis/trans isomerism of olefinic products. As the equilibrium ratio of these isomers is generally impure (trans:cis \sim 4:1 to 9:1), catalysts that provide either pure trans or pure cis formation are desired.¹ Given the thermodynamic preference for trans olefin, the synthesis of pure cis product is anticipated to be particularly difficult. The development of a *cis*-selective catalytic route, however, remains particularly attractive due to an abundance of cis olefins in natural products (Figure 1). For instance, the stereoselective synthesis of the cis olefins contained in the

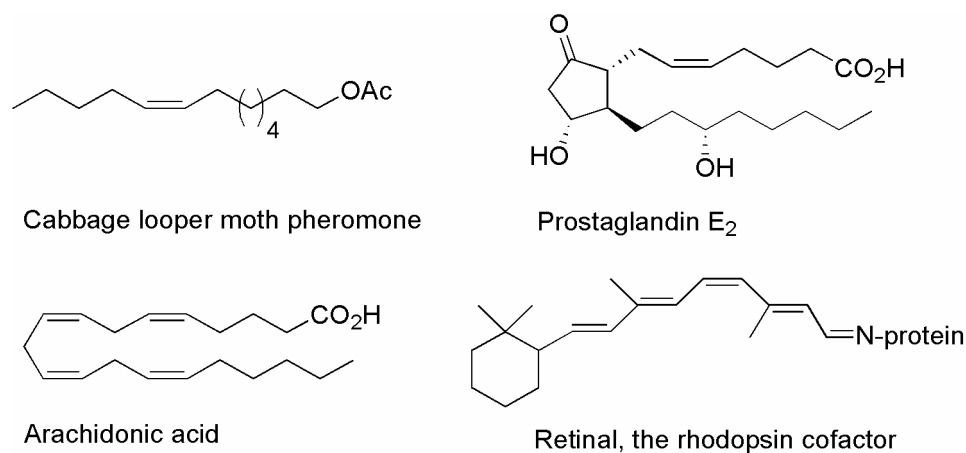


Figure 1. Cis double bonds in natural products.

majority of insect pheromones derived from C12 through C23 fatty acids is often critical since the trans isomer may inhibit the activity of its cis counterpart.^{2,3} Many biological processes involve the isomerization of a particular olefin from cis to trans, and investigation of these processes depends on the development of methods for cis olefin synthesis.^{4,5} Furthermore, cis olefins are present in a large number of bioactive molecules, including the prostaglandins.⁶⁻⁹

The occurrences of *cis* selectivity reported in the synthesis of small molecules via olefin metathesis are few. Early, ill-defined systems composed of tungsten or molybdenum salts and organotin/organoaluminums are capable of facilitating ROMP to give high *cis* polymer.^{10,11} Well-defined systems that display some measure of *cis*-selectivity (Figure 2) include the cyclometallated aryloxy alkylidene tungsten (VI) catalyst (**4.1**)¹² and *cis*-dialkyl-Cp*-diene tantalum complex (**4.2-4.3**).¹³ These catalysts effect the ring-opening metathesis polymerization (ROMP) of norbornene resulting in polymers with greater than 98% *cis* linkages. Additionally, the tungsten catalyst has demonstrated high *cis*-selectivity in cross metathesis, albeit at low conversions. However, these systems are highly sensitive to water and maintain a low compatibility with functional groups, making the development of user-friendly, *cis*-selective catalysts a worthwhile goal.

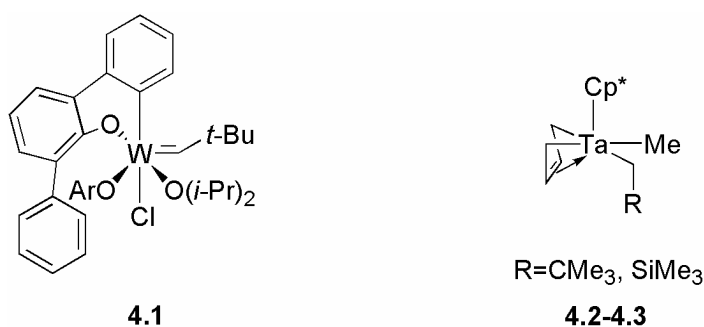


Figure 2. Olefin metathesis catalysts that exhibit *cis* selectivity.

With readily modifiable ligands which do not dissociate from the metal center during metathesis,¹⁴ the *N*-heterocyclic-carbene-ligated ruthenium-based olefin metathesis catalysts are particularly suitable candidates to modify for *cis*/*trans* selective purposes. However, these complexes also pose two major challenges to *cis*/*trans* development. First, the stereochemistry of the intermediates involved in the mechanism

of these complexes remains relatively obscure—whether the mode of olefin binding and metallacyclobutane formation is at a site cis or trans to the *N*-heterocyclic carbene of the organometallic complex is expected to hold major implications for developing selective catalysts. Second, the *N*-heterocyclic carbene complexes of ruthenium are so active for metathesis that product olefin isomerization is rapid. This isomerization renders the observation of the kinetic selectivity of these complexes difficult.

The stereochemistry of the intermediates involved in the olefin metathesis reaction is expected to be of major importance in controlling product stereochemistry. In particular, it is unknown as to whether the olefin binds cis or trans to the L-type ligand (see Chapter 3, *Stereochemical Model*). This binding mode holds major implications for the stereochemistry of the olefinic products. For example, in anticipation of an olefin-complex intermediate with the olefin bound trans to the NHC ligand, efforts in our research group led to the design of a large NHC ligand with biaryl side-groups designed to reach into a quadrant of the ligand sphere where they can impart a steric influence on the region trans to the NHC ligand (4.4, Figure 3).¹⁵ Although complex 4.4 is not *cis*-

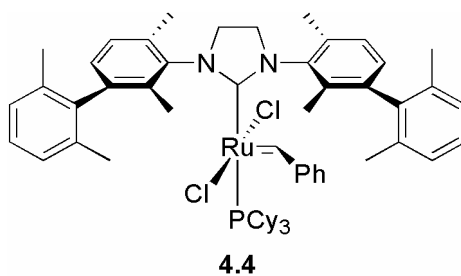
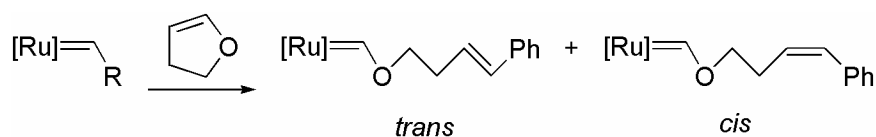


Figure 3. Attempted *cis*-selective catalyst design.

selective, its design is demonstrative of the challenges anticipated for a trans binding mode; other approaches center around synthetically difficult modifications of the X-type

ligands. On the other hand, if olefin-binding is cis to the NHC ligand, it is perhaps surprising that the large steric bulk of the NHC does not lead to cis product formation.

The rapidity of olefin isomerization with the active NHC-ligated of olefin metathesis complexes is anticipated to pose a challenge to the development of systems which lead to stereopure products. Presently, however, this high activity makes it difficult to identify the cis/trans selectivity of NHC-ligated catalysts. With our understanding of the stereoselectivity of these systems in its infancy, it is extremely important to develop a means of determining their inherent stereoselectivity. To this end, the work presented here includes efforts to develop the reaction of ruthenium complexes with dihydrofuran in a single-turnover reaction to yield a metathesis-inactive Fischer-



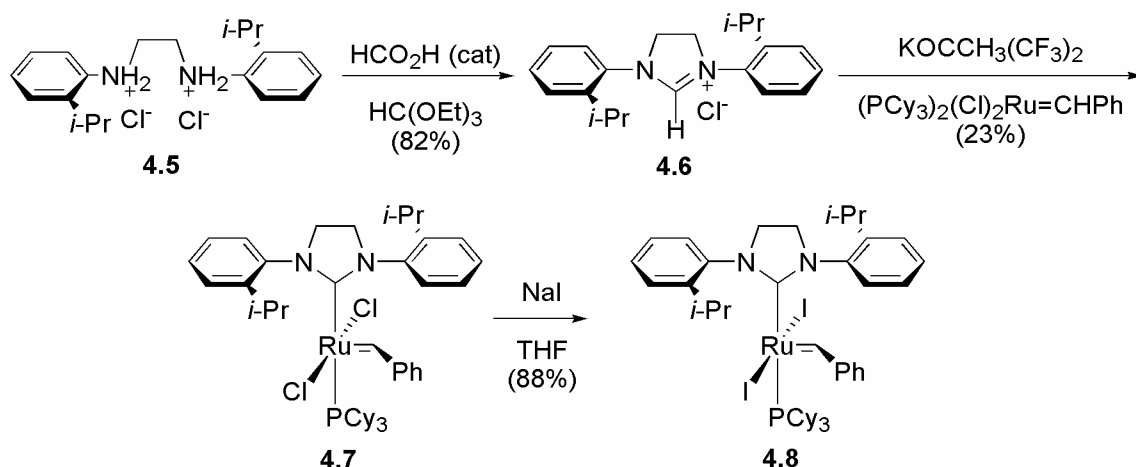
Scheme 1. Single-turnover reactions with dihydrofuran.

alkylidene complex with a quantifiable E:Z product ratio (Scheme 1).¹⁶ We have found that this reaction proceeds cleanly and quantitatively, without isomerization from secondary metathesis. Furthermore, the removal of all volatiles allows for the outcome of the reaction to be measured by three separate spectroscopic handles: the ^1H NMR spectroscopic signals of the Fischer-carbene and olefin protons, and the ^{31}P NMR spectroscopic signals of the rebound phosphorus ligand.

Results

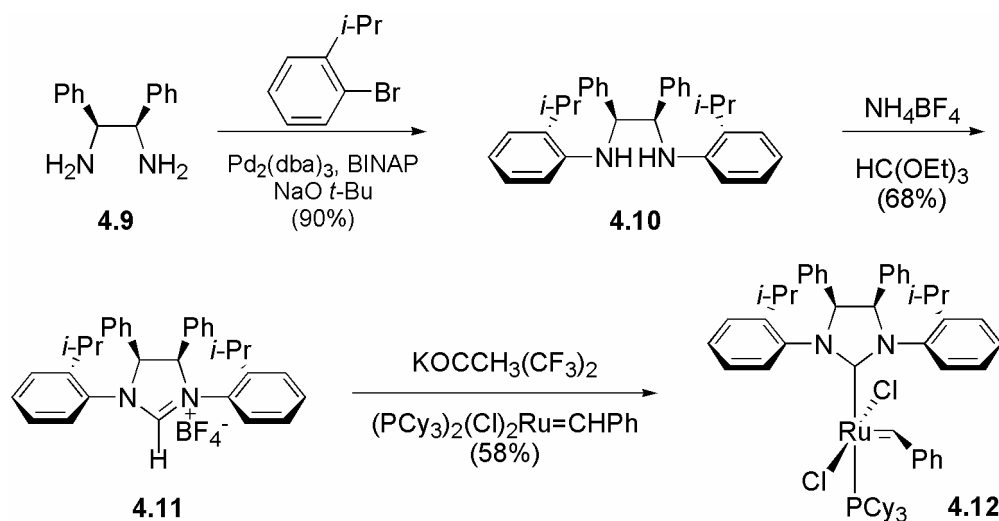
Catalyst synthesis

Three novel organometallic complexes are introduced in this chapter for the purpose of this study. Diamine salt **4.5**, the protonated form of a literature-reported diamine,¹⁷ is heated overnight in refluxing triethyl orthoformate in the presence of catalytic quantities of formic acid to give *N*-heterocyclic carbene precursor **4.6**. This ligand is in turn subjected to potassium hexafluoro-*t*-butoxide and heated with $\text{RuCl}_2(\text{PCy}_3)_2=\text{CHPh}$ to displace a phosphine ligand and form *N*-heterocyclic carbene complex **4.7**. Complex **4.7** is treated with NaI to form diiodide complex **4.8** (Scheme 2).



Scheme 2. Synthesis of complexes **4.7** and **4.8**.

Commercially available *meso*-diamine **4.9** is subjected to aryl bromide under standard Pd-catalyzed aryl amination conditions to yield diamine **4.10**. This compound is then heated overnight in refluxing triethyl orthoformate in the presence of stoichiometric amounts of NH_4BF_4 to form *N*-heterocyclic carbene precursor **4.11**. This ligand is in turn subjected to potassium hexafluoro-*t*-butoxide and heated with $\text{RuCl}_2(\text{PCy}_3)_2=\text{CHPh}$ to displace a phosphine ligand and form *N*-heterocyclic carbene complex **4.12** (Scheme 3).



Scheme 3. Synthesis of complex **4.12**.

Reactions with dihydrofuran

In addition to newly synthesized complexes **4.7**, **4.8**, and **4.12**, data were collected for sixteen olefin metathesis catalysts of interest—some of which are reported in the elsewhere in this thesis (**4.13-4.14**, **4.20-4.21**), are reported in the literature (**4.16-4.18**,¹⁸ **4.19**,¹⁹ **4.23**,¹⁸ **4.24**,²⁰ **4.25**,²¹ **4.26**¹⁸), or were provided by other members of the group (**4.15**, Steven Goldberg; **4.22**, Jacob Berlin; **4.27-4.28**, Jennifer Love). These complexes react cleanly and completely with dihydrofuran and an E:Z product ratio is assignable by one or more spectroscopic handles. The results of these reactions are reproducible, but it is important to point out that the measurements are approximate measures of the inherent stereoselectivity of the complexes. For this reason, the results of these reactions are conveniently divided into three major categories: E:Z > 19:1; E:Z ~4:1 or 5:1; E:Z ~ 2:1 (Figure 4).

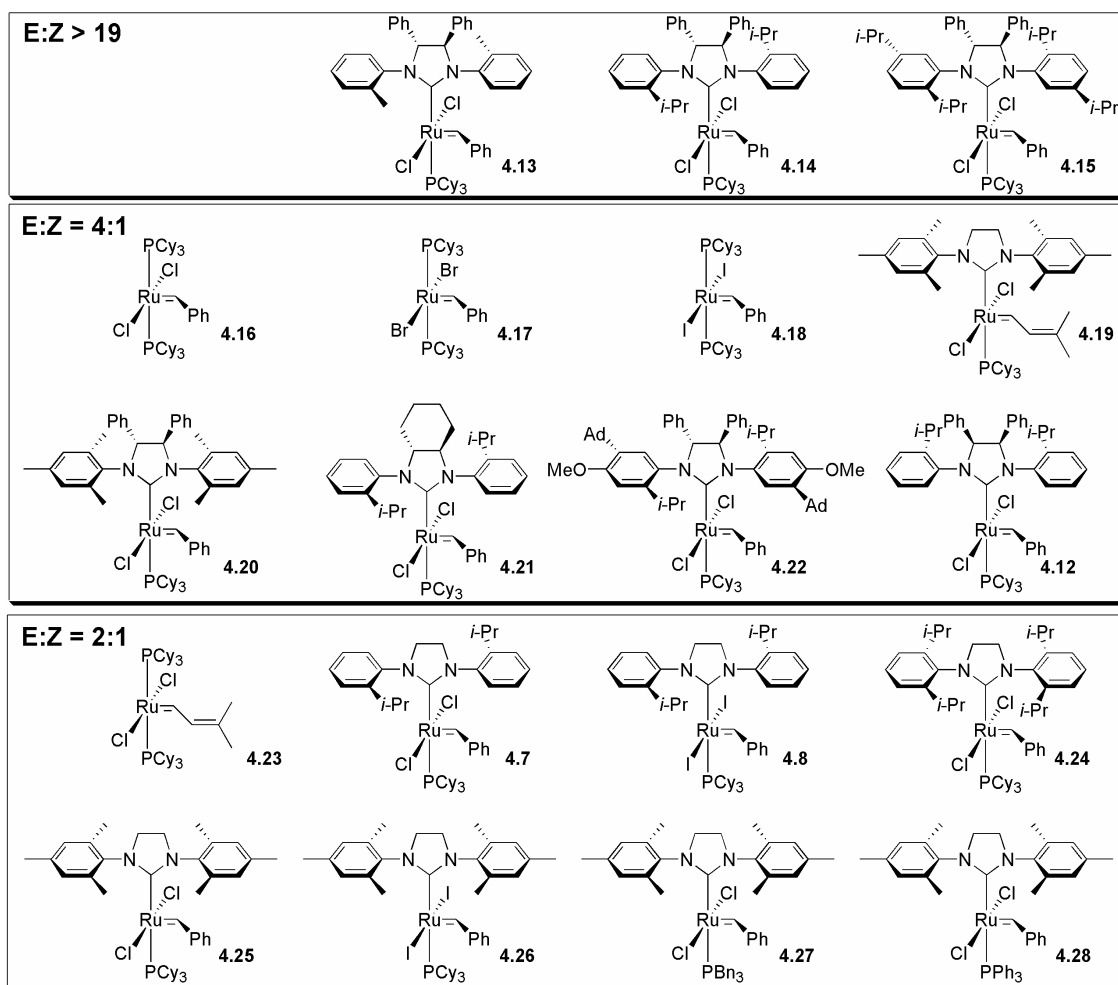


Figure 4. E:Z ratios of reactions of dihydrofuran with olefin metathesis complexes.

When complex **4.7** is reacted with dihydrofuran, a pair of doublets is observed in the alkylidene region of the ^1H NMR spectrum: δ 14.22 (d, $J = 8.9$ Hz), 14.20 (d, $J = 8.3$ Hz) which by intensity occur in the ratio of 1.7:1. Following removal of volatiles, the olefinic region shows two doublets assigned to the Z and E isomers, respectively: δ 6.52 (d, $J = 11.7$ Hz) and 6.45 (d, $J = 16.5$ Hz) in a ratio of 2.1:1 E/Z (E and Z assignments are based on coupling constants). The ^{31}P NMR spectrum shows what appear to be two doublets: δ 29.42 (d, $J = 110$ Hz) and 29.17 (d, $J = 101$ Hz) which by intensity occur in a ratio of 2.4:1.

On reaction with dihydrofuran, the ^1H NMR spectrum of complex **4.8** shows little useful information in the alkylidene region with unresolved peaks at δ 13.643 and 14.635. The olefinic region, on the other hand, shows a pair of doublets: δ 6.49 (d, $J= 11.3$ Hz) and 6.40 (d, $J= 16.0$ Hz) with an E:Z ratio of 2.2:1. This is consistent with the ^{31}P NMR, which shows a pair of doublets: δ 30.50 (d, $J= 53.4$ Hz) and 29.88 (d, $J= 55.0$ Hz) in a ratio of 2.1:1.

On reaction with dihydrofuran, complex **4.12** exhibits two singlets in the alkylidene region of the ^1H NMR spectrum: δ 14.34 and 14.29 in a ratio of 5.8:1. The olefinic region shows two doublets: δ 6.53 (d, $J= 12.0$ Hz) and δ 6.45 (d, $J= 15.9$ Hz) which suggest an E:Z ratio of 3.9:1. The ^{31}P NMR spectrum shows two singlets: δ 27.37 and 27.51 in a ratio of 4.3:1.

On reaction with dihydrofuran, complex **4.13** gives difficult spectra due to the presence of many observable rotational isomers. In the alkylidene region of the ^1H NMR spectrum, around four peaks are observed: δ 14.16-14.24. The ^{31}P NMR spectrum is also difficult to interpret with several peaks. In the olefinic region of the ^1H NMR, however, there is a clear doublet observed with a faint signal where the cis doublet is normally observed in an E:Z ratio of 42:1. δ 6.45 (d, $J= 16.0$ Hz).

On reaction with dihydrofuran, complex **4.14** shows a pair of doublets in the alkylidene region of the ^1H NMR spectrum: δ 14.56 (d, $J= 3.1$ Hz) and 14.31 (d, $J= 3.1$ Hz) which integrate in a ratio of 19:1. It is suspected that the smaller peak in this region is a rotational isomer rather than the cis product as a similar ratio of alkylidene signals is observed in the parent complex. In the olefinic region, only the trans product is observed: δ 6.43 (d, $J= 15.7$ Hz). Only one ^{31}P NMR signal is observed: δ 29.15.

On reaction with dihydrofuran, complex **4.15** shows similar spectra to **4.14**. In the alkylidene region of the ^1H NMR spectrum, two poorly resolved peaks are observed at δ 14.16 and 14.15. In the olefinic region, only the trans product is observed: δ 6.52 (d, $J = 15.0$ Hz). The ^{31}P NMR spectrum shows two peaks at δ 30.39 and 30.23 in a ratio of 9:1. Two peaks are probably observed in the alkylidene region of the ^1H NMR spectrum and the ^{31}P spectrum due to the presence of rotational isomers.

On reaction with dihydrofuran, the alkylidene region of the ^1H NMR of complex **4.17** is not resolved, showing a peak at δ 14.62 with a visible shoulder. On the other hand, the olefinic spectrum shows two doublets: δ 6.49 (d, $J = 11.5$ Hz) and 6.38 (d, $J = 16.0$ Hz) with an E:Z ratio of 3.7. This ratio is confirmed by the ^{31}P NMR spectrum, which shows two peaks: δ 35.11 and 35.38 in a ratio of 3.9.

On reaction with dihydrofuran, the ^1H NMR spectrum of complex **4.18** shows only one alkylidene peak at δ 14.14. The olefin region shows two doublets: δ 6.44 (d, $J = 10.5$ Hz) and 6.31 (d, $J = 16.0$ Hz) with an E:Z ratio of 4.4:1. The ^{31}P NMR spectrum shows two singlets: δ 35.03 and 34.69 in a ratio of 3.4:1.

On reaction with dihydrofuran, complex **4.19** shows only one peak in the alkylidene region of the ^1H NMR spectrum at δ 14.11. In the olefinic region, doublets of triplets are compared: δ 5.59 and 5.39 with an E:Z ratio of 4.1:1. The ^{31}P NMR spectrum shows two singlets: δ 31.17 and 31.06 in a ratio of 4.9:1.

On reaction with dihydrofuran, complex **4.20** shows two doublets in the alkylidene region of the ^1H NMR spectrum: δ 14.15 (d, $J = 1.2$ Hz) and 14.11 (d, $J = 1.2$ Hz) in a ratio of 3.6:1. In the olefinic region, two doublets are observed: δ 6.48 (d, $J =$

11.4 Hz) and 6.40 (d, $J = 16.2$ Hz) with an E:Z ratio of 4.0:1. The ^{31}P NMR spectrum shows two singlets: δ 29.97 and 29.64 in a ratio of 3.9:1.

On reaction with dihydrofuran, the NMR spectra of complex **4.21** can be rather complex due to the presence of many rotational isomers. In the alkylidene region of the ^1H NMR spectrum, approximately seven peaks are observed in the region δ 14.15-14.25. Furthermore, there are more than six peaks in the ^{31}P NMR: δ 28.2-28.9. The olefinic region is clearer—by picking out all of the doublets in a certain region and using their coupling constants to determine cis and trans, and E:Z ratio of 4.3 is determined: δ 6.54 (d, $J = 12.0$ Hz), 6.48 (d, $J = 16.0$ Hz), 6.47 (d, $J = 15.5$ Hz).

On reaction with dihydrofuran, the ^1H NMR spectrum of complex **4.22** shows two singlets in the alkylidene region: δ 14.09 and 14.08 in a ratio of 3.5:1. The olefinic region shows two doublets: δ 6.50 (d, $J = 12.0$ Hz) and 6.40 (d, $J = 15.0$ Hz) in an E:Z ratio of 4.7:1. Furthermore, the ^{31}P NMR spectrum shows two singlets: δ 30.68 and 30.55 in a ratio of 3.3:1.

The reaction of complex **4.23** with dihydrofuran was somewhat difficult to analyze—the olefinic region of the ^1H NMR spectrum was very difficult to interpret. The alkylidene region shows two poorly resolved singlets: δ 14.87 and 14.84 which suggest a ratio of 1.9:1 by peak intensity. The ^{31}P NMR spectrum shows two poorly resolved singlets: δ 35.69 and 35.66 which show a ratio of 2.1:1 by peak intensity.

On reaction with dihydrofuran, the ^1H NMR spectrum of complex **4.24** shows two singlets in the alkylidene region: δ 14.25 and 14.21 in a ratio of 2.1:1. The olefinic region shows two doublets: δ 6.51 (d, $J = 11.7$ Hz) and 6.41 (d, $J = 16.2$ Hz) with an E:Z ratio of 2.8:1. The ^{31}P NMR shows two singlets: 30.72 and 30.87 with a ratio of 2.0:1.

The reaction of complex **4.25** with dihydrofuran proved to be the most problematic to analyze by spectroscopy; it is likely that some kind of extraneous complex forms and wreaks havoc with the NMR integrations. On account of these difficulties, complexes **4.27** and **4.28** were of particular interest since they have the same active species in the catalytic turnover. In the best experiment with **4.25**, the ^{31}P NMR shows a larger peak at δ 30.88 and a smaller peak at δ 31.19, which show a ratio of 2.6:1 based on intensity. In the olefinic region of the ^1H NMR spectrum, doublets are observed which confirm an E:Z ratio of 2.6: δ 6.55 (d, $J= 12.0\text{Hz}$) and 6.47 (d, $J= 15.5\text{ Hz}$). These results correlate well with complexes **4.27** and **4.28**.

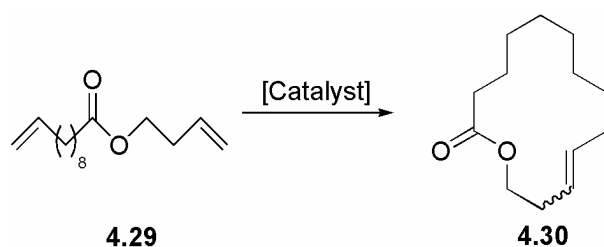
On reaction of complex **4.26** with dihydrofuran, the ^1H NMR spectrum shows two peaks in the alkylidene region: δ 13.57 and 13.54 in a ratio of 2.0:1. The olefinic region shows two doublets: δ 6.48 (d, $J = 11.4\text{ Hz}$) and 6.38 (d, $J = 15.9\text{ Hz}$) with an E:Z ratio of 2.1:1. The ^{31}P NMR spectrum shows two singlets: δ 27.44 and 27.85 in a ratio of 1.8:1.

On reaction of complex **4.27** with dihydrofuran, the ^1H NMR spectrum shows two unresolved singlets in the alkylidene region: δ 13.51 and 13.49 suggest a ratio of 1.8:1 by peak intensity. The olefinic region shows two doublets: δ 6.29 (d, $J = 12.0\text{ Hz}$) and 6.18 (d, $J = 16.0\text{ Hz}$) with an E:Z ratio of 2.3:1. The ^{31}P NMR spectrum shows only one singlet at δ 38.38.

On reaction of complex **4.28** with dihydrofuran, the ^1H NMR spectrum shows only one peak in the alkylidene region: δ 13.55. In the olefin region, two doublets are observed: δ 6.39 (d, $J = 12.0\text{ Hz}$) and 6.20 (d, $J = 16.0\text{ Hz}$) with an E:Z ratio of 2.3:1. The ^{31}P NMR spectrum two singlets at δ 36.03 and 36.12 in a ratio of 2.4:1.

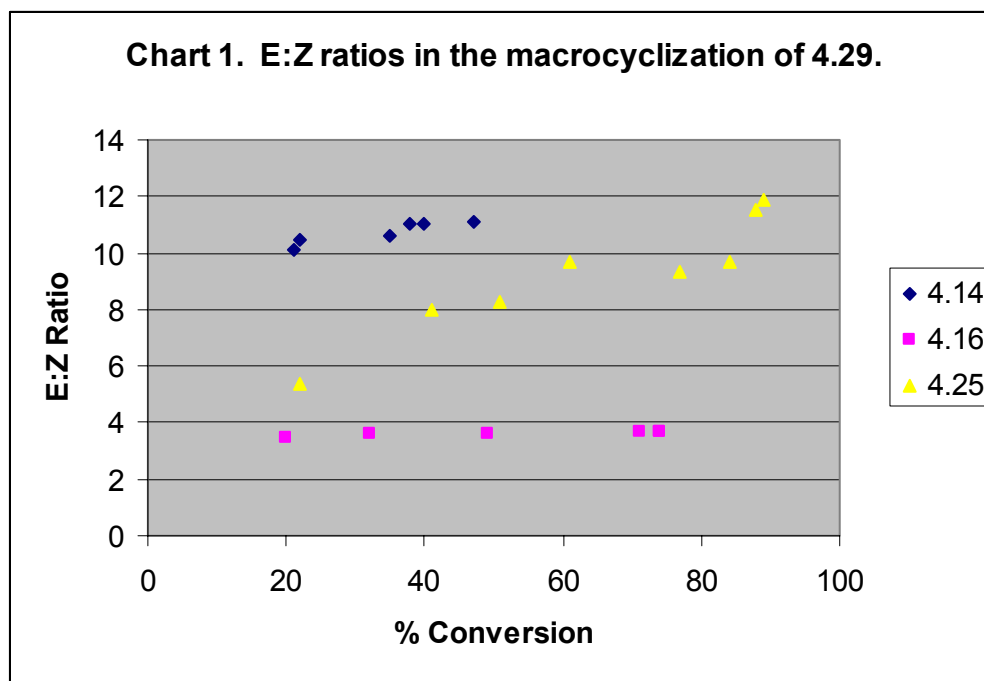
Reactions with other substrates

With single-turnover data in hand, it is of considerable interest to apply these complexes to a catalytic reaction and monitor the E:Z ratios with respect to conversion. To this end, one complex from each of three categories was chosen (**4.14**, **4.16**, and **4.25**) and employed in the ring-closing metathesis of substrate **4.29** to yield macrocyclic product **4.30** (Scheme 4).²² GC analysis was used to measure conversion and product



Scheme 4. Macrocyclization through ring-closing metathesis.

E:Z ratios over the course of the reactions (Chart 1). From these data, several interesting phenomena are observed. Notably, bisphosphine complex **4.1**, which is not expected to engage in rapid secondary isomerization, initially gives a products with E:Z ratios close to the predicted value (~4:1) and these ratios remain steady throughout the course of the reaction. The commonly employed *N*-heterocyclic-carbene-ligated complex **4.25**, on the other hand, initially gives lower E:Z ratios as predicted, and then shows isomerization throughout the reaction to result finally in an E:Z ratio of ~12:1. Finally, NHC-ligated chiral complex **4.14** gives relatively high E:Z ratios at low conversions as anticipated. These results demonstrate the importance of developing methods to monitor the inherent stereoselectivity of olefin metathesis complexes, and the utility of the dihydrofuran reaction is confirmed by the close correlation of these data to the observed single-turnover E:Z ratios.



Discussion

Reactions with dihydrofuran

From the E:Z data collected for the reaction of these complexes with dihydrofuran, it is useful to attempt to identify trends in selectivity with the hopes that an understanding of these catalysts may emerge which will lead to the successful design of stereoselective catalysts. For example, it is interesting to note that the stereoselectivity of these complexes does not change with symmetrical variation of their X-type ligands. This is true for the bisphosphine complexes, which give an E:Z ratio of ~4:1 even as the halide ligands increase in size from Cl⁻ (**4.16**) to Br⁻ (**4.17**) to I⁻ (**4.18**). Additionally, the IMesH₂ catalyst (IMesH₂ = 1,3-dimesityl-4,5-dihydroimidazol-2-ylidene) exhibits an E:Z selectivity of ~2:1 with variation from Cl⁻ (**4.25**) to I⁻ (**4.26**), as do mono-*ortho*-substituted complexes **4.7** and **4.8**.

The alteration of the alkylidene moiety does not produce a discernible trend. In the case of the bisphosphine **4.16**, the benzylidene moiety leads to higher *trans* selectivity (E:Z ~ 4:1) than the dimethylvinyl moiety **4.23** (E:Z ~ 2:1). However, just the opposite effect is observed in IMesH₂-ligated complexes, where the benzylidene-ligated complex **4.25** leads to lower *trans* selectivity (E:Z ~ 2:1) than the dimethylvinyl-ligated complex **4.19**.

Based on the assumption that the low steric requirements of the mono-substituted aryl side groups of NHC complexes such as **4.7**, **4.14**, and **4.21** could allow for facile *transoid* binding of the dihydrofuran substrate cis to the L-type ligand (see Chapter 3), it was predicted that this class of catalysts would provide high *trans*-olefin product selectivity. Interestingly, however, a distinct trend is observed with *trans*-selectivity increasing with increasing chiral steric bulk in the backbone of the NHC ligands (Figure 5). For example, while achiral complex **4.7** provides an E:Z ratio of ~2:1, the analogous complex **4.21** with a cyclohexyl-substituted NHC ligand provides a ratio of ~4:1. Furthermore, complex **4.14** (the most enantioselective catalyst) provides high *trans* selectivity with E:Z ratios greater than 19:1.

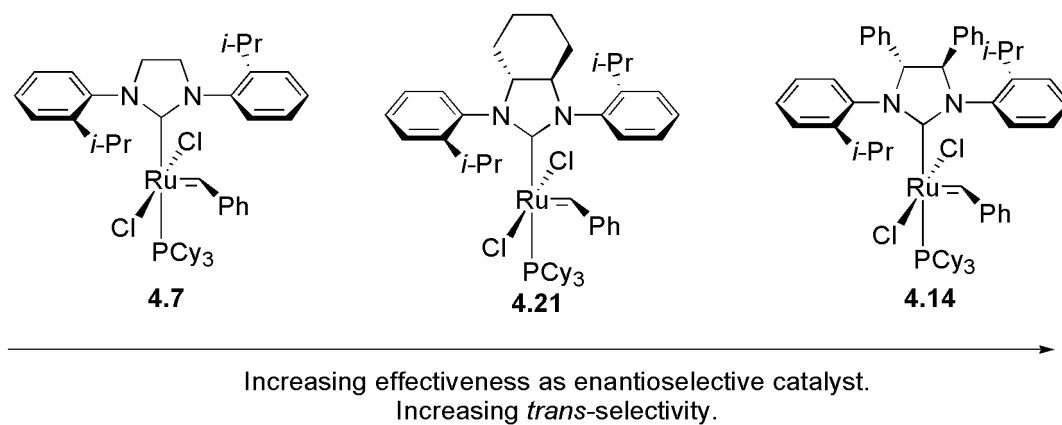


Figure 5. Enantioselectivity/*trans*-selectivity correlation.

Based on the understanding of the rotational isomers developed in Chapter 2 of this thesis, it is plain that this trend also correlates to the degree of organization imparted onto the aryl side-groups of the ligands by the substitution in the backbone. The least *trans*-selective catalyst, complex **4.7**, is also the complex which is anticipated to contain a significant proportion of *syn* rotamers in addition to *anti* rotamers (Figure 6). On the

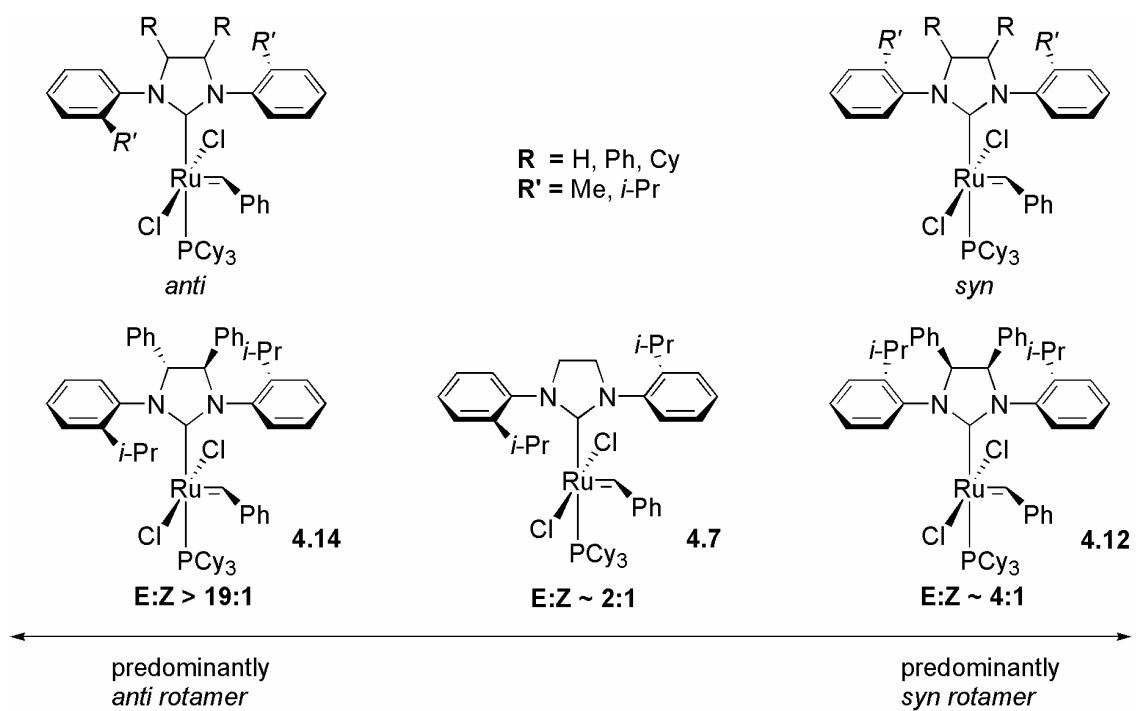


Figure 6. *Syn* and *anti* rotamers in cis/trans selectivity.

other hand, the most *trans*-selective catalyst, complex **4.14**, is anticipated to have the greatest organization of its ligand and to consist primarily of *anti* rotamer. This observation begs the question as to whether the *syn* rotamer is primarily responsible for cis product formation and, subsequently, whether the *anti* rotamer is primarily responsible for trans product formation. To address this question, we focus our attention on the relative E:Z selectivities of complexes **4.14**, **4.7**, and **4.12**. Since the *meso* complex **4.12** is expected to consist primarily of *syn* rotamer and its E:Z selectivity is

intermediate to those of complexes **4.7** and **4.14**, it is apparent that cis/trans selectivity for these complexes is controlled by more than simple organization of the aryl side groups of the NHC ligand. For further confirmation of this, it is observed that the di-*ortho*-substituted complex **4.24** offers the same E:Z selectivity as analogous mono-*ortho*-substituted complex **4.7**.

Stereochemical model

With these data in hand, it is useful to contemplate a plausible stereochemical model that is consistent with the observed outcome of the reactions. In concordance with the stereochemical model proposed in Chapter 3, the degree of variation of E:Z stereoselectivity with subtle variation of the NHC ligand implies olefin-complex intermediates in which the olefin binds cis to the L-type ligand—it is difficult to imagine the NHC having so strong an impact on binding events trans to it. Certainly, too, our results indicate that cis/trans selectivity is not controlled by the *syn* and *anti* rotational isomers of the complexes. Certainly, high trans selectivity seems to have a strong correlation with chirality—this may correspond to the role that the alkylidene moiety can play in cis/trans selectivity.

It is useful to suggest a stereochemical model which is consistent with our present understanding of the geometry of olefin binding. In the crystal structure of chiral ruthenium pyridine complex **2.22** described in Chapter 2, the alkylidene moiety is rotated approximately 45° out of the plane of the chlorides—presumably due to the interaction of the *ortho*-proton of the aryl side group of the NHC (Figure 7). Clearly, too, the alkylidene moiety experiences a steric interaction with the isopropyl moiety, causing it to occupy a position *anti* to the isopropyl despite its negative interaction with the aryl *ortho*-

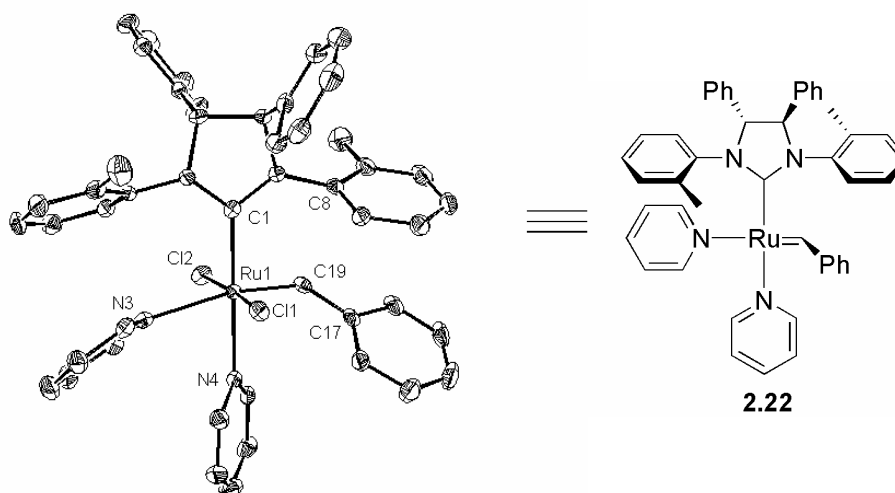


Figure 7. X-Ray crystal structure of complex **2.22**.

proton. This interaction may hold key implications for the stereoselectivity of chiral complexes; if, in the course of the reaction, the alkyldiene occupies the same quadrant which it occupies in the crystal structure, it may serve to direct the orientation of the incoming dihydrofuran molecule, strongly disfavoring the formation of the *cis* product (Figure 8). On the other hand, achiral analogue **4.7**, with its low steric demands, has much greater rotational freedom for the aryl groups of the NHC. As a result, a strong influence of the NHC on the alkyldiene moiety is not expected and *cis* product formation is readily allowed.

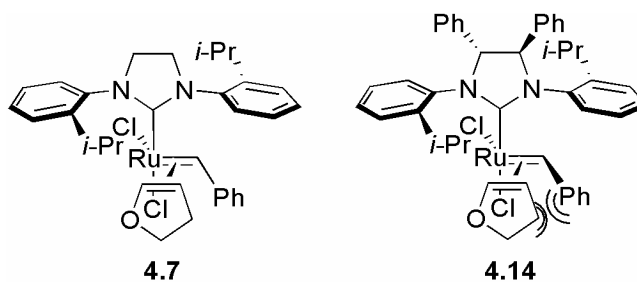


Figure 8. Disfavoring of *cis* product formation through alkyldiene steric interaction.

Experimental Section

General Procedures

When specified, manipulation of organometallic compounds was performed using standard Schlenk techniques under an atmosphere of dry argon or in a nitrogen-filled Vacuum Atmospheres drybox ($O_2 < 2$ ppm). Argon was purified by passage through columns of BASF R3-11 catalyst (Chemalog) and 4Å molecular sieves (Linde). NMR spectra were recorded on a Varian Inova (499.85 MHz for 1H ; 202.34 MHz for ^{31}P) or a Varian Mercury 300 (299.817 for 1H ; 121.39 MHz for ^{31}P). Chemical shifts are referenced to internal solvent resonances and are reported relative to tetramethylsilane. ^{31}P NMR spectra were referenced using H_3PO_4 ($\delta = 0$ ppm) as an external standard.

Materials and Methods

Toluene, dichloromethane, tetrahydrofuran, and benzene were dried and degassed by passage through solvent purification columns containing activated alumina and copper. Dihydrofuran was purified by distillation from calcium hydride. Silica gel used in organometallic complex purification was obtained from TSI. Ruthenium-based starting materials were used as received from Materia (Pasadena, CA). All others were purchased from Aldrich, and all liquids were purified by distillation.

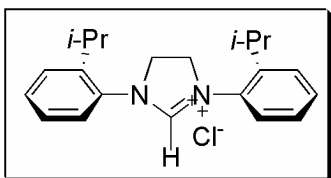
General procedure with dihydrofuran

Catalyst (0.0103 mmol) is weighed into a vial in the glovebox, followed by addition of 0.6 ml C_6D_6 and transfer to an NMR tube with a septum-centered screw cap. This sample is then analyzed by NMR, followed by addition of 20 equivalents of dihydrofuran (16 μL ; 0.212 mmol). The reaction is then monitored by 1H and ^{31}P NMR; heating is employed if necessary to achieve reasonable rates of reaction. Following

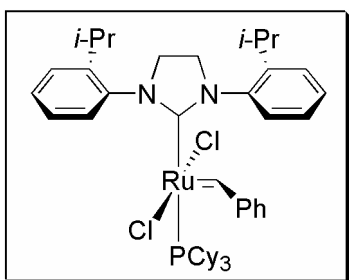
complete conversion, all volatiles are removed *in vacuo*, and the sample is again analyzed by ^1H and ^{31}P NMR.

Synthetic procedures

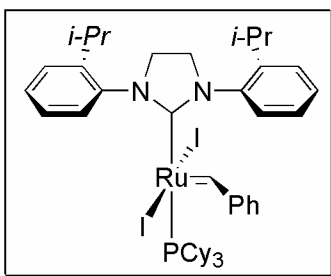
All syntheses are performed in close analogy to those reported in Chapter 2.



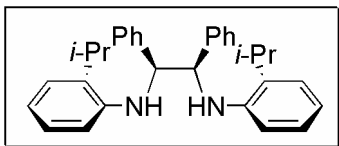
Compound **4.6**. (82%). ^1H NMR (300 MHz, CD_2Cl_2): δ 1.32 (d, $J=6.9$ Hz, 12H), 3.11 (m, $J=6.9$ Hz, 2H), 4.68 (s, 4H), 7.32-7.50 (m, 6H), 8.06 (d, $J=7.8$ Hz, 2H), 8.44 (s, 1H).



Compound **4.7**. (23%). ^1H NMR (500 MHz, C_6D_6) exists as mixture of atropisomers (1:1): δ 0.9-2.3 (br m), 3.1-3.9 (br m), 6.4-7.7 (br m), 8.95 (br t), 19.54 (s, Ru=CHPh), 19.72 (s, Ru=CHPh). ^{31}P NMR (202 MHz, C_6D_6): δ 27.47.

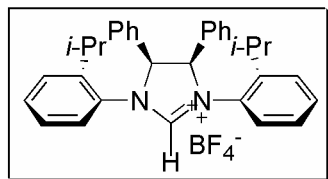


Compound **4.8**. (88%). ^1H NMR (300 MHz, C_6D_6): δ 0.9-1.9 (br m), 2.7-3.0 (br m), 3.2-4.1 (br m), 6.4-7.3 (br m), 9.2 (br d), . ^{31}P NMR (121 MHz, C_6D_6) (visible as a mixture of atropisomers 1.2:1): δ 30.30, 31.81.

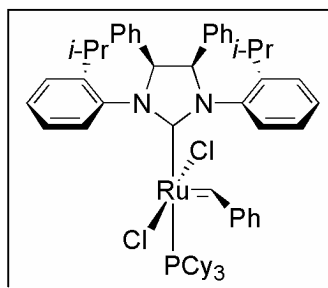


Compound **4.10**. (90%). ^1H NMR (300 MHz, CDCl_3): δ 1.26 (d, $J=6.6$ Hz, 6H), 1.32 (d, $J=6.6$ Hz, 6H), 2.92 (m, $J=$

7.2 Hz, 2H), 4.70 (br d, $J = 5.4$ Hz, 2H), 5.00 (br d, $J = 5.7$ Hz, 2H), 6.36 (d, $J = 6.9$ Hz, 2H), 6.71 (d of d, 2H), 6.92 (d of d, 2H), 6.96-7.04 (br m, 4H), 7.16 (d, $J = 7.5$ Hz, 2H), 7.22-7.30 (br m, 6H).



Compound **4.11**. (68%). ^1H NMR (300 MHz, CDCl_3): δ 1.36 (d, $J = 6.6$ Hz, 6H), 1.41 (d, $J = 7.2$ Hz, 6H), 3.39 (m, $J = 6.6$ Hz, 2H), 6.67 (s, 2H), 7.11 (s, 10H), 7.25-7.31 (m, 2H), 7.36-7.44 (m, 4H), 7.66 (d, $J = 7.8$ Hz, 2H), 8.33 (s, 1H).



Compound **4.12**. (58%). ^1H NMR (500 MHz, CDCl_3): δ 0.80-2.0 (br m), 3.43 (m), 6.6-8.0 (br m), 10.03 (s), 19.32 (s).
 ^{31}P NMR (121 MHz, C_6D_6): δ 22.75.

References and Notes

1. Corey, E. J.; Cheng, X.-M. *The Logic of Chemical Synthesis*; Wiley: New York, 1995; Vol. 2.
2. Nakanishi, K., Ed. *Natural Products Chemistry*; Academic Press: New York, 1974; Vol. 2.
3. Mori, K. *Biosci. Biotechnol. Biochem.* **1996**, *60*, 1925-1932.
4. Hubbard, R.; Kropf, A. *Proc. Natl. Acad. Sci. U. S. A.* **1958**, *44*, 130-139.
5. Jiang, H. L.; Kruger, N.; Lahiri, D. R.; Wang, D. R.; Vatele, J. M.; Balazy, M. *J. Biol. Chem.* **1999**, *274*, 16235-16241.
6. Ramwell, P. W. *The Prostaglandins*; Plenum: New York, 1973.
7. von Euler, U. S.; Eliasson, R. *Prostaglandins*; Academic Press: New York, 1967.
8. Benedetto, C., Ed. *Prostaglandins and Related Substances: A Practical Approach*; IRL Press: Washington, D. C., 1987.
9. Bergstrom, S. *Science* **1967**, *157*, 382.
10. Ivin, K. J.; Mol, J. C. *Olefin Metathesis and Metathesis Polymerization*; Academic Press: San Diego, 1997.
11. Dimonie, M.; Coca, S.; Dragutan, V. *J. Mol. Catal. A: Chem.* **1992**, *76*, 79-91.
12. Basset, J. M.; Leconte, M.; Lefebvre, F.; Hamilton, J. G.; Rooney, J. J. *Macromol. Chem. Phys.* **1997**, *198*, 3499-3506.
13. Mashima, K.; Kaidzu, M.; Tanaka, Y.; Nakayama, Y.; Nakamura, A.; Hamilton, J. G.; Rooney, J. J. *Organometallics* **1998**, *17*, 4183-4195.
14. Sanford, M.; Ulman, M.; Grubbs, R. *J. Am. Chem. Soc.* **2001**, *123*, 749-750.
15. Love, J. A. *Unpublished results*.

16. This idea was initially formulated and developed by Melanie Sanford.
17. Kim, Y. K.; Livinghouse, T. *Angew. Chem., Int. Ed.* **2002**, *41*, 3645-3647.
18. Sanford, M. S.; Love, J. A.; Grubbs, R. H. *J. Am. Chem. Soc.* **2001**, *123*, 6543-6554.
19. Chatterjee, A.; Morgan, J.; Scholl, M.; Grubbs, R. *J. Am. Chem. Soc.* **2000**, *122*, 3783-3784.
20. Dinger, M. B.; Mol, J. C. *Adv. Synth. Catal.* **2002**, *344*, 671-677.
21. Scholl, M.; Ding, S.; Lee, C. W.; Grubbs, R. H. *Org. Lett.* **1999**, *1*, 953-956.
22. Lee, C. W.

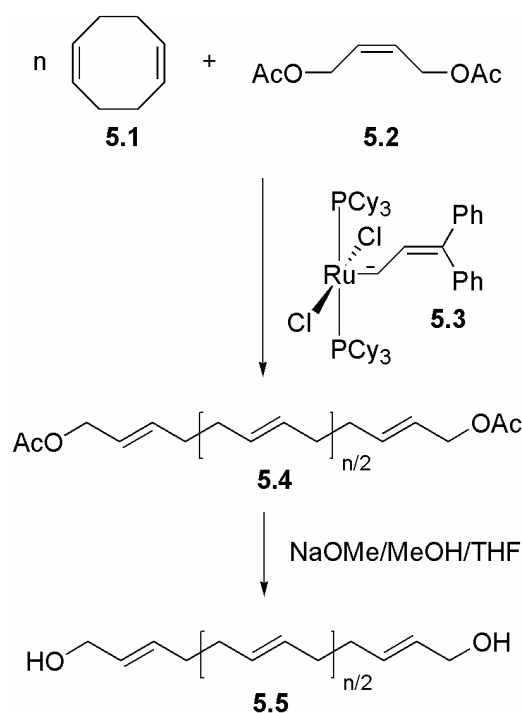
**Chapter 5: Novel Method for the Synthesis of Telechelic
Poly(oxanorbornene)**

Abstract

Chloro-functionalized telechelic and semitelechelic poly(oxanorbornene) was synthesized *via* ring-opening metathesis polymerization (ROMP) by catalyst precursors $\text{RuCl}_2(=\text{PhH})(\text{PCy}_3)_2$, **5.6**, and $\text{RuCl}_2(=\text{CHCH}_2\text{Cl})(\text{PCy}_3)_2$ **5.11** followed by end-capping with chain-transfer agent *cis*-1,4-dichloro-2-butene **5.9**. Although **5.11** exhibits incomplete initiation, good molecular weight control was achieved and polydispersities were narrow.

Introduction

Owing to their utility in block copolymer synthesis, reaction injection molding, chain extension processes, and network formation,^{1,2} telechelic polymers are particularly interesting synthetic targets. The high functional-group tolerance of ruthenium-alkylidene complexes³ has generally led to their successful employment as ring-opening metathesis polymerization (ROMP) catalysts; moreover, these complexes are useful in the synthesis of telechelic polymers, allowing for well-controlled molecular weights and



Scheme 1. Ru-catalyzed preparation of HTPBD **5.5**.

introduction of terminal functional groups. These properties have been established in our group⁴⁻⁶ with the preparation hydroxy end-functionalization of poly(butadiene) (HTPBD) **5.5**. In this approach, polymerization of cyclooctadiene **5.1** (COD) in the presence of α,ω -difunctional olefin chain-transfer agent **5.2** with olefin metathesis catalyst **5.3**

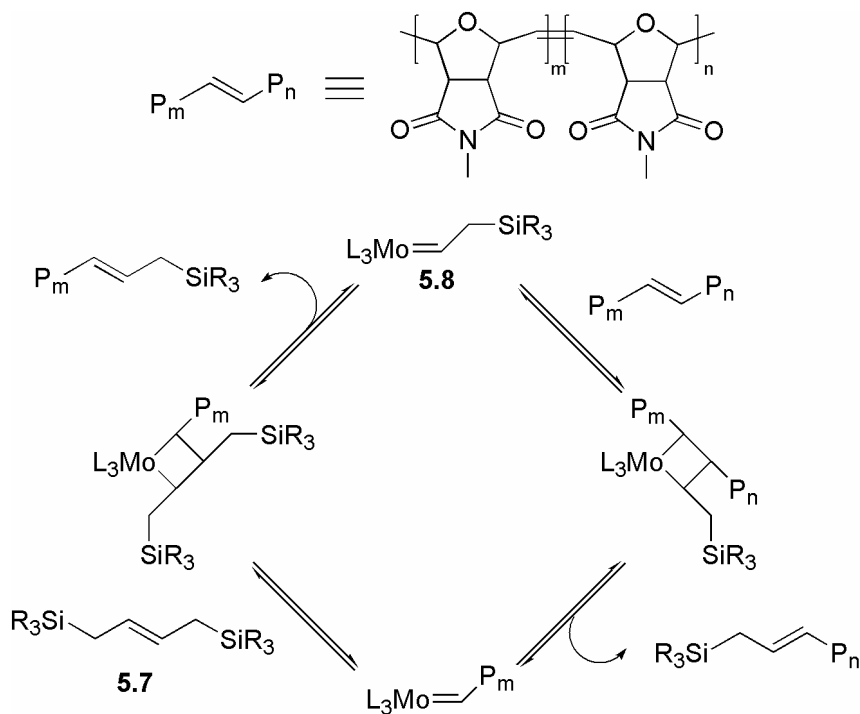
produces telechelic poly(butadiene) (PBD) **5.4** with a functionality approaching two (Scheme 1).

The efficacy of this approach lies in the functional termination of a polymer chain with an acyclic chain transfer agent, accompanied by the regeneration of a catalytically active metal species bearing a functionalized alkylidene moiety. Further polymerization and functional termination lead to telechelic polymers. As observed in the literature, the polymer functionality *approaches* two because “polymer end-groups that do not contain residues from the chain-transfer agent are those from the initiating alkylidene and the end-capping reagent.” While this synthetic approach is effective for relatively low-strain monomers where rates of propagation are comparable to rates of chain transfer, it results in semitelechelic polymers for high-strained bicyclic monomers with relatively rapid rates of polymer propagation. In such cases, since the generation of a functionalized alkylidene species does not occur until the termination of polymerization, the polymer functionality does not approach two. The synthetic approach presented here serves to address this challenge through the judicious selection of olefin metathesis complexes bearing functionalized alkylidene moieties.

The highly strained bicyclic monomer 7-oxanorbornene **5.5** was chosen for this study due to its relative ease of handling and the narrow polydispersities resulting from its ROMP by $\text{RuCl}_2(=\text{HPh})(\text{PCy}_3)_2$ **5.6**.^{7,8} Additionally, poly(oxanorbornene) prepared by ROMP has exhibited interesting properties as ion-permeable films,⁹ the utility of which might be enhanced by the processing possibilities introduced by telechelic functionality.¹⁰ Silicon-derivatized block copolymer poly(oxanorbornene) has received interest in possible utility in high resolution photoresists,⁷ and Kiessling *et al.* have

shown that carbohydrate functionalized poly(oxanorbornene)s have been of some utility in biological systems.^{11,12}

The synthetic method presented here is an improvement over previously reported syntheses of telechelic poly(oxanorbornene)¹³ in which aqueous ring-opening polymerization is followed by depolymerization through acyclic diene metathesis (ADMET) with chain-transfer agent 1,1,8,8-Tetramethyl-2,7-disilaoct-4-ene **5.7** in the presence of an olefin metathesis catalyst. The effectiveness of this approach again lies in the regeneration of the appropriately functionalized catalyst, **5.8**, upon reaction with the chain-transfer agent. This method has the obvious disadvantage of requiring the synthesis of high molecular weight polymer prior to the introduction of functionality and the



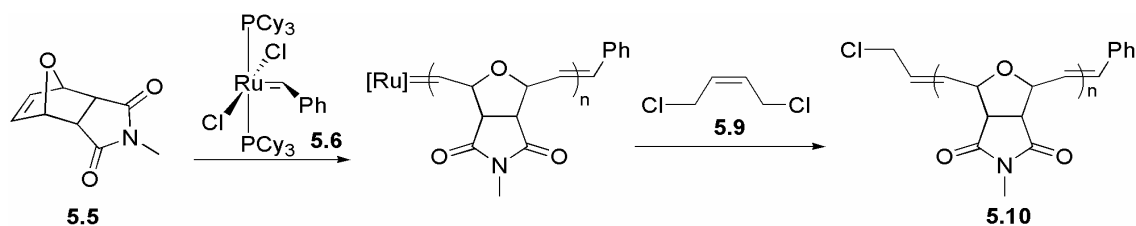
Scheme 2. ADMET/depolymerization synthesis of telechelic poly(oxanorbornene).

relatively high polydispersity indices (PDIs) of 2 or greater which necessarily accompany such an approach.

Results and Discussion

Semitelechelic poly(oxanorbornene)

As an initial test of the effectiveness of introducing terminal functionality to poly(oxanorbornene), the benzylidene ruthenium catalyst, **5.6**, was employed in the ROMP of 7-oxanorbornene **5.5** to prepare polymers of three different molecular weights, followed by addition of excess α,ω -difunctional olefin chain-transfer agent **5.9** to give semitelechelic poly(oxanorbornene) **5.10** (Scheme 3). The reaction was terminated by purification of the polymer via precipitation in methanol.



Scheme 3. Synthesis of semitelechelic poly(oxanorbornene).

To prove the versatility of this reaction, polymers of molecular weight 2,000, 10,000, and 50,000 were targeted. Assuming rapid and complete initiation, catalyst mol % loading was calculated based on [monomer molecular weight]/[polymer molecular weight]. Molecular weight of the lowest weight polymer was determined based on integration of the polymer protons vs. the protons characteristic of the terminal phenyl and chloromethylene groups by ¹H NMR spectroscopy (Figure 1). NMR spectroscopy was found to be ineffective for larger molecular weight chains, since the signals

characteristic of the terminal groups are obscure. These data indicate that polymers of ~13 units were achieved, which is in good accord with the target molecular weight.

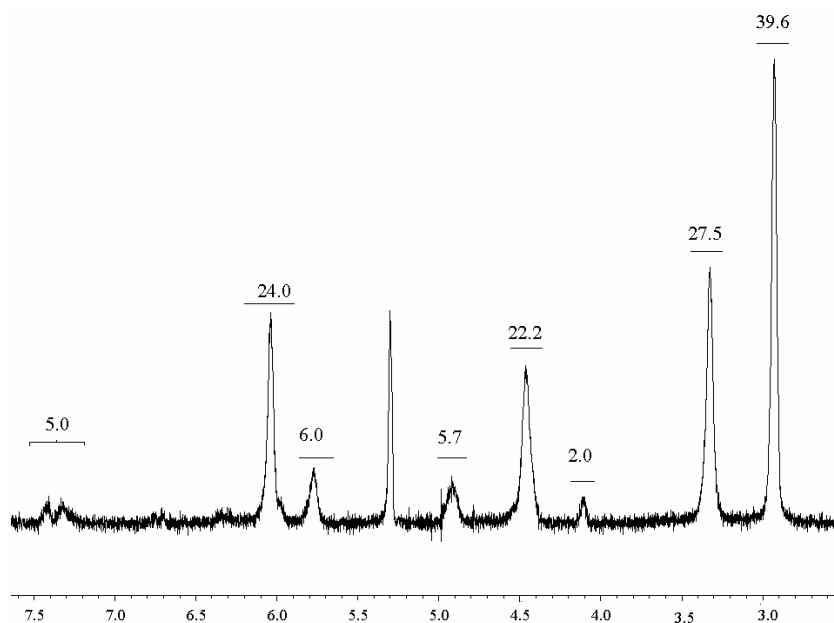


Figure 1. ^1H NMR spectrum of low-molecular-weight semitelechelic poly(oxanorbornene) **5.10** in CD_2Cl_2 : terminal phenyl protons occur around δ 7.4; terminal methylene protons occur around δ 4.1; N-methyl protons occur around δ 2.9; molecular weight is determined by relative integration.

The polymers were further characterized by gel permeation chromatography (GPC) in dimethyl formamide (DMF) based on poly(ethylene glycol) (PEG) standards.¹⁴ The polydispersities of the resulting polymers were found to be narrow.

Table 1. Data for semitelechelic poly(oxanorbornene) **5.10**.

Target M_w	$M_w \times 10^3$ by GPC	PDI	M_w by NMR	Yield
2000	1.6	—*	2500	quantitative
10000	14.7	1.1	—	quantitative
50000	107.9	1.1	—	quantitative

* solvent and product peaks overlap

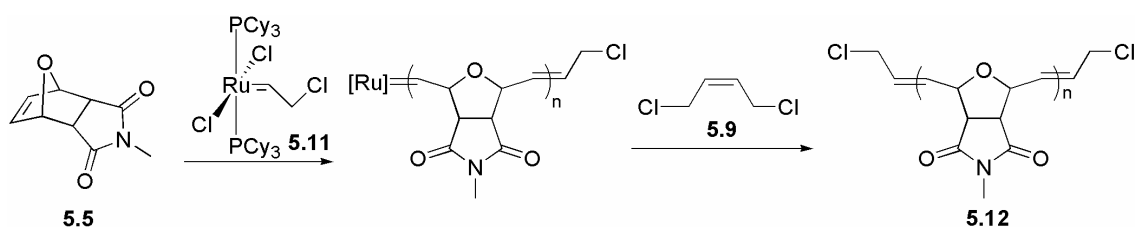
Synthesis of functionalized catalyst precursor

Although reported in the literature, the synthesis of $\text{RuCl}_2(=\text{CHCH}_2\text{Cl})(\text{PCy}_3)_2$ **5.11** is unsuccessful as described. Reaction of $\text{RuCl}_2(=\text{CPhH})(\text{PCy}_3)_2$ **5.6** with 10 equivalents of allyl chloride shows complete conversion of the catalyst to the chloroethylidene by ^1H and ^{31}P NMR. However, on scale-up, an incomplete conversion of ~60% is observed. Presumably, this incomplete conversion is attributable to a disruption of the product equilibrium during removal of all volatile components *in vacuo*—allyl chloride is much lower boiling than styrene. Numerous approaches to correct this problem were attempted, including precipitation of the product from the reaction mixture, removal of volatile components *in vacuo* under temperatures lower than those required for metathesis activity, and use of *cis*-1,4-dichloro-2-butene in the place of allyl chloride. The best conversions achieved were around only 80%. Pure production of the catalyst was ultimately achieved by employing an iterative approach to its synthesis, first isolating a 60:40 mixture of target alkylidene to benzylidene catalyst, and then subjecting this mixture again to 20 equiv. allyl chloride followed by an identical work-up.

Chloro-functionalized telechelic poly(oxanorbornene)

In order to synthesize telechelic poly(oxanorbornene), the well-defined chloroethylidene catalyst **5.11** was utilized to catalyze ROMP of oxanorbornene **5.5**, followed by chain-transfer with agent **5.9**, in order to afford telechelic polymer **5.12** (Scheme 4).

Again, in order to demonstrate the versatility of this approach, polymers of target molecular weights 2,000; 10,000; and 50,000 were synthesized. Assuming rapid and complete catalyst initiation, mol % catalyst loading was calculated based on [monomer



Scheme 4. Synthesis of telechelic poly(oxanorbornene) **5.12**.

molecular weight]/[polymer molecular weight]. Molecular weight of the lowest weight polymer was determined based on integration of the polymer protons vs. the protons characteristic of the terminal methylene chloro groups by ^1H NMR spectroscopy (Figure 2). NMR spectroscopy was found to be ineffective for analyzing larger molecular weight chains since the peaks characteristic of the terminal groups are obscure. These data indicate that polymers of ~ 35 units were achieved, which is about three times the target molecular weight. This discrepancy is further demonstrated by the GPC data (Table 2).

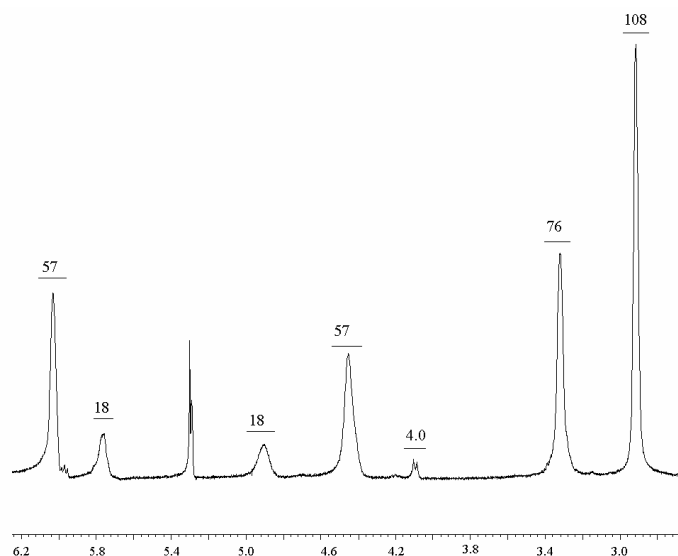


Figure 2-- ^1H NMR spectrum of low molecular weight telechelic poly(oxanorbornene) **5.12** in CD_2Cl_2 : terminal methylene protons occur around δ 4.1; N-methyl protons occur around δ 2.9; molecular weights determined by relative integration suggest poor molecular weight control.

Table 2. Data for telechelic poly(oxanorbornene) **5.12**.

Target M_w	$M_w \times 10^3$ by GPC	PDI	M_w by NMR	Yield
2000	—	—	6400	quantitative
10000	49.1	1.4	—	80%
50000	115.8	1.2	—	82%

In order to probe the source of poor molecular weight targeting, polymerization was conducted and monitored by NMR spectroscopy, using anthracene as an internal standard. For the benzylidene ruthenium catalyst, the active species alkylidene peak typically is distinct from the alkylidene peak of the precursor itself. For chloroethylidene **5.11**, on the other hand, the active species and precursor peaks are indistinguishable. However, by comparing the integration of the terminal methylene chloro groups to the catalyst alkylidene species, it could be observed that approximately 1/3 of catalyst **5.11** is initiating in the course of the reaction. Furthermore, these NMR studies showed that the 1/3 catalyst initiation remained constant throughout the polymerization. In order to effect more complete catalyst initiation, polymerization at an elevated temperature was effected, but afforded even poorer molecular weight control (at 55°C, a target polymerization of 10 monomer units gave polymer of 65 units in length).

In order to overcome the challenges presented by incomplete initiation, polymerizations were again effected with catalyst loadings based on incomplete initiation. Employing the same conditions and assuming one-third catalyst initiation, mol % catalyst loading is calculated based on $3 * [\text{monomer molecular weight}]/[\text{polymer molecular weight}]$. Molecular weight of the lowest weight polymer was determined based on integration of the polymer protons vs. the protons characteristic of the terminal

chloromethylene groups. These data indicate that polymers of ~15 units were produced, which is in reasonably good accord with the target molecular weight. The efficacy of adjusting the catalyst loading is further supported by the GPC data. Again, relatively narrow polydispersities are achieved (Table 3).

Table 3. Data for telechelic poly(oxabornene) **5.12** with adjusted catalyst loadings.

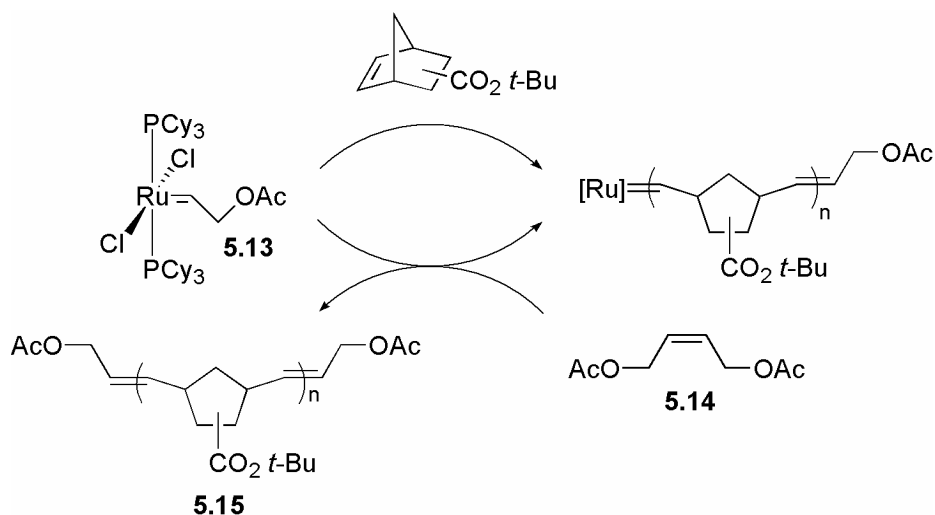
Target M_w	$M_w \times 10^3$ by GPC	PDI	M_w by NMR	Yield
2000	3.6	—*	2800	quantitative
10000	10.6	—*	—	—
50000	43.7	1.1	—	88%

* solvent and product peaks overlap

Conclusion

Despite the reported challenges with initiation of catalyst **5.11**, these results show that telechelic poly(oxanorborene) synthesized from the appropriate catalyst precursor in a well-controlled system with narrow polydispersities and molecular weight control. While these results lay the groundwork for further studies including the development of simpler methodologies involving the generation of complex **5.11** *in situ*, a literature report¹⁵ revealed that this work had been of interest to a competing research group. In this communication, Gibson and coworkers tell of the first telechelic poly(norborene) **5.15** derivative synthesized by initiation with well-defined alkylidene species **5.13** followed by termination with α,ω -difunctional olefin chain-transfer agent, **5.14** (Scheme 5). By employing a pulsed injection approach, it was shown that upon termination of the polymer chains with chain-transfer agent, the active catalyst was regenerated. These results confirm the applicability of the described route to telechelic polymers on a

different system. Good functionalization control, molecular weight control, and narrow polydispersities were achieved.



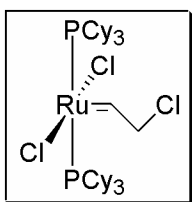
Scheme 5. Synthesis of telechelic poly(norbornene) derivative **5.15**.

Experimental Section

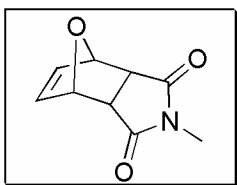
General considerations. Manipulations of organometallic complexes were performed using standard Schlenk techniques under an atmosphere of argon. Argon was purified by passage through columns of BASF R3-11 catalyst (Chemalog) and 4Å molecular sieves (Linde). Polymerizations were performed in a nitrogen-filled Vacuum Atmospheres drybox. NMR spectra were recorded using either a JEOL 400 (400 MHz for ^1H ; 100 MHz for ^{13}C ; 162 MHz for ^{31}P), or a QE-300 Plus instrument (300 MHz for ^1H ; 75 MHz for ^{13}C). Chemical shifts are referenced to internal solvent resonances and are reported relative to tetramethylsilane. ^{31}P NMR spectra were referenced using H_3PO_4 ($\delta = 0$ ppm) as an external standard. Gel permeation chromatography was performed on an HPLC

system using an Altex model 110A pump, a Rheodyne model 7125 injector with a 100 μL injection loop, two American Polymer Standards 10 μL

Materials. Dichloromethane and ethyl ether were dried and degassed by passage through solvent purification columns containing activated alumina and Cu. Dichloromethane- d_6 was purified by vacuum transfer from CaH. Dichloroethane was degassed under argon. Ruthenium benzylidene complex was used as received from Materia. *Cis*-1,4-dichloro-2-butene and allyl chloride were purchased from Aldrich and purified by distillation. All other materials were acquired from commercial sources and used as received.



Complex **5.11**. 283mg (0.344 mmol) $\text{RuCl}_2(=\text{PhH})(\text{PCy}_3)_2$ **5.6** were dissolved in 5 mL CH_2Cl_2 under Ar and cooled to -20°C . To this mixture, 280 μL (10 equiv.) allyl chloride were added via syringe. The reaction mixture was brought to room temperature over the course of 10 min, followed by removal of volatile components *in vacuo*. Solids were treated with three 10mL washings of ice cold methanol, followed by removal of volatile components *in vacuo*. This procedure was then repeated to give pure **5.11** in $\sim 50\%$ yield. Spectral data reported in the literature.⁸



7-oxanorbornene **5.5**. A thick-walled Schlenk flask was charged with 10.1 g (90.93 mmol) *N*-methylmaleimide and evacuated and filled with argon three times. 50 mL of dry, degassed ethyl ether were then added *via* cannula followed by 12.4g (181.9 mmol) degassed furan. The

reaction mixture was then heated at 90°C as a closed system for 4 h. The diethyl ether was decanted under ambient conditions and the white solid was washed once with diethyl ether. Pure product was recrystallized from deionized water at ~30% yield. ¹H NMR (300MHz, CDCl₃): δ 6.5 (d, 2H); 5.3 (t, 2H); 3.1 (s, 3H); 2.9 (d, 2H).

General procedure for semitelechelic polymerization. Under nitrogen, the appropriate amount of 7-oxanorbornene **5.5** was weighed into a vial and dissolved in 2 mL dry, degassed dichloromethane. 10 mg of RuCl₂(=PhH)(PCy₃)₂ **5.6** were diluted in 1 mL dichloromethane. This catalyst solution was then quickly injected into the vial containing the monomer solution with vigorous stirring. After ~20 min, an excess (3 drops) of chain transfer agent *cis*-1,4-dichloro-2-butene **5.9** were added to the reaction mixture and allowed to react for ~5 minutes. The polymer was then precipitated in excess methanol under ambient conditions. ¹H NMR (300MHz, CD₂Cl₂, target 2000 molecular weight): δ 7.1-7.4 (br m, 5H); 6.05 (br s, 21H); 5.75 (br s, 6H); 4.9 (br s, 6H); 4.4 (br s, 22H); 4.1 (br s, 2H); 3.3 (br s, 27H); 2.95 (br s, 40H).

General procedure for telechelic polymerization. Under nitrogen, the appropriate amount of 7-oxanorbornene **5.5** was weighed into a vial and dissolved in 2 mL dry, degassed dichloromethane. 10 mg of RuCl₂(=CHCH₂Cl)(PCy₃)₂ **5.11** were diluted in 1 mL dichloromethane. The catalyst solution was quickly injected into the vial containing the monomer solution with vigorous stirring. After ~20 min, an excess (3 drops) of chain transfer agent *cis*-1,4-dichloro-2-butene **5.9** were added to the reaction mixture and allowed to react for ~5 minutes more. The polymer was then precipitated in excess

methanol under ambient conditions. ^1H NMR (300MHz, CD_2Cl_2 , target 2000 molecular weight with corrected catalyst loading): δ 6.05 (br s, 25H); 5.75 (br s, 7H); 4.9 (br s, 6H); 4.4 (br s, 23H); 4.1-4.3 (4H); 3.3 (br s, 29H); 2.95 (br s, 45H).

References and Notes

1. Goethals, E. J. *Telechelic Polymers: Synthesis and Applications*; CRC Press: Boca Raton, FL, 1989.
2. Nuyken, O.; Pask, S. In *Encyclopedia of Polymer Science and Technology*; Kroschwitz, J. I., Ed.; Wiley-Interscience: New York, 1989; Vol. 16, pp 494-532.
3. Schwab, P.; Grubbs, R. H.; Ziller, J. W. *J. Am. Chem. Soc.* **1996**, *118*, 100-110.
4. Hillmyer, M. A.; Grubbs, R. H. *Macromolecules* **1993**, *26*, 872-874.
5. Hillmyer, M. A.; Grubbs, R. H. *Macromolecules* **1995**, *28*, 8662-8667.
6. Hillmyer, M. A.; Nguyen, S. T.; Grubbs, R. H. *Macromolecules* **1997**, *30*, 718-721.
7. Kanaoka, S.; Grubbs, R. H. *Macromolecules* **1995**, *28*, 4707-4713.
8. Weck, M.; Schwab, P.; Grubbs, R. H. *Macromolecules* **1996**, *29*, 1789-1793.
9. Novak, B. M.; Ph.D. Thesis: Pasadena, CA, 1989.
10. Novak, B. M.; Grubbs, R. H. *J. Am. Chem. Soc.* **1988**, *110*, 960-961.
11. Mortell, K. H.; Gingras, M.; Kiessling, L. L. *J. Am. Chem. Soc.* **1994**, *116*, 12053-12054.
12. Mortell, K. H.; Weatherman, R. V.; Kiessling, L. L. *J. Am. Chem. Soc.* **1996**, *118*, 2297-2298.
13. Viswanathan, T.; Gomez, F.; Wagener, K. B. *J. Polym. Sci. Pol. Chem.* **1994**, *32*, 2469-2477.
14. Polystyrene standards would have been preferred for this polymer, but technical challenges in their use were encountered and dichloromethane GPC was unavailable.
15. Gibson, V. C.; Okada, T. *Macromolecules* **2000**, *33*, 655-656.

Appendix: X-Ray Crystallographic Data

Table 1. Crystal data and structure refinement for complex 3.23.

Empirical formula	C ₄₆ H ₄₂ N ₄ Cl ₂ Ru	
Formula weight	822.81	
Crystallization Solvent	Benzene/pentane	
Crystal Habit	Fragment	
Crystal size	0.27 x 0.14 x 0.13 mm ³	
Crystal color	Green	
Data Collection		
Preliminary Photos	Rotation	
Type of diffractometer	Bruker SMART 1000	
Wavelength	0.71073 Å MoK α	
Data Collection Temperature	98(2) K	
θ range for 15797 reflections used in lattice determination	2.31 to 28.39°	
Unit cell dimensions	a = 12.1001(9) Å b = 13.4513(10) Å c = 12.3012(9) Å	β = 108.5860(10)°
Volume	1897.7(2) Å ³	
Z	2	
Crystal system	Monoclinic	
Space group	P2 ₁	
Density (calculated)	1.440 Mg/m ³	
F(000)	848	
Data collection program	Bruker SMART v5.054	
θ range for data collection	1.75 to 28.49°	
Completeness to θ = 28.49°	95.0 %	
Index ranges	-15 ≤ h ≤ 16, -17 ≤ k ≤ 17, -16 ≤ l ≤ 16	
Data collection scan type	ω scans at 7 ϕ settings	
Data reduction program	Bruker SAINT v6.022	
Reflections collected	39564	
Independent reflections	8908 [R _{int} = 0.0714]	
Absorption coefficient	0.593 mm ⁻¹	
Absorption correction	None	
Max. and min. transmission	0.9269 and 0.8562	

Table 1 (cont.)

Structure Solution and Refinement	
Structure solution program	SHELXS-86 (Sheldrick, 1990)
Primary solution method	Direct methods
Secondary solution method	Difference Fourier map
Hydrogen placement	Geometric positions
Structure refinement program	SHELXL-97 (Sheldrick, 1997)
Refinement method	Full matrix least-squares on F^2
Data / restraints / parameters	8908 / 1 / 480
Treatment of hydrogen atoms	Riding
Goodness-of-fit on F^2	1.148
Final R indices [$I > 2\sigma(I)$, 7352 reflections]	$R1 = 0.0333$, $wR2 = 0.0544$
R indices (all data)	$R1 = 0.0481$, $wR2 = 0.0570$
Type of weighting scheme used	Sigma
Weighting scheme used	$w = 1/\sigma^2(Fo^2)$
Max shift/error	0.001
Average shift/error	0.000
Absolute structure parameter	-0.020(18)
Largest diff. peak and hole	0.819 and -0.572 e. \AA^{-3}

Special Refinement Details

Refinement of F^2 against ALL reflections. The weighted R-factor (wR) and goodness of fit (S) are based on F^2 , conventional R-factors (R) are based on F , with F set to zero for negative F^2 . The threshold expression of $F^2 > 2\sigma(F^2)$ is used only for calculating R-factors(gt) etc. and is not relevant to the choice of reflections for refinement. R-factors based on F^2 are statistically about twice as large as those based on F , and R-factors based on ALL data will be even larger.

All esds (except the esd in the dihedral angle between two l.s. planes) are estimated using the full covariance matrix. The cell esds are taken into account individually in the estimation of esds in distances, angles and torsion angles; correlations between esds in cell parameters are only used when they are defined by crystal symmetry. An approximate (isotropic) treatment of cell esds is used for estimating esds involving l.s. planes

Table 2. Atomic coordinates ($\times 10^4$) and equivalent isotropic displacement parameters ($\text{\AA}^2 \times 10^3$) for 3.23 (CCDC 208627). $U(\text{eq})$ is defined as the trace of the orthogonalized U^{ij} tensor.

	x	y	z	U_{eq}
Ru(1)	7128(1)	981(1)	9725(1)	14(1)
Cl(1)	9061(1)	979(1)	9597(1)	20(1)
Cl(2)	5172(1)	1145(1)	9825(1)	23(1)
N(1)	6074(2)	1304(2)	7146(2)	16(1)
N(2)	6434(2)	-264(2)	7527(2)	15(1)
N(3)	7294(2)	2726(2)	9710(2)	21(1)
N(4)	7803(2)	1341(2)	11555(2)	17(1)
C(1)	6998(2)	-352(2)	10096(2)	18(1)
C(2)	7778(3)	-1017(2)	10915(2)	21(1)
C(3)	8927(3)	-784(2)	11532(2)	25(1)
C(4)	9634(3)	-1453(2)	12289(3)	35(1)
C(5)	9209(3)	-2379(3)	12446(3)	38(1)
C(6)	8082(3)	-2626(2)	11866(3)	35(1)
C(7)	7367(3)	-1965(2)	11105(3)	26(1)
C(8)	6502(2)	657(2)	8028(2)	15(1)
C(9)	5555(2)	829(2)	6015(2)	18(1)
C(10)	6095(2)	-221(2)	6259(2)	18(1)
C(11)	4228(2)	853(3)	5631(2)	18(1)
C(12)	3623(3)	449(2)	6314(3)	31(1)
C(13)	2417(3)	429(2)	5938(3)	36(1)
C(14)	1812(3)	833(3)	4886(3)	34(1)
C(15)	2404(3)	1273(2)	4225(3)	32(1)
C(16)	3602(3)	1277(2)	4598(2)	23(1)
C(17)	7135(3)	-397(2)	5852(3)	20(1)
C(18)	7050(3)	-1075(2)	4988(2)	24(1)
C(19)	7992(3)	-1248(2)	4594(3)	32(1)
C(20)	9024(3)	-758(2)	5081(3)	31(1)
C(21)	9131(3)	-89(2)	5966(3)	26(1)
C(22)	8186(3)	98(2)	6343(2)	22(1)
C(23)	5867(3)	2360(2)	7207(2)	18(1)
C(24)	5023(3)	2692(2)	7646(2)	22(1)
C(25)	4838(3)	3706(3)	7715(3)	29(1)
C(26)	5474(3)	4367(2)	7300(3)	33(1)
C(27)	6269(3)	4033(2)	6809(3)	31(1)
C(28)	6485(3)	3022(2)	6747(2)	24(1)
C(29)	7397(3)	2684(3)	6233(3)	35(1)
C(30)	6947(2)	-1190(2)	8030(2)	18(1)
C(31)	8153(2)	-1283(2)	8468(2)	21(1)
C(32)	8658(3)	-2193(2)	8874(3)	28(1)
C(33)	7951(3)	-2998(2)	8823(3)	29(1)
C(34)	6760(3)	-2918(2)	8406(3)	29(1)
C(35)	6228(3)	-2009(2)	7999(2)	24(1)
C(36)	4932(3)	-1926(3)	7587(3)	33(1)
C(37)	8150(3)	3202(2)	9445(2)	22(1)
C(38)	8484(3)	4165(2)	9775(3)	28(1)
C(39)	7912(3)	4680(2)	10396(3)	34(1)
C(40)	6999(3)	4219(2)	10641(3)	32(1)

C(41)	6723(3)	3255(2)	10289(2)	24(1)
C(42)	8764(2)	1909(2)	11985(2)	23(1)
C(43)	9173(3)	2188(2)	13123(3)	28(1)
C(44)	8607(3)	1871(2)	13855(3)	30(1)
C(45)	7651(3)	1262(2)	13441(2)	28(1)
C(46)	7278(2)	1025(3)	12293(2)	19(1)

Table 3. Selected bond lengths [\AA] and angles [$^\circ$] for 3.23 (CCDC 208627).

Ru(1)-C(1)	1.868(3)	C(1)-Ru(1)-C(8)	90.71(11)
Ru(1)-C(8)	2.028(3)	C(1)-Ru(1)-N(4)	89.67(10)
Ru(1)-N(4)	2.190(2)	C(8)-Ru(1)-N(4)	179.61(10)
Ru(1)-N(3)	2.357(2)	C(1)-Ru(1)-N(3)	166.27(11)
Ru(1)-Cl(1)	2.3931(7)	C(8)-Ru(1)-N(3)	102.17(9)
Ru(1)-Cl(2)	2.4194(7)	N(4)-Ru(1)-N(3)	77.45(8)
		C(1)-Ru(1)-Cl(1)	100.09(9)
		C(8)-Ru(1)-Cl(1)	89.13(7)
		N(4)-Ru(1)-Cl(1)	90.90(6)
		N(3)-Ru(1)-Cl(1)	85.02(6)
		C(1)-Ru(1)-Cl(2)	85.16(9)
		C(8)-Ru(1)-Cl(2)	91.20(7)
		N(4)-Ru(1)-Cl(2)	88.73(6)
		N(3)-Ru(1)-Cl(2)	89.78(6)
		Cl(1)-Ru(1)-Cl(2)	174.74(4)

Table 4. Bond lengths [Å] and angles [°] for 3.23 (CCDC 208627).

Ru(1)-C(1)	1.868(3)	C(20)-C(21)	1.386(4)
Ru(1)-C(8)	2.028(3)	C(20)-H(20)	0.9500
Ru(1)-N(4)	2.190(2)	C(21)-C(22)	1.387(4)
Ru(1)-N(3)	2.357(2)	C(21)-H(21)	0.9500
Ru(1)-Cl(1)	2.3931(7)	C(22)-H(22)	0.9500
Ru(1)-Cl(2)	2.4194(7)	C(23)-C(24)	1.373(4)
N(1)-C(8)	1.358(3)	C(23)-C(28)	1.393(4)
N(1)-C(23)	1.449(3)	C(24)-C(25)	1.389(4)
N(1)-C(9)	1.477(3)	C(24)-H(24)	0.9500
N(2)-C(8)	1.374(3)	C(25)-C(26)	1.376(5)
N(2)-C(30)	1.440(3)	C(25)-H(25)	0.9500
N(2)-C(10)	1.483(3)	C(26)-C(27)	1.364(4)
N(3)-C(37)	1.343(4)	C(26)-H(26)	0.9500
N(3)-C(41)	1.343(4)	C(27)-C(28)	1.391(4)
N(4)-C(46)	1.333(3)	C(27)-H(27)	0.9500
N(4)-C(42)	1.350(3)	C(28)-C(29)	1.507(4)
C(1)-C(2)	1.449(4)	C(29)-H(29A)	0.9800
C(1)-H(1)	0.9500	C(29)-H(29B)	0.9800
C(2)-C(3)	1.391(4)	C(29)-H(29C)	0.9800
C(2)-C(7)	1.415(4)	C(30)-C(31)	1.391(4)
C(3)-C(4)	1.380(4)	C(30)-C(35)	1.397(4)
C(3)-H(3)	0.9500	C(31)-C(32)	1.388(4)
C(4)-C(5)	1.384(5)	C(31)-H(31)	0.9500
C(4)-H(4)	0.9500	C(32)-C(33)	1.370(4)
C(5)-C(6)	1.363(5)	C(32)-H(32)	0.9500
C(5)-H(5)	0.9500	C(33)-C(34)	1.371(4)
C(6)-C(7)	1.378(4)	C(33)-H(33)	0.9500
C(6)-H(6)	0.9500	C(34)-C(35)	1.397(4)
C(7)-H(7)	0.9500	C(34)-H(34)	0.9500
C(9)-C(11)	1.523(3)	C(35)-C(36)	1.491(5)
C(9)-C(10)	1.544(4)	C(36)-H(36A)	0.9800
C(9)-H(9)	1.0000	C(36)-H(36B)	0.9800
C(10)-C(17)	1.514(4)	C(36)-H(36C)	0.9800
C(10)-H(10)	1.0000	C(37)-C(38)	1.380(4)
C(11)-C(16)	1.379(4)	C(37)-H(37)	0.9500
C(11)-C(12)	1.389(4)	C(38)-C(39)	1.369(4)
C(12)-C(13)	1.383(4)	C(38)-H(38)	0.9500
C(12)-H(12)	0.9500	C(39)-C(40)	1.382(4)
C(13)-C(14)	1.379(4)	C(39)-H(39)	0.9500
C(13)-H(13)	0.9500	C(40)-C(41)	1.375(4)
C(14)-C(15)	1.378(4)	C(40)-H(40)	0.9500
C(14)-H(14)	0.9500	C(41)-H(41)	0.9500
C(15)-C(16)	1.374(4)	C(42)-C(43)	1.379(4)
C(15)-H(15)	0.9500	C(42)-H(42)	0.9500
C(16)-H(16)	0.9500	C(43)-C(44)	1.362(4)
C(17)-C(18)	1.379(4)	C(43)-H(43)	0.9500
C(17)-C(22)	1.391(4)	C(44)-C(45)	1.375(4)
C(18)-C(19)	1.392(4)	C(44)-H(44)	0.9500
C(18)-H(18)	0.9500	C(45)-C(46)	1.375(4)
C(19)-C(20)	1.369(4)	C(45)-H(45)	0.9500
C(19)-H(19)	0.9500	C(46)-H(46)	0.9500

		C(11)-C(9)-C(10)	114.8(3)
C(1)-Ru(1)-C(8)	90.71(11)	N(1)-C(9)-H(9)	109.7
C(1)-Ru(1)-N(4)	89.67(10)	C(11)-C(9)-H(9)	109.7
C(8)-Ru(1)-N(4)	179.61(10)	C(10)-C(9)-H(9)	109.7
C(1)-Ru(1)-N(3)	166.27(11)	N(2)-C(10)-C(17)	111.2(2)
C(8)-Ru(1)-N(3)	102.17(9)	N(2)-C(10)-C(9)	101.4(2)
N(4)-Ru(1)-N(3)	77.45(8)	C(17)-C(10)-C(9)	115.1(2)
C(1)-Ru(1)-Cl(1)	100.09(9)	N(2)-C(10)-H(10)	109.6
C(8)-Ru(1)-Cl(1)	89.13(7)	C(17)-C(10)-H(10)	109.6
N(4)-Ru(1)-Cl(1)	90.90(6)	C(9)-C(10)-H(10)	109.6
N(3)-Ru(1)-Cl(1)	85.02(6)	C(16)-C(11)-C(12)	118.6(3)
C(1)-Ru(1)-Cl(2)	85.16(9)	C(16)-C(11)-C(9)	120.7(3)
C(8)-Ru(1)-Cl(2)	91.20(7)	C(12)-C(11)-C(9)	120.7(3)
N(4)-Ru(1)-Cl(2)	88.73(6)	C(13)-C(12)-C(11)	120.5(3)
N(3)-Ru(1)-Cl(2)	89.78(6)	C(13)-C(12)-H(12)	119.7
Cl(1)-Ru(1)-Cl(2)	174.74(4)	C(11)-C(12)-H(12)	119.7
C(8)-N(1)-C(23)	128.0(2)	C(14)-C(13)-C(12)	119.7(3)
C(8)-N(1)-C(9)	114.4(2)	C(14)-C(13)-H(13)	120.2
C(23)-N(1)-C(9)	116.4(2)	C(12)-C(13)-H(13)	120.2
C(8)-N(2)-C(30)	129.2(2)	C(15)-C(14)-C(13)	120.2(3)
C(8)-N(2)-C(10)	113.2(2)	C(15)-C(14)-H(14)	119.9
C(30)-N(2)-C(10)	115.0(2)	C(13)-C(14)-H(14)	119.9
C(37)-N(3)-C(41)	116.3(3)	C(16)-C(15)-C(14)	119.7(3)
C(37)-N(3)-Ru(1)	123.41(19)	C(16)-C(15)-H(15)	120.1
C(41)-N(3)-Ru(1)	117.6(2)	C(14)-C(15)-H(15)	120.1
C(46)-N(4)-C(42)	116.8(2)	C(15)-C(16)-C(11)	121.2(3)
C(46)-N(4)-Ru(1)	121.80(18)	C(15)-C(16)-H(16)	119.4
C(42)-N(4)-Ru(1)	121.37(19)	C(11)-C(16)-H(16)	119.4
C(2)-C(1)-Ru(1)	132.5(2)	C(18)-C(17)-C(22)	119.0(3)
C(2)-C(1)-H(1)	113.8	C(18)-C(17)-C(10)	119.5(3)
Ru(1)-C(1)-H(1)	113.8	C(22)-C(17)-C(10)	121.5(3)
C(3)-C(2)-C(7)	117.1(3)	C(17)-C(18)-C(19)	120.7(3)
C(3)-C(2)-C(1)	123.8(3)	C(17)-C(18)-H(18)	119.6
C(7)-C(2)-C(1)	119.1(3)	C(19)-C(18)-H(18)	119.6
C(4)-C(3)-C(2)	121.2(3)	C(20)-C(19)-C(18)	120.0(3)
C(4)-C(3)-H(3)	119.4	C(20)-C(19)-H(19)	120.0
C(2)-C(3)-H(3)	119.4	C(18)-C(19)-H(19)	120.0
C(3)-C(4)-C(5)	120.2(3)	C(19)-C(20)-C(21)	120.0(3)
C(3)-C(4)-H(4)	119.9	C(19)-C(20)-H(20)	120.0
C(5)-C(4)-H(4)	119.9	C(21)-C(20)-H(20)	120.0
C(6)-C(5)-C(4)	120.1(3)	C(20)-C(21)-C(22)	120.0(3)
C(6)-C(5)-H(5)	119.9	C(20)-C(21)-H(21)	120.0
C(4)-C(5)-H(5)	119.9	C(22)-C(21)-H(21)	120.0
C(5)-C(6)-C(7)	120.3(3)	C(21)-C(22)-C(17)	120.3(3)
C(5)-C(6)-H(6)	119.9	C(21)-C(22)-H(22)	119.8
C(7)-C(6)-H(6)	119.9	C(17)-C(22)-H(22)	119.8
C(6)-C(7)-C(2)	121.1(3)	C(24)-C(23)-C(28)	121.0(3)
C(6)-C(7)-H(7)	119.5	C(24)-C(23)-N(1)	120.1(3)
C(2)-C(7)-H(7)	119.5	C(28)-C(23)-N(1)	118.8(3)
N(1)-C(8)-N(2)	105.5(2)	C(23)-C(24)-C(25)	119.8(3)
N(1)-C(8)-Ru(1)	127.34(18)	C(23)-C(24)-H(24)	120.1
N(2)-C(8)-Ru(1)	127.16(19)	C(25)-C(24)-H(24)	120.1
N(1)-C(9)-C(11)	111.9(2)	C(26)-C(25)-C(24)	119.5(4)
N(1)-C(9)-C(10)	100.8(2)	C(26)-C(25)-H(25)	120.2

C(24)-C(25)-H(25)	120.2	C(35)-C(36)-H(36B)	109.5
C(27)-C(26)-C(25)	120.4(3)	H(36A)-C(36)-H(36B)	109.5
C(27)-C(26)-H(26)	119.8	C(35)-C(36)-H(36C)	109.5
C(25)-C(26)-H(26)	119.8	H(36A)-C(36)-H(36C)	109.5
C(26)-C(27)-C(28)	121.2(3)	H(36B)-C(36)-H(36C)	109.5
C(26)-C(27)-H(27)	119.4	N(3)-C(37)-C(38)	123.5(3)
C(28)-C(27)-H(27)	119.4	N(3)-C(37)-H(37)	118.2
C(27)-C(28)-C(23)	117.9(3)	C(38)-C(37)-H(37)	118.2
C(27)-C(28)-C(29)	119.6(3)	C(39)-C(38)-C(37)	119.1(3)
C(23)-C(28)-C(29)	122.5(3)	C(39)-C(38)-H(38)	120.5
C(28)-C(29)-H(29A)	109.5	C(37)-C(38)-H(38)	120.5
C(28)-C(29)-H(29B)	109.5	C(38)-C(39)-C(40)	118.5(3)
H(29A)-C(29)-H(29B)	109.5	C(38)-C(39)-H(39)	120.8
C(28)-C(29)-H(29C)	109.5	C(40)-C(39)-H(39)	120.8
H(29A)-C(29)-H(29C)	109.5	C(41)-C(40)-C(39)	119.0(3)
H(29B)-C(29)-H(29C)	109.5	C(41)-C(40)-H(40)	120.5
C(31)-C(30)-C(35)	120.4(3)	C(39)-C(40)-H(40)	120.5
C(31)-C(30)-N(2)	119.9(2)	N(3)-C(41)-C(40)	123.6(3)
C(35)-C(30)-N(2)	119.5(3)	N(3)-C(41)-H(41)	118.2
C(32)-C(31)-C(30)	120.4(3)	C(40)-C(41)-H(41)	118.2
C(32)-C(31)-H(31)	119.8	N(4)-C(42)-C(43)	122.5(3)
C(30)-C(31)-H(31)	119.8	N(4)-C(42)-H(42)	118.7
C(33)-C(32)-C(31)	118.9(3)	C(43)-C(42)-H(42)	118.7
C(33)-C(32)-H(32)	120.5	C(44)-C(43)-C(42)	119.5(3)
C(31)-C(32)-H(32)	120.5	C(44)-C(43)-H(43)	120.3
C(32)-C(33)-C(34)	121.5(3)	C(42)-C(43)-H(43)	120.3
C(32)-C(33)-H(33)	119.3	C(43)-C(44)-C(45)	118.8(3)
C(34)-C(33)-H(33)	119.3	C(43)-C(44)-H(44)	120.6
C(33)-C(34)-C(35)	120.8(3)	C(45)-C(44)-H(44)	120.6
C(33)-C(34)-H(34)	119.6	C(44)-C(45)-C(46)	118.7(3)
C(35)-C(34)-H(34)	119.6	C(44)-C(45)-H(45)	120.6
C(34)-C(35)-C(30)	118.0(3)	C(46)-C(45)-H(45)	120.6
C(34)-C(35)-C(36)	120.1(3)	N(4)-C(46)-C(45)	123.6(3)
C(30)-C(35)-C(36)	121.9(3)	N(4)-C(46)-H(46)	118.2
C(35)-C(36)-H(36A)	109.5	C(45)-C(46)-H(46)	118.2

Table 5. Anisotropic displacement parameters ($\text{\AA}^2 \times 10^4$) for 3.23 (CCDC 208627). The anisotropic displacement factor exponent takes the form: $-2\pi^2 [h^2 a^{*2} U^{11} + \dots + 2 h k a^* b^* U^{12}]$.

	U^{11}	U^{22}	U^{33}	U^{23}	U^{13}	U^{12}
Ru(1)	154(1)	134(1)	142(1)	-2(1)	41(1)	-6(1)
Cl(1)	179(3)	200(3)	234(3)	-24(5)	76(3)	-21(5)
Cl(2)	168(3)	295(6)	234(3)	29(3)	76(3)	-5(3)
N(1)	142(12)	156(12)	160(12)	-6(9)	25(10)	3(9)
N(2)	138(14)	167(13)	141(13)	1(10)	45(11)	-1(11)
N(3)	192(14)	225(13)	166(13)	10(11)	3(11)	-3(11)
N(4)	172(13)	154(12)	169(13)	1(9)	22(10)	4(9)
C(1)	206(16)	183(15)	156(16)	-53(12)	55(13)	-41(13)
C(2)	305(18)	181(15)	187(16)	-43(13)	125(14)	40(14)
C(3)	308(19)	223(17)	238(18)	0(14)	101(15)	55(14)
C(4)	370(20)	380(20)	292(19)	69(16)	67(16)	150(16)
C(5)	540(30)	320(20)	320(20)	138(16)	178(19)	235(18)
C(6)	640(30)	170(17)	300(20)	79(14)	233(19)	71(17)
C(7)	380(20)	217(18)	214(18)	-37(14)	155(16)	6(15)
C(8)	108(14)	160(15)	187(15)	28(11)	49(12)	-17(10)
C(9)	191(13)	210(19)	109(12)	3(13)	26(10)	-16(13)
C(10)	187(16)	170(14)	142(15)	-21(12)	16(13)	3(12)
C(11)	192(13)	171(18)	169(13)	-4(14)	40(11)	69(14)
C(12)	223(17)	368(19)	315(19)	112(15)	44(15)	58(15)
C(13)	252(19)	410(20)	430(20)	83(17)	125(17)	36(16)
C(14)	169(15)	320(30)	447(19)	-60(19)	0(14)	61(17)
C(15)	272(18)	380(20)	243(17)	1(14)	-27(14)	131(14)
C(16)	255(17)	215(18)	214(16)	-20(12)	57(13)	32(12)
C(17)	233(18)	180(16)	206(17)	56(13)	81(14)	75(13)
C(18)	298(18)	238(16)	181(17)	1(13)	62(14)	46(14)
C(19)	400(20)	342(18)	239(18)	-15(15)	122(16)	112(16)
C(20)	340(20)	362(19)	311(19)	110(16)	209(16)	125(16)
C(21)	209(17)	296(18)	286(18)	95(14)	80(15)	27(14)
C(22)	261(17)	213(17)	205(17)	-6(13)	94(14)	23(13)
C(23)	188(17)	124(14)	166(16)	-17(12)	-22(14)	-11(12)
C(24)	283(17)	184(16)	178(16)	21(13)	54(13)	23(13)
C(25)	330(20)	263(19)	260(20)	-4(16)	56(17)	83(16)
C(26)	390(20)	136(16)	370(20)	-29(15)	-15(18)	-10(15)
C(27)	340(20)	190(16)	350(20)	42(14)	20(16)	-83(15)
C(28)	200(17)	228(16)	227(17)	13(13)	-1(14)	-13(13)
C(29)	300(20)	300(20)	490(20)	26(17)	169(18)	-100(16)
C(30)	245(17)	164(14)	150(15)	-9(12)	77(13)	23(12)
C(31)	246(17)	198(15)	187(16)	6(12)	66(13)	12(13)
C(32)	326(19)	293(18)	219(18)	-4(14)	95(15)	100(15)
C(33)	500(20)	171(16)	229(17)	29(13)	142(16)	75(15)
C(34)	470(20)	164(16)	270(18)	-42(13)	170(16)	-51(14)
C(35)	297(18)	221(16)	187(16)	-24(13)	71(14)	-63(14)
C(36)	340(20)	310(20)	340(20)	25(17)	99(19)	-108(18)
C(37)	217(17)	228(16)	215(17)	51(13)	57(14)	29(13)
C(38)	350(19)	199(17)	306(19)	8(14)	116(16)	-60(14)
C(39)	510(20)	169(15)	330(20)	3(15)	105(17)	-52(17)
C(40)	450(20)	227(18)	280(20)	-3(15)	127(18)	77(16)

C(41)	238(17)	238(16)	234(17)	5(13)	82(14)	26(13)
C(42)	254(17)	189(15)	234(16)	3(13)	66(13)	-17(14)
C(43)	236(18)	271(18)	254(18)	-33(14)	-12(14)	-16(14)
C(44)	318(19)	374(19)	191(17)	-17(15)	44(14)	69(16)
C(45)	309(17)	340(20)	199(15)	46(13)	109(13)	93(13)
C(46)	205(13)	167(12)	207(13)	20(18)	66(10)	55(18)

Table 6. Hydrogen coordinates ($\times 10^4$) and isotropic displacement parameters ($\text{\AA}^2 \times 10^3$) for 3.23 (CCDC 208627).

	x	y	z	U_{iso}
H(1)	6282	-651	9663	22
H(3)	9231	-152	11429	30
H(4)	10416	-1279	12705	43
H(5)	9702	-2842	12958	46
H(6)	7788	-3257	11988	42
H(7)	6586	-2150	10700	31
H(9)	5839	1169	5432	21
H(10)	5482	-732	5916	21
H(12)	4041	184	7046	37
H(13)	2008	139	6402	43
H(14)	984	806	4617	40
H(15)	1985	1574	3514	39
H(16)	4006	1577	4136	28
H(18)	6342	-1427	4659	29
H(19)	7918	-1706	3987	39
H(20)	9666	-878	4813	37
H(21)	9851	241	6313	32
H(22)	8257	567	6939	27
H(24)	4568	2229	7903	26
H(25)	4277	3941	8045	35
H(26)	5358	5061	7355	40
H(27)	6682	4498	6505	37
H(29A)	7714	3263	5948	53
H(29B)	7044	2227	5597	53
H(29C)	8027	2344	6820	53
H(31)	8634	-720	8490	25
H(32)	9481	-2256	9183	33
H(33)	8292	-3626	9083	35
H(34)	6290	-3487	8392	35
H(36A)	4697	-1330	7917	50
H(36B)	4592	-2516	7825	50
H(36C)	4655	-1877	6749	50
H(37)	8547	2856	9007	27
H(38)	9102	4468	9575	34
H(39)	8139	5338	10651	41
H(40)	6568	4564	11047	38
H(41)	6095	2945	10465	28
H(42)	9173	2125	11485	27
H(43)	9845	2597	13394	33
H(44)	8867	2067	14637	36
H(45)	7257	1010	13938	33
H(46)	6610	613	12011	23

